Characterization and modeling of the cure-induced shrinkage of an epoxy resin used in organic laminate based electronic modules

Master Thesis

by

Julia Verena Zündel

submitted to the

Institute of Material Science and Testing of Polymers
at the Montanuniversität Leoben

prepared at

AT&S Austria Technologie & Systemtechnik AG

Thesis supervisor: Dipl.-Ing. Thomas Krivec, Dipl.-Ing. Qi Tao

Academic supervisor: Univ.-Prof. Dr. Gerald Pinter

Leoben, January 2018

EIDESSTATTLICHE ERKLÄRUNG

Ich erkläre an Eides statt, dass ich diese Arbeit selbstständig verfasst, andere als die angegebenen Quellen und Hilfsmittel nicht benutzt und mich auch sonst keiner unerlaubter Hilfsmittel bedient habe.

AFFIDAVIT

I declare in lieu of oath, that I wrote this thesis and performed the associated research myself, using only literature cited in this volume.

LEOBEN, January 2018

(Julia Verena Zündel)

ACKNOWLEDGMENT

KURZFASSUNG

Der Trend zur Miniaturisierung und insbesondere das Einbetten von elektronischen Komponenten in die epoxidharzbasierten, faserverstärkten Innenlagen führen zu einer zunehmenden Komplexität von Leiterplatten und deren Herstellungsprozess. Numerische Simulationen mittels der Finite-Elemente-Methode gewinnen daher zunehmen an Bedeutung, da mit ihrer Hilfe die Herstellbarkeit und Funktionalität sowohl der Leiterplatten als auch der vereinzelten elektronischen Module bereits vor ihrer tatsächlichen Fertigung ermittelt und bewertet werden können. Eine grundlegende Voraussetzung für aussagekräftige Simulationsergebnisse ist die detaillierte Kenntnis des zeit- und temperaturabhängigen Verhaltens der verwendeten Materialien. Bisher wird die Bildung von inneren Spannungen auf Grund des härtungsbedingten Schrumpfens der Harzkomponente und die damit einhergehende Verwerfung von elektronischen Modulen in Finite-Elemente-Simulationen allerdings größtenteils vernachlässigt.

Eine Hauptzielsetzung der vorliegenden Arbeit lag daher in der Bestimmung des Härtungsschrumpfens eines Epoxidharzes, welches gegenwärtig in der Herstellung von Leiterplatten Anwendung findet. Zu diesem Zweck wurden verschiedene Messmethoden auf ihre Anwendbarkeit untersucht und die Reproduzierbarkeit der Messergebnisse sowie ihre Vergleichbarkeit untereinander überprüft. Des Weiteren wurde der Einfluss von Druck und Temperatur bei der Prüfkörperherstellung auf das Materialverhalten des Harzes und damit einhergehend auf die messbaren Schrumpfwerte untersucht. Der zweite Teil dieser Arbeit befasst sich mit der Implementierung des ermittelten Schrumpfwertes in das Materialmodell des Harzes in der Finite-Elemente-Software Abaqus FEA. Ein einfacher Implementierungsansatz wurde gewählt, bei dem der Wärmeausdehnungskoeffizient des Harzes und der Schrumpfwert zu einem temperaturabhängigen Materialkennwert kombiniert wurden.

Es konnte gezeigt werden, dass die thermomechanische Analyse im Vergleich zu den anderen untersuchten Messmethoden die zuverlässigsten Ergebnisse lieferte. Während des raschen Aufheizens der Prüfkörper und des anschließenden vollständigen Aushärtens des Harzes unter isothermen Bedingungen wurden die Prüfkörperabmessungen kontinuierlich aufgezeichnet. Die Auswertung der Messdaten ergab einen Wert von 1% für das Härtungsschrumpfen des untersuchten Harzes. Die temperaturmodulierte thermomechanische Analyse zeigte großes Potential hinsichtlich einer kontinuierlichen Schrumpfmessung während des Aushärtevorgangs, es empfiehlt sich daher eine

detailliertere Auseinandersetzung mit dieser komplexen Messmethode in weiterführenden Arbeiten. Mit den weiteren Messmethoden, konkret den Dichtemessungen und den Messungen am Platte-Platte-Rheometer, konnten in Kombination mit der gewählten Art der Prüfkörperherstellung keine zufriedenstellenden Ergebnisse im Bezug auf das Härtungsschrumpfen erzielt werden.

ABSTRACT

Regarding printed circuit board industry, miniaturization and the technique of embedding electrical components in the internal organic laminate based layers lead to an ever increasing complexity of the designs as well as the manufacturing processes of the boards. As a consequence, reliable finite element simulations have become more important because they can support the investigation of both the producibility and the reliability of the requested electronic modules prior to manufacturing. Detailed knowledge about the time- and temperature-dependent material behavior of all components is essential for this purpose. However, deformation and internal stresses due to resin shrinkage are mostly neglected in finite element simulations of electronic modules until now.

The primary focus of the present master thesis was therefore to determine the cure-induced shrinkage of an epoxy resin of an organic laminate commonly used in printed circuit board manufacturing. For this purpose, various measurement methods were investigated and evaluated with regard to reproducibility and comparability. The influences of the temperature and the pressure applied during specimen preparation on the material behavior of the resin and consequently on the measured shrinkage values were investigated as well. The second part of the thesis focused on the implementation of the determined shrinkage into the material model of the resin in the finite element software Abaqus FEA. A simple implementation approach was chosen, combining the effects of thermal expansion and cure-induced shrinkage into one temperature-dependent material characteristic.

It could be shown that thermomechanical analysis is the most suitable method among the examined measurement techniques. Isothermal measurements at the curing temperature of the resin were performed and the dimensional changes of the specimens were recorded. By evaluating the measured data a shrinkage value of approximately 1% was obtained for the investigated resin. Temperature modulated thermomechanical analysis has the potential to be used for online shrinkage measurement; further research of this complex technique is needed though. The combination of the other investigated measurement methods, namely density measurements and rheometry, and the chosen specimen preparation method turned out to be not suitable for the determination of the resin shrinkage.

TABLE OF CONTENTS

1   INTRODUCTION AND OBJECTIVE

Miniaturization and the trend of embedding electrical components in the internal organic laminate based layers are currently leading to an ever increasing complexity of printed circuit boards (PCBs) and their manufacturing. The multitude of organic and non-organic materials and the mismatch in their coefficients of thermal expansion (CTEs) can cause internal stresses in the PCB. The use of reinforced composites can be an additional source of stresses due to the resin shrinkage which occurs during the curing of the resin substrate. Consequently, production processes under thermal loads as well as non-symmetric lay-ups contribute to the development of stresses and a subsequent deflection of the PCB. Such a deformation can cause problems during the PCB manufacturing and may as well have an impact on the reliability of the finished electronic modules (Schuerink et al. 2013, Kravchenko et al. 2014).

For this reason, improving the predictability of the warpage behavior of the PCBs and the individual electronic modules becomes all the more important. Computer-aided simulations of the boards prior to manufacturing can save both manufacturing time and money. The finite element analysis (FEA) is a powerful simulation tool that performs more effectively the more detailed and realistic the characteristics of the materials can be implemented in the used simulation software. While some material characteristics can easily be obtained either from supplier datasheets or from measurements that can be performed using a rather simple test setup, the determination of others is considerably more complex and time-consuming. As a consequence, the accuracy of a finite element based warpage analysis is often limited by the assumptions made for developing the required material models or by missing material data (Stommel et al. 2011).

Generally, the organic laminates used for PCB production at Austria Technologie & Systemtechnik AG (AT&S) consist of glass-fiber reinforced epoxy resins. Experience showed that considering only the dimensional changes of these composites due to thermal expansion and contraction is not sufficient for an accurate prediction of the warpage behavior of the electronic modules. The cure-induced shrinkage of the resin material has to be taken into account as well.

The main scope of this thesis was therefore the determination of the cure-induced shrinkage of the epoxy resin of a laminate commonly used at AT&S. For this purpose, the resin matrix had to be separated from the fiber fabric in order to prepare pure resin

specimens. The shrinkage behavior of these specimens was then analyzed using several test procedures based on different measurement principles. The investigated test procedures were chosen on condition that they can be performed with equipment available at AT&S or at least with measurement instruments with reasonable acquisition costs. This thesis compares the shrinkage values obtained by applying the investigated measuring methods, with a special focus on the influence of the specimen preparation on the measured results. The measurement parameters and the specimens chosen for each of the experiments are explained in detail, as well as possible influence factors on the measurements. Finally, the most promising test procedure was identified.

The last part of this thesis focuses on performing a FEA of a test carrier in order to validate the experimentally determined shrinkage value of the investigated epoxy resin. For this purpose, the shrinkage value had to be implemented into the material model of the resin. A quite simple approach was chosen, whereby the resin shrinkage could be combined with the coefficient of thermal expansion of the resin. The similarities and differences between the model and the test carrier are presented within this thesis, as well as explanations for the occurring discrepancies in the resulting deformation.

2 BASIC CONSIDERATIONS

2.1 Composite materials used in the electronics industry

Generally speaking, the laminates used in PCBs consist of reinforced resin substrates that are clad with copper on both sides. Figure 2-1 shows the conventional manufacturing process of laminates. As a first step, the chosen reinforcement material is pre-impregnated with the resin. Glass fibers are commonly chosen as reinforcement materials due to their good mechanical and electrical properties and the low costs. Usually the glass fibers are bundled to yarns and then woven to fabrics prior to the impregnation in order to enable easy handling of the material. In a next step, the now pre-impregnated fibers or prepregs are exposed to heat. This process dedicated to achieve a partial curing of the resin is known as B-staging. The prepregs are then cut in length and stacked according to the defined lay-up of the laminate. Finally, the stacks are clad with copper foils on both sides and laminated in a press by applying temperature, pressure and vacuum (Coombs 2001).

Epoxy resins are the most widely used resins for PCBs due to their good mechanical, physical, and electrical properties and the low costs compared to other resin systems. Basically, epoxy resins are a class of thermosetting polymers that contain cyclic ethers called epoxide groups (Fig. 2-2a). Depending on the area of application, there exists a wide range of additives which can or have to be added to the resin system to ensure the
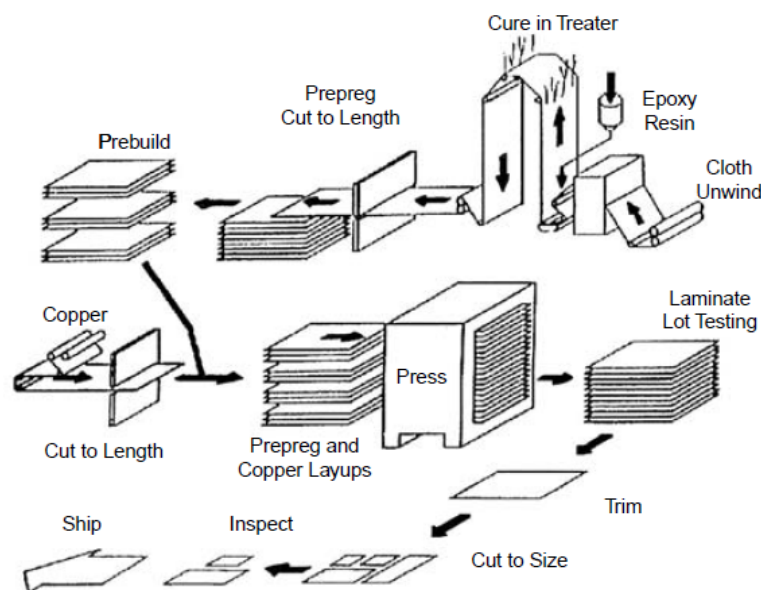
Fig. 2-1: Conventional laminate manufacturing process (Coombs 2001).

(a)   (b)
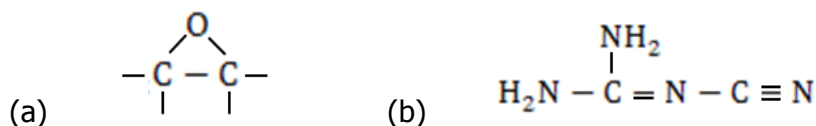
Fig. 2-2: Structural formulas of (a) the functional group of an epoxy resin and of (b) dicyandiamide (Gilbert 1988).

required material behavior. Curing agents and accelerators directly affect the curing reaction, while additives like modifiers, flame retardants, and organic and inorganic fillers have an impact on the material characteristics of the partially or fully cured resin. Dicyandiamide (dicy) is a latent hardener commonly used in epoxy resin systems because of the good mechanical properties and the resistance to both acids and bases which can be achieved. Compared to other epoxy resin systems, the combination of epoxy and dicy is also able to form strong bonds to copper, which is an essential characteristic regarding PCB manufacturing. The chemical structure of dicy is depicted in Fig. 2-2b (Gilbert 1988, Coombs 2001).

The chemical reaction between the functional groups of an epoxy resin and dicy as the curing agent is represented schematically in Fig. 2-3. The depicted primary amine reacts with the epoxide group of the resin. The addition of a primary or secondary amine to the epoxide results in a secondary or tertiary amine respectively, as well as a hydroxyl group. Reactions with tertiary amines occur as well; they are either a result of the unshared electron pair of the nitrogen or of the addition of a hydroxyl group to the epoxide. All four nitrogen atoms of the dicy molecule are able to react with epoxide groups. However, it has been found that the formation of hydroxyl groups by primary and secondary amine reactions catalyze the curing reaction, with the reaction rate increasing with increasing degree of cure (Gilbert 1988, Boyle et al. 2001).

Primary amine   Epoxide   Secondary amine + Hydroxyl
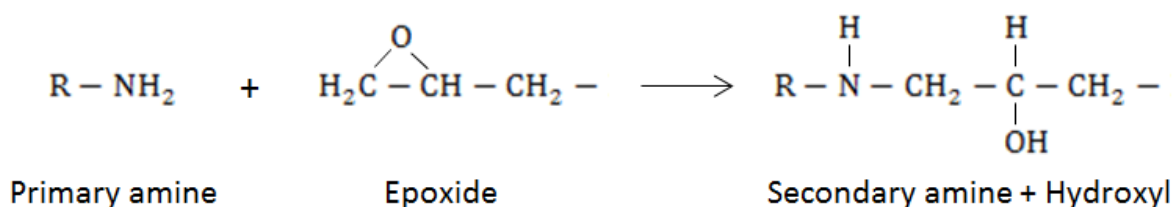
Fig. 2-3: Epoxy/amine reaction: the primary amine reacts with the functional group of the resin (Boyle et al. 2001).

2.2 Warpage behavior of electronic modules

Basically, the design of a PCB as well as the characteristics of the used materials contribute to the deformation behavior of the boards under thermal loads. Non-symmetric lay-ups and the mismatch in the CTEs of the different layer materials are two major influence factors. During manufacturing, several press steps involve heating of the lay-up under pressure in order to chemically bond the individual layers together. The deformation evolving due to the differences in CTE of two materials is depicted schematically in Fig. 2-4. As can be seen, the unbound layers (i) and (ii) show a different deformation behavior than the bonded layers (iii) and (iv). Increasing the temperature leads to an expansion of both materials. Unbound layers of equal size can expand freely and therefore remain straight; the dimensions of the expanded layers may differ significantly though. By contrast, the expansion of the bonded layers is impeded at the contact surface, which leads to the formation of internal stresses. The stresses in symmetric builds counteract each other and again the bonded layers remain straight. However, any deviation from symmetry leads to a deformation of the build, with the extent of the deformation depending on the characteristics of the two materials (Schuerink et al. 2013).

The warpage of a PCB can be explained by two overlapping deformation modes, bow and twist, which lead to a deviation from the flat state of the board. Bow describes the deformation due to the formation of a cylindrical curvature as in Fig. 2-5a, whereas twist describes a deformation that occurs parallel to a diagonal across the surface of the panel as is Fig. 2-5b. As can easily be imagined, these deformations lead to severe difficulties regarding the board manufacturing. Many process steps require a certain degree of flatness because the panels are transported between rolls; the automatic feeding would not work properly if the panels were overly warped. Other processes require flat or at least flexible panels because vacuum suction is used in order to align and fix the panels. But even if the PCBs can be manufactured despite being warped, internal stresses and
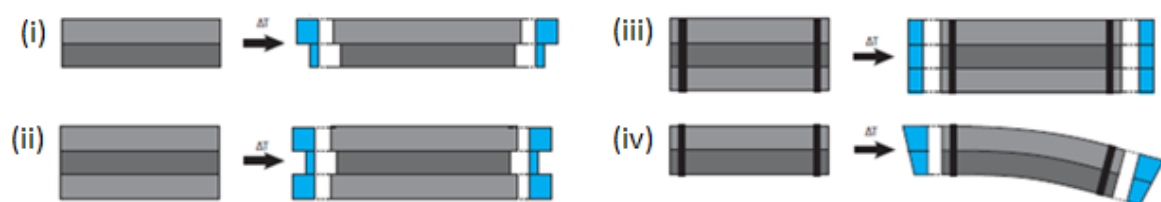
Fig. 2-4:   Deformation of (i, ii) unbound and (iii, iv) bonded layers due to thermal expansion (Schuerink et al. 2013).
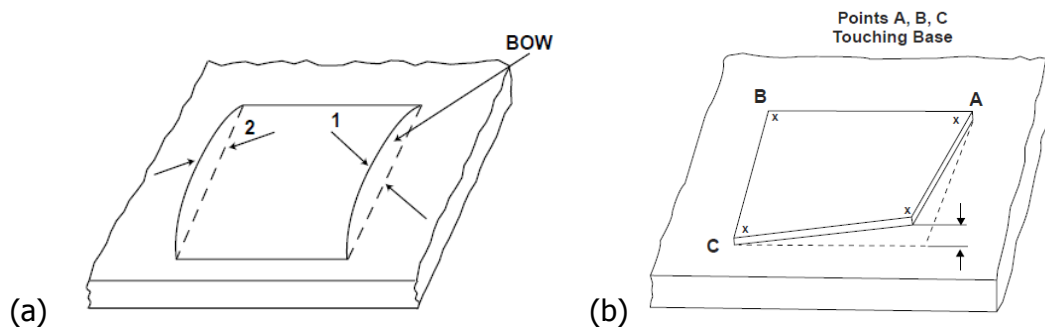
Fig. 2-5: Schematic representation of (a) bow and (b) twist of a panel (IPC - Association Connecting Electronics Industries 1999).

board deformations can lead to a series of further problems. Experience showed that interface delamination or die cracking can be a direct result of residual stresses and affect the reliability of the finished electronic modules (IPC - Association Connecting Electronics Industries 1999, Coombs 2001).

2.3 Experimental principles

2.3.1 Density measurements

The density of a resin specimen increases during curing, whereas its volume decreases. This material behavior is caused by the formation of a network of cross-links between the molecular chains. Covalent bonds instead of van der Waals bonds lead to reduced distance of separation between the molecules. Therefore, density measurement is one of the possible measurement techniques to determine the volumetric cure shrinkage of a material (Khoun and Hubert 2010).

Pycnometry

A pycnometer is a laboratory flask which at a certain temperature holds an exact volume of a working liquid. Distilled water is commonly used as the working liquid since its temperature-dependent density values can be easily retrieved from literature. The weight of the pycnometer m_p is measured in dry state. Additionally, the weight of the pycnometer with the inserted solid m_{p+s} and filled with the working liquid m_{p+l} respectively is measured, as well as the weight of the pycnometer filled with both liquid and solid m_{p+l+s}. The density of the specimen can then be calculated using equation (2.1). When using a working liquid with unknown density, its density can be calculated by measuring

the weight of the liquid and dividing this value by the known volume of the glass-flask (Ortega-Rivas 2012).

$$\rho_{specimen} = \frac{m_{p+s} - m_p}{(m_{p+l} - m_p) - (m_{p+l+s} - m_{p+s})} * \rho_{liquid} \qquad (2.1)$$

Hydrostatic weighing

Hydrostatic weighing is a technique directly based on Archimedes' principle of determining the density of a solid specimen (Fig. 2-6). Basically, the buoyancy of the specimen in a measurement fluid is used to calculate the density of the specimen. The weight of the specimen is determined first in air m_{air} and then immersed in the liquid m_{liquid}. When immersed in the liquid, the specimen experiences buoyancy, with the buoyant force being equal to the weight of the water that the specimen displaces. The density of the specimen $\rho_{specimen}$ can therefore be calculated using equation (2.2), if the density of the liquid ρ_{liquid} is known at the defined measuring temperature (Frick and Stern 2011).

$$\rho_{specimen} = \frac{m_{air}}{m_{air} - m_{liquid}} * \rho_{liquid} \qquad (2.2)$$
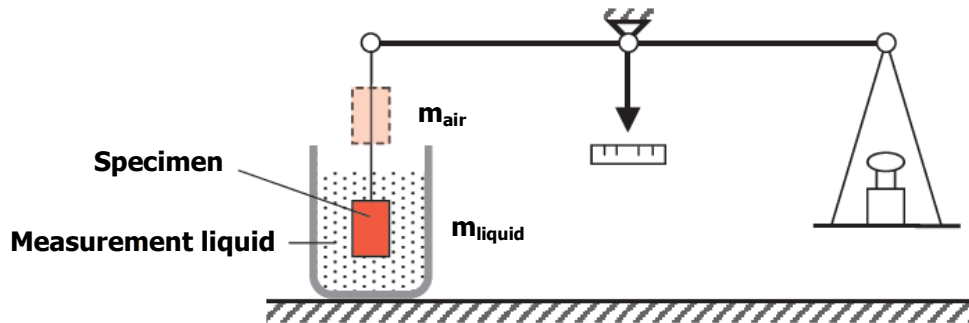
Fig. 2-6: Hydrostatic weighing as a direct application of Archmides' principle (Frick and Stern 2011).

2.3.2 Differential scanning calorimetry

Differential scanning calorimetry (DSC) enables the determination of the changes in internal energy or enthalpy of a substance due to physical and chemical reactions. Processes like melting or glass transition increase the enthalpy, whereas crystallization or curing are processes that lead to a decrease in enthalpy (Ehrenstein et al. 2004).

In heat-flux DSC, basically both the specimen and a reference material are located in a furnace (Fig. 2-7a). The temperatures of both materials T_S and T_R are measured continuously during an experiment. As long as no reactions take place in the investigated material, the temperatures match and the heat flux into the materials remains constant, whereas any physical or chemical reaction leads to a change in the heat flux. The heat flux $\dot{Q}$ describes the quantity of heat transferred from the furnace either to the reference material $\dot{Q}_{OR}$ or to the specimen $\dot{Q}_{OS}$. Figure 2-7b shows a schematic DSC diagram. The reactions and transitions can be interpreted as deviations of the heat flow curve from the baseline. The baseline marks the temperature regions in which no reactions take place in the material (Ehrenstein et al. 2004).

The specific heat capacity c_p of a material indicates the energy needed in order to increase the temperature of 1g of the material by 1°C at constant pressure. $\dot{Q}$ is directly proportional to c_p but requires less elaborate equipment to measure. Equation (2.3) describes the relation between these two parameters. As can be seen, the heating rate v and the mass m of the specimen have an influence on $\dot{Q}$ (Ehrenstein et al. 2004, Frick and Stern 2006).

$$\dot{Q} = v * c_p * m \tag{2.3}$$

DSC measurements can be used to characterize the cure kinetics of a resin. In this study, the Vyazovkin model-free kinetic algorithm was applied in order to determine the degree of cure as a function of both curing time and temperature. The conversion rate of the cure reaction $d\alpha/dt$ can be predicted using the Arrhenius expression in equation (2.4),

(a)   (b)
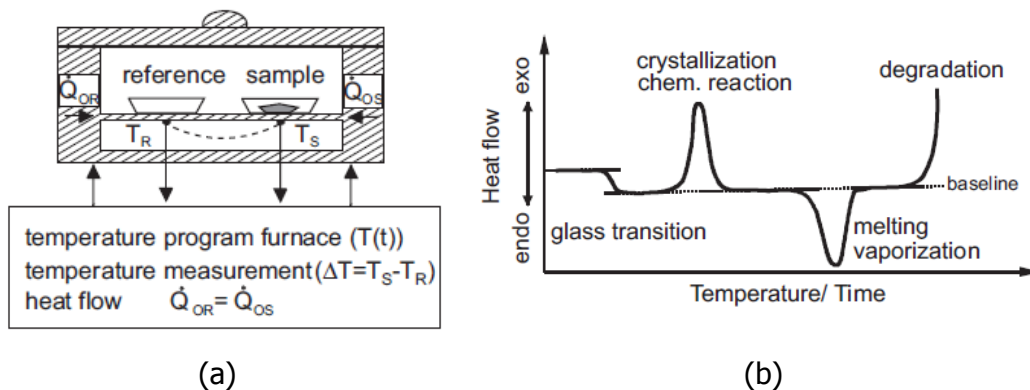
Fig. 2-7:   (a) Specimen and reference material in the furnace of a heat-flux DSC (Ehrenstein et al. 2004).

(b) Schematic diagram of a DSC curve showing possible endothermic and exothermic transitions (Ehrenstein et al. 2004).

where k_0 is the pre-exponential factor, $E(\alpha)$ the activation energy as a function of the conversion α, R the universal gas constant, T the temperature, and $f(\alpha)$ a mathematical expression describing the reaction model as a function of α. By performing measurements with at least 3 different heating rates, $E(\alpha)$ can be determined numerically for each degree of conversion without knowing the exact expression of $f(\alpha)$. As a next step, these data can be used to predict the degree of cure as a function of time and temperature (Mettler Toledo 2003, Wang et al. 2005).

$$\frac{d\alpha}{dt} = k_0 * \exp\left(\frac{-E(\alpha)}{R*T}\right) * f(\alpha) \tag{2.4}$$

2.3.3 Dynamic-mechanical analysis

In dynamic mechanical analysis (DMA), a sinusoidal force is applied to a specimen and thus creates a sinusoidal deformation of the material. Polymeric materials show a time-delayed response to the applied force due to their viscoelastic behavior (Fig. 2-8a). In the linear viscoelastic region at small stresses, the deformation depends only on time but not on the extent of mechanical loading. In this region, stress σ is directly proportional to strain ε. Therefore, in analogy to Hooke's Law, the complex modulus E^* can be calculated from stress and strain amplitudes using equation (2.5) (Frick and Stern 2011).

$$|E^*| = \frac{\sigma_A}{\varepsilon_A} = \frac{E'}{\cos\delta} = \frac{E''}{\sin\delta} \tag{2.5}$$

(a)   (b)
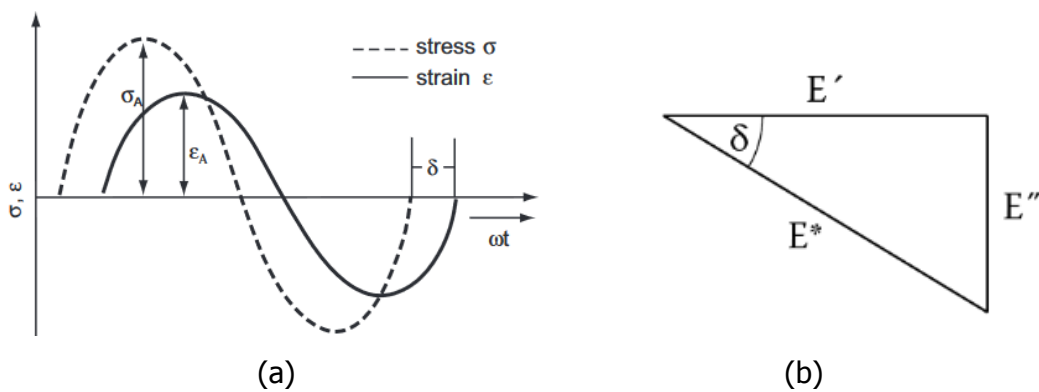
Fig. 2-8:   (a) Deformation response of a viscoelastic material to an applied sinusoidal force (Ehrenstein et al. 2004).

(b) Graphical representation of the relation between complex modulus E^*, storage modulus E', loss modulus E'' and loss factor δ (Menard 2008).
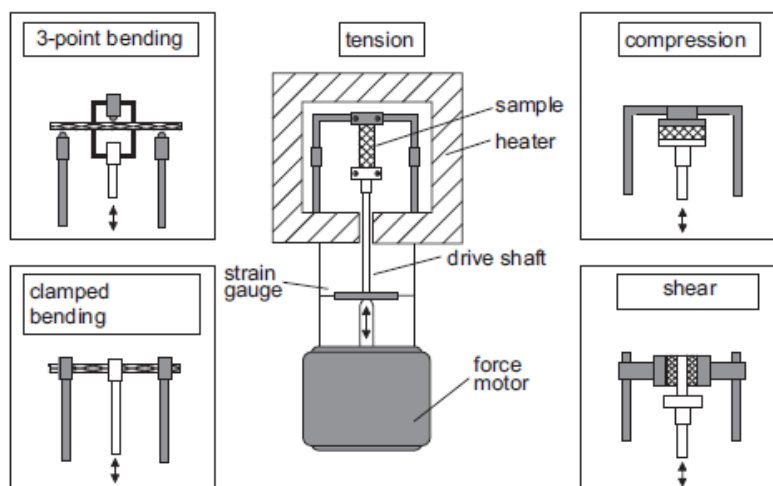
Fig. 2-9: Different test arrangements under vertical load of a dynamic-mechanical analyzer (Ehrenstein et al. 2004).

The complex modulus combines the storage modulus E' and the loss modulus E". The storage modulus describes the stiffness of the specimen, whereas the loss modulus is a measure of the dissipated energy during loading. Using the phase shift between the stress and strain curves, E' and E" can be calculated according to equation (2.5). The mathematical correlations between the different moduli are depicted graphically in Fig. 2-8b (Frick and Stern 2011).

Various test arrangements exist in order to investigate the mechanical properties of all kinds of polymeric specimens (Fig. 2-9). Measurements under shear loading can be used to investigate the rheological properties of viscoelastic materials. In this work, shear mode was used to determine the gelation temperature of the investigated epoxy resin. The 3-point bending configuration enabled to measure the curvature of the bi-material specimens evolving due to the curing of the resin layer at elevated temperatures (Ehrenstein et al. 2004).

2.3.4 Rheometry

The rotational rheometer enables the investigation of the viscosity of a specimen as a function of shear rate and temperature. In oscillatory mode, both the rheometric and the viscoelastic properties of the specimen can be determined. By analogy with the shear mode in DMA, a sinusoidal load is applied to the specimen and the time-delayed response of the material is recorded (Fig. 2-10b). In the parallel plate configuration, the specimen is placed between the two concentric plates. The torque M(t) is introduced by the
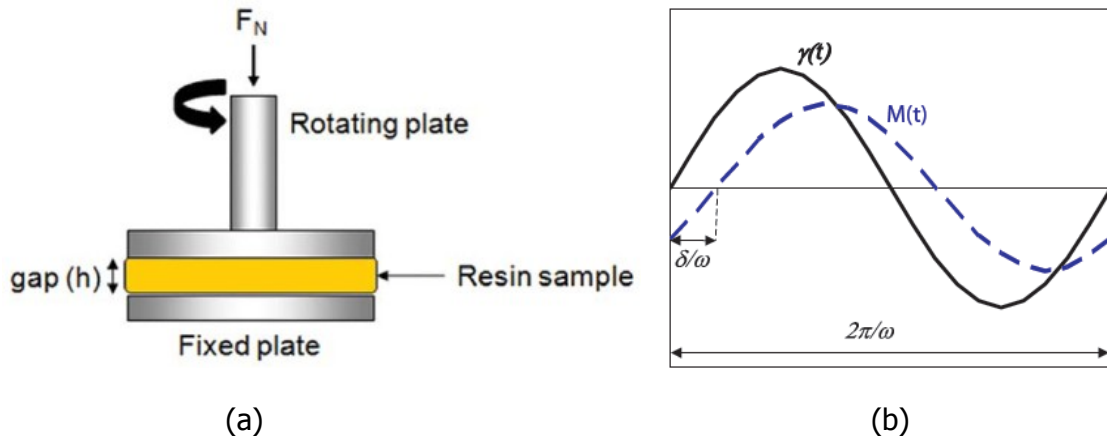
Fig. 2-10: (a) Resin specimen fixed between the parallel plates of a rotational rheometer (Khoun and Hubert 2010).

(b) Curve progression of shear deformation and torque over time.

oscillation of one of the plates, as depicted in Fig. 2-10a. Applying only small shear amplitudes $\gamma(t)$ ensures measurements in the linear viscoelastic region of the material (Frick and Stern 2011).

In addition, a small normal force (F_N) has to be applied to the specimen in order to ensure permanent contact between the specimen and the rheometer plates. However, the force influences the material behavior, especially so at the beginning of the measurement when the resin is still uncured. This is why some literature recommends to apply the normal force only after gelation of the resin material (Khoun and Hubert 2010).

The volumetric cure shrinkage ε_V of the specimens can be calculated using equation (2.6), where h_0 is the initial gap size and h is the actual gap size at a given time. This equation is valid as long as the in-plane strains in the resin specimens are assumed to be zero. Furthermore the resin material is assumed to be incompressible (Haider et al. 2007).

$$\varepsilon_V = \left[1 + \frac{1}{3} * \left(\frac{h - h_0}{h_0}\right)\right]^3 - 1 \tag{2.6}$$

2.3.5 Thermomechanical analysis

Thermomechanical analysis (TMA) is used to determine the dimensional changes of a specimen as a function of temperature. In expansion or dilatometric mode, the specimen is placed on the sample holder of the test instrument and a constant load is applied via a quartz glass probe. Probes with large contact areas are used in order to determine the
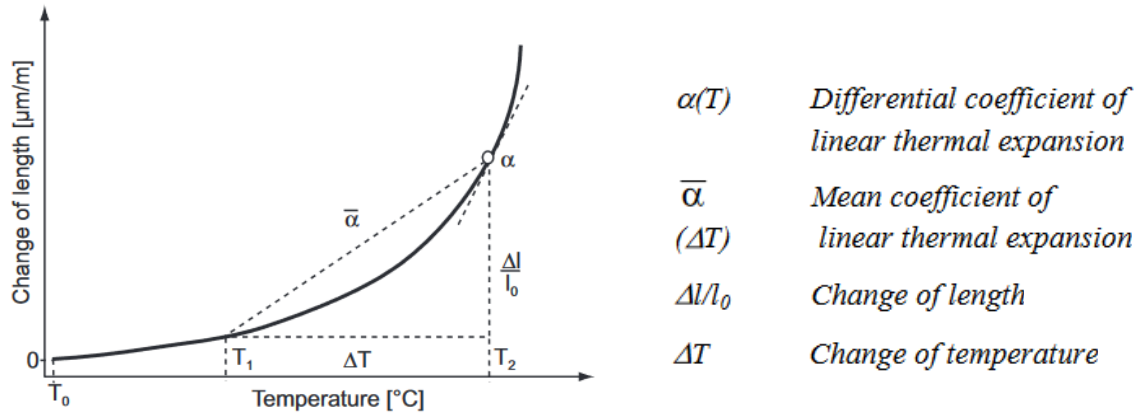
Fig. 2-11: Mean and differential coefficients of linear thermal expansion $\bar{\alpha}(\Delta T)$, $\alpha(T)$ (Ehrenstein et al. 2004).

coefficient of linear thermal expansion (CTE) of the investigated material. The combination of small loads and large contact areas ensures that both expansion and contraction of the specimen can be measured accurately without the probe losing contact with the specimen. However, even a small load counteracts thermal expansion and induces a compressive force. Consequently, the recorded dimensional changes of the specimen are always the result of the interaction of material changes and external influences (Ehrenstein et al. 2004).

When plotting the dimensional changes over temperature, the CTE of the material can be evaluated in two ways. As can be seen in Fig. 2-11, the mean coefficient of linear thermal expansion $\bar{\alpha}(\Delta T)$ describes the dimensional change Δl_{th} over the whole measured temperature range ΔT. However, since Δl_{th} is dependent on ΔT, $\bar{\alpha}(\Delta T)$ cannot be used as a material constant. In comparison, the differential coefficient of linear thermal expansion $\alpha(T)$ describes l_{th} as a function of the current temperature T_2, using the initial temperature T_1 as a reference. The coefficients can be calculated using the expressions given in equation (2.7). Both calculations are based on the initial dimension value l_0 of the specimen (Ehrenstein et al. 2004).

$$\bar{\alpha}(\Delta T) = \frac{1}{l_0} * \frac{\Delta l_{th}}{\Delta T} \, , \, \alpha(T) = \frac{1}{l_0} * \frac{dl_{th}}{dT} \tag{2.7}$$

$\bar{\alpha}(\Delta T)$ can be calculated out of $\alpha(T)$ by applying equations (2.8) and (2.9). In a first step, the corresponding thermal strains $\varepsilon^{(th)}$ are calculated for the chosen temperature steps. Afterwards the values for $\bar{\alpha}(\Delta T)$ can be determined with regard to T_1 (Dassault Systèmes 2017).

$$\varepsilon_n^{(th)} = \varepsilon_{n-1}^{(th)} + \alpha(T)_n * (T_n - T_{n-1}) \tag{2.8}$$

$$\bar{\alpha}(T)_n = \frac{\varepsilon_n^{(th)}}{T_n - T_1} \tag{2.9}$$

Regarding polymers, the CTE is not a constant value but changes in accordance with the temperature-dependent changes in their material behavior. During curing, the dimensions of a thermosetting polymer change additionally due to the formation of cross-links. Therefore suggestions to use TMA measurements not only in order to determine the CTE but also to investigate the cure shrinkage of resin materials can be found in literature (Yu et al. 2005).

However, interpreting the dimensional changes recorded in expansion mode only works well as long as no other effects than thermal expansion affect the dimensions of the specimen. During heating, the dimensions of a resin specimen both increase due to thermal expansion and decrease due to the cure-induced shrinkage. It is not possible to separate these two effects when performing conventional TMA measurements. Temperature modulated TMA is a special technique which enables to study the thermal properties and the shrinkage behavior of a specimen simultaneously. During the measurements, the average heating rate is superimposed by an oscillating temperature change. The specimen shrinks irreversibly during heating, whereas the thermal expansion in each oscillation step is reversible. Thus it is possible to separate the total measured dimensional change L_{total} into a non-reversing part $L_{non-reversing}$ due to shrinkage and a reversing part $L_{reversing}$ due to thermal expansion according to equation (2.10) (Riesen 2000).

$$L_{total} = L_{reversing} + L_{non-reversing} \tag{2.10}$$

The thermomechanical analyzer can be equipped with a 3-point bending accessory. The device made of quartz glass can be combined with any sample holder and measurement probe. Thus it was possible to measure the curvature of the investigated bi-material strips by analogy with the 3-point bending mode of DMA. Usually, TMA measurements in 3-point bending mode are used to investigate the elasticity of stiff samples (Mettler Toledo 1997).

2.4 Principles of finite element analysis

The finite element analysis (FEA) is a technique to numerically solve complex mathematical problems. The geometry of the simulation model is approximated by a discrete number of elements. The interconnection points between two or more elements are called nodes. Independent equations can be established for each of these nodes. In this way, partial differential equations describing the original problem are transformed into a discrete set of equations. The resulting system of equations can be expressed as shown in equation (2.11), where {F} is the load vector, [K] is the coefficient matrix and {u} is the displacement vector. The elements of {F} represent all the nodal forces and moments, whereas the elements of {u} describe the nodal displacements. [K], also called the stiffness matrix, describes the relation between {F} and {u}. For a given load, the numerical solution of this system of equations provides the resulting displacement of all element nodes (Stommel et al. 2011).

$$\{F\} = [K] * \{u\} \tag{2.11}$$

Usually, software suited for FEA is used for the formulation of the system of equations. The basic procedure to create a computer-aided simulation model using FEA is illustrated in Fig. 2-12. In a first step called pre-processing, the geometry of the model is created
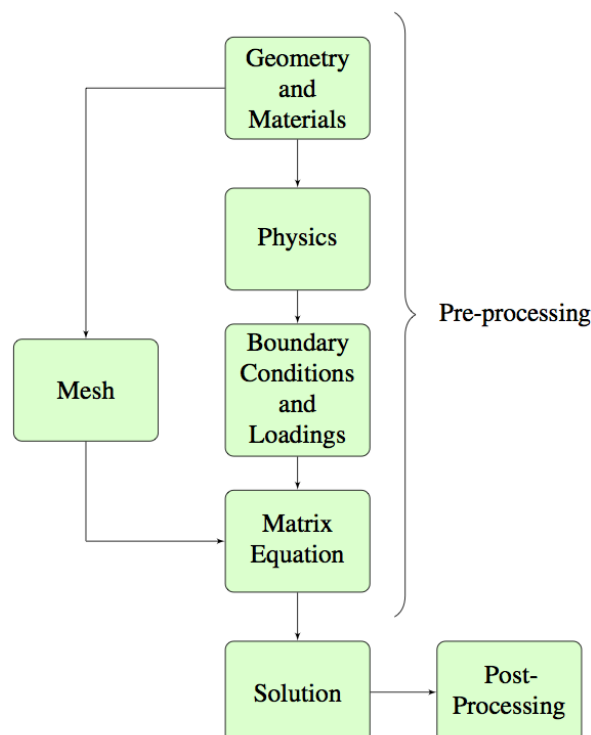
Fig. 2-12: Basic steps of a finite element analysis (Rovitto 2016).

and the relevant material properties are assigned. Boundary conditions and loads are applied in order to represent the original mechanical conditions. The discretization into finite elements is achieved by assigning a mesh to the model. Based on this information the FEA software formulates the matrix equation. The pre-processing is followed by the solution of the matrix equation. Depending on the used solver, a specific iteration scheme is implemented which performs a step-wise approximation to a mathematical solution with sufficient accuracy. In the post-processing step the results can finally be depicted graphically and evaluated with regard to the initial problem definition (Rovitto 2016).

3 EXPERIMENTAL

3.1 Materials and specimens

Prepregs were used as the basic material for both the investigation of the lamination process and the material characterization of the resin. The prepregs consist of woven glass fibers and an epoxy resin; information about the exact composition of the resin system is not provided by the prepreg manufacturer though. However, investigations at AT&S prior to this work using fourier transform infrared (FTIR) spectroscopy could prove that dicy is added to the resin as a latent hardener.

3.1.1 Specimen preparation for the analysis of the cure shrinkage

Specimens out of pure resin were needed for the cure shrinkage measurements. For this purpose, the resin powder had to be separated from the glass fibers. This was achieved by crushing and grinding the prepregs in a sealed bag until most of the powder was segregated from the fiber fabric. A sieve with US standard mesh size 60 was used afterwards to remove as many of the remaining fibers as possible. In so doing resin powder with a high degree of purity was obtained (Fig. 3-1a).

The next step was to fill and squeeze the resin powder into a mold cut out of copper plated panels in order to produce compact resin plates (Fig. 3-1b). The resin was marginally cured in a UVL 5.0 laboratory press from Maschinenfabrik Lauffer GmbH & Co.KG at 3 different temperatures. The essential press parameters are listed in Table 3-1.

(a)   (b)
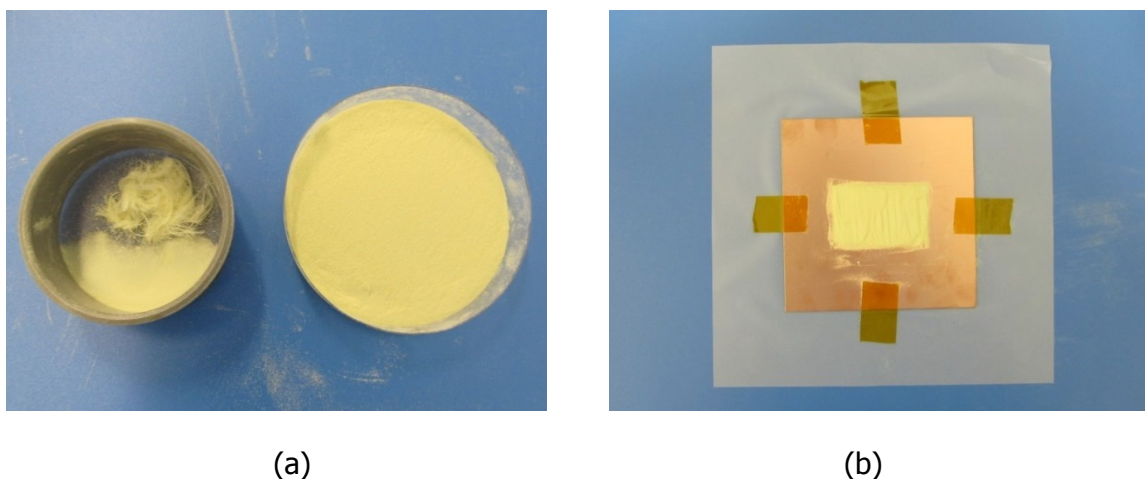
Fig. 3-1:   (a) Resin and glass fibers were separated using a sieve.

(b) Resin pressed into the mold of the copper plated panel, attached to a release film.

Table 3-1: Applied parameters and device used for the preparation of pure resin specimens.

Curing temperature	Holding time	Pressure	Preparation device
[°C]	[min]	[N/cm²]	-
110	60	100	Press
120	60	100	Press
120	60	-	DSC crucibles
140	60	100	Press

No curing of the resin was expected at 110°C, whereas at 140°C the curing was expected to be already well-advanced. Finally, the specimens for the density measurements and the TMA measurements in expansion mode were cut out of the pressed resin plates. In addition, specimens were prepared in DSC crucibles at 120°C without applying any pressure.

3.1.2 Specimen preparation for the analysis of the prepreg lamination process

Bi-material panels were fabricated out of prepregs and aluminum sheets under pressure and at high temperatures in order to identify the influence of the press temperature on the warpage behavior of the panels. A P 250-3-VK press from HML Haseneder Maschinenbau e.K. was used for the preparation of these panels. Panels with both fully cured and partially cured resin layers were prepared. Regarding the partially cured panels, again 3 different press temperatures were chosen; the press parameters are listed in Table 3-2.

Specimens were cut out of the panels for the TMA measurements in 3-point bending mode. The panels that were prepared at a press temperature of 110°C turned out to be not suitable for further investigations because no sufficient adhesion between the prepreg and the aluminum layer was obtained. As a consequence, strips were cut out only of the panels that were prepared at 120°C and 140°C.

Table 3-2: Press parameters applied for the preparation of bi-material panels with both partially and fully cured prepreg layers.

Curing temperature	Holding time	Pressure
[°C]	[min]	[kp/cm²]
110	45	20
120	45	20
140	45	20
200	80	30

3.2 Density measurements

Pycnometry

Small pycnometers with a volume of 4ml were used in order to determine the density of the resin specimens (Fig. 3-2). At first distilled water was used as the working liquid. However, it turned out that bubbles could not be avoided when using only distilled water. For this reason, a small drop of a detergent was added to the water. In so doing, the surface tension of the water was reduced and wetting of the specimens could be improved. An AE 260 DeltaRange Analytical Balance Scale from Mettler-Toledo Inc. was

Fig. 3-2: Pycnometers used for density measurements.

used to carry out the weight measurements. In a first step the weight of various specimens which were prepared at a press temperature of 110°C (Resin 110) and 140°C (Resin 140) respectively was determined. The specimens were then cured in DSC crucibles at 200°C for 60min. Afterwards the specimens were weighed again and the densities before and after curing were calculated.

Hydrostatic weighing

Further density measurements were performed at the Polymer Competence Center Leoben (PCCL) using an analytical balance XS205DU from Mettler-Toledo Inc. (Fig. 3-3). Distilled water mixed with a few drops of a release agent was used as the measurement liquid. The balance is provided with a special program for density measurements which allows an easy handling of the device. Using a thermometer, the temperature of the water is determined with an accuracy of 0,1°C prior to the measurements. The specimens are weighed first in dry state and next immersed in the beaker filled with the measurement liquid. The balance internally calculates the density of the specimen which can finally be read from the digital display. Figure 3-4 illustrates the fixtures needed for the density measurements.

In order to ensure reproducibility of the measurements, several specimens were prepared and tested under identical conditions. More precisely, resin specimens that were prepared in the press at 120°C (Resin 120) and 140°C were examined. By also measuring the
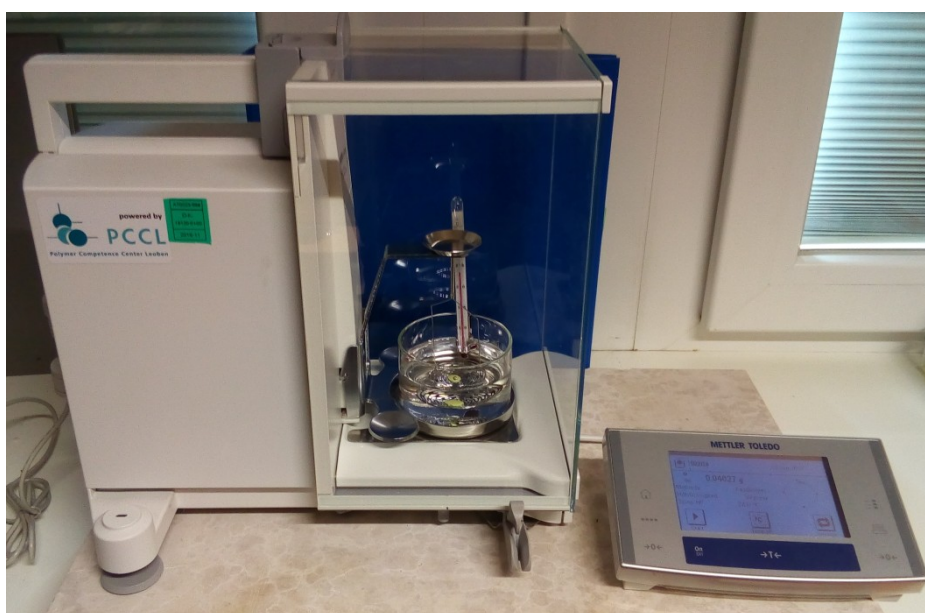
Fig. 3-3: Analytical balance XS205DU from Mettler-Toledo Inc., equipped with the density measurement kit.

Table 3-3: Parameters applied in order to fully cure the specimens that were used for hydrostatic weighing.

Resin	Curing device	Normal force	Heating rate	Curing temperature	Curing time
-	-	[N]	[°C/min]	[°C]	[min]
Resin 120	Oven	No	-	200	60
Resin 120	TMA	0,01	20	200	60
Resin 140	Oven	No	-	200	60
Resin 140	TMA	0,01	20	200	60
Resin DSC	Oven	No	-	200	60

densities of specimens that were prepared in the DSC crucibles at 120°C (Resin DSC), the influence of the pressure applied during the specimen preparation could be investigated. The densities of all specimens were determined prior to further treatment. The next step was to cure one half of the specimens in a heating chamber and the other half in a thermomechanical analyzer and again determine the densities. Thus the influence of pressure during the curing process on the shrinkage of the resin could be investigated as well. The parameters relevant for the measurements are summarized in Table 3-3.
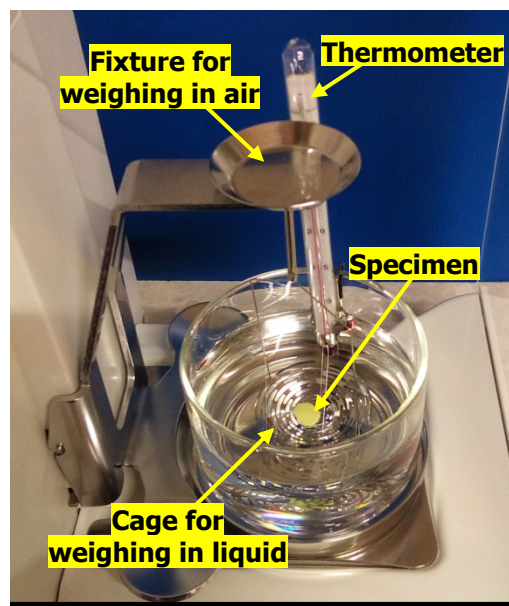
Fig. 3-4: Specimen placed in the weighing cage of the analytical balance and immersed in the measurement liquid.

3.3   Differential scanning calorimetry

The cure characteristics of the resin specimens were analyzed using a DSC823^e Differential Scanning Calorimeter from Mettler-Toledo Inc. (Fig. 3-5). The test instrument can be cooled with liquid nitrogen and enables both rapid heating and cooling. The calorimeter works according to the principle of heat-flux DSC.

In order to study the curing characteristics of the epoxy resin and to be able to apply the model-free kinetic algorithm as described in chapter 2.3.2, temperature scans of the resin powder had to be performed at different heating rates. The resin powder was heated from ambient temperature to 350°C at six different heating rates between 1°C/min and 10°C/min. The parameters chosen for the measurements are listed in the column "Model-free kinetics" of Table 3-4.

Isothermal measurements at 200°C were performed to fully cure the specimens that were prepared in the press at different temperatures. Resin powder was analyzed using the same measurement parameters in order to compare the differences in curing enthalpy. In so doing, the degrees of cure of the different resin specimens could be compared based on the enthalpy value of the untreated resin powder. This was important because the more cured the specimens were after specimen preparation, the less cure shrinkage would be measurable afterwards. In addition to the isothermal measurements, dynamic measurements were performed at a heating rate of 5°C/min for comparison (Table 3-4, column "Analysis of different specimens").
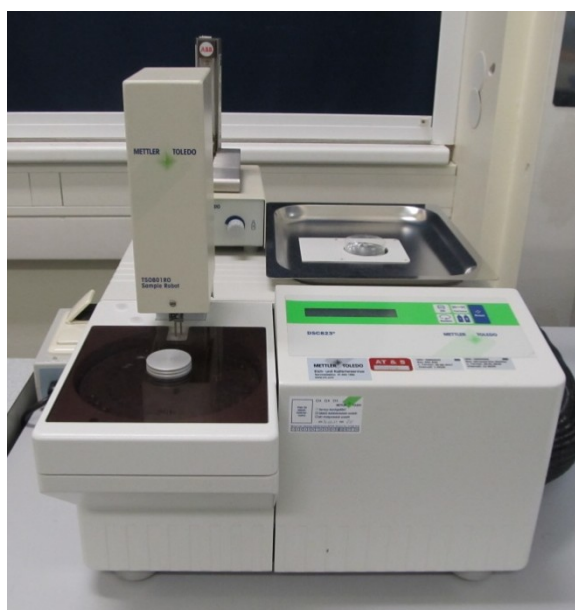
Fig. 3-5:   DSC823^e Differential Scanning Calorimeter from Mettler-Toledo Inc..

Table 3-4: Test parameters for isothermal and non-isothermal DSC measurements of the resin powder and of specimens prepared at different temperatures.

		Model-free kinetics	**Analysis of different specimens**		**Analysis of the curing reaction**
Specimen	-	Resin powder	Resin powder / Resin 110 / Resin 120 / Resin 140		Resin powder
Measuring mode	-	Dynamic	Dynamic	Isothermal	Isothermal
Temperature range	[°C]	30 … 350	30 … 350	-	-
Heating rate	[°C/min]	1 / 2 / 3 / 5 / 8 / 10	5	-	-
Temperature (isothermal)	[°C]	-	-	200	100 / 110 / 120
Time (isothermal)	[min]	-	-	100	100

Since there was no information available about the exact composition of the investigated resin, DSC measurements were performed in order to acquire knowledge about the temperature needed for the curing reaction to start. The melting point of dicy is rather high with approximately 210°C. By adding accelerators, the cure temperature of the dicy/epoxy formulation can be lowered. Therefore the curing was expected to start above a specific temperature; at temperatures below this critical temperature no signs of cross-linking were to be expected. Isothermal measurements were performed at several temperatures in the expected temperature range. The test parameters are listed in the column "Analysis of the curing reaction" of Table 3-4. Resin powder was exposed to a temperature of 100°C, 110°C and 120°C respectively for 100min (Gilbert 1988).

3.4   Dynamic-mechanical analysis

The dynamic mechanical measurements were carried out with a DMA/SDTA861[e] Dynamic Mechanical Analyser from Mettler-Toledo Inc. under 2 different types of loading modes (Fig. 3-6). Measurements under shear loading allowed the determination of the gelation

temperature of the epoxy material; 3-point bending mode was used to measure the deformation of the bi-material strips evolving during the curing of the resin.

Figure 3-7 displays the shear clamp with mounted specimens, installed in the clamping assembly of the test instrument. The shear clamp consists of three disks supporting two dimensionally similar specimens when pressed together in the clamp holder. When pressing the plates together, force should be applied only enough to fix the specimens but not to deform or crush them. For the thin epoxy films, it is sufficient to fasten the locking screws with the appropriate wrench until the slightest resistance is noticeable. The thermocouple is inserted in the hole at the side of the shear clamp which is specifically designed to measure the specimen temperature as accurate as possible during the experiments (Ehrenstein et al. 2004).

When heating up to high temperatures, both the dimensions of the specimen and the clamping device change slightly. The METTLER TOLEDO STAR[e] system offers several different types of offset control to compensate the temperature-caused deformation of the test instrument. "Zero displacement" offset control was used to reposition the moveable part of the clamping device into the zero position continuously throughout the whole experiment. This is the position in which the specimen can be installed free of force in the sample holder (Mettler Toledo 2005).

The test parameters are listed in Table 3-5. The modulus values were recorded in a temperature range between +25°C and +200°C at a frequency of 1Hz. With a heating

Fig. 3-6:   DMA/SDTA861[e] Dynamic Mechanical Analyser from Mettler-Toledo Inc..
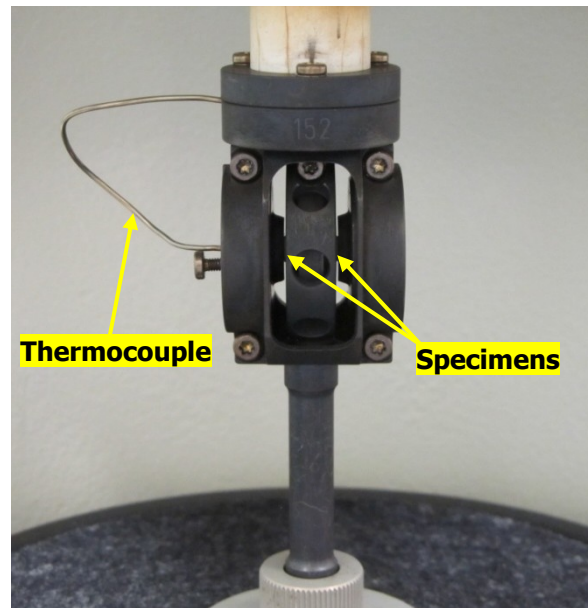
Fig. 3-7: Specimens mounted symmetrically in the shear clamp of the DMA/SDTA861[e].

rate of 3°C/min, the thin resin specimens should be able to follow the change in temperature easily. A force scan of the resin films was performed at room temperature prior to the measurements in order to determine the maximum force and displacement in the linear viscoelastic region of the material. This region can be identified by aligning a tangent to the force-displacement curve. Beyond the point where the slope of the curve starts to deviate from the tangent line, linear viscoelastic approaches are not valid anymore (Fig. A-1).

Table 3-5: Test parameters for measurements in the shear mode of the DMA/SDTA861[e].

Average specimen thickness	**[mm]**	4,5
Average specimen diameter	**[mm]**	0,35
Temperature range	**[°C]**	+25 … +200
Heating rate	**[°C/min]**	3
Maximum force	**[N]**	1
Maximum displacement	**[µm]**	0,05
Frequency	**[Hz]**	1
Mode of offset control	**-**	zero displacement

Figure 3-8 shows a bi-material specimen mounted in the 3-point bending clamp of the DMA/SDTA861^e. The ends of the strip are not fastened into place with the clamps but rest on two knife-edges in the clamps. A third knife-edge is attached to the moveable part of the clamp holder and supports the middle part of the strip (Mettler Toledo 2005).

This test setup makes it possible to measure the strip curvature evolving because of the temperature-induced cure shrinkage of the resin material during heating. In addition, the CTE values of the prepreg and the aluminum differ significantly from each other and thus lead to an additional bending of the strip during the heating process. After cooling down to room temperature, the bi-material strip remains curved due to the cure shrinkage. The strip deformation can only be recorded by the test instrument as long as the maximum deflection of the strip is smaller than the maximum displacement of the displacement sensor core. The maximum displacement provided by the DMA/SDTA861^e is 1500µm. Due to the geometry of the clamping device, the minimum specimen length must not be less than 30mm (Mettler Toledo 2005).

Table 3-6 lists the test parameters used for the 3-point bending measurements. The lengths of the specimens were varied from 30mm to 80mm, the widths were all 10mm. The measurements were carried out in a temperature range between 30°C and 220°C with a heating rate of 5°C/min. The force of 8mN was specifically chosen to offset the weight of the lightest strips and therefore to prevent a non cure- or CTE-related lowering of the moveable knife-edge.
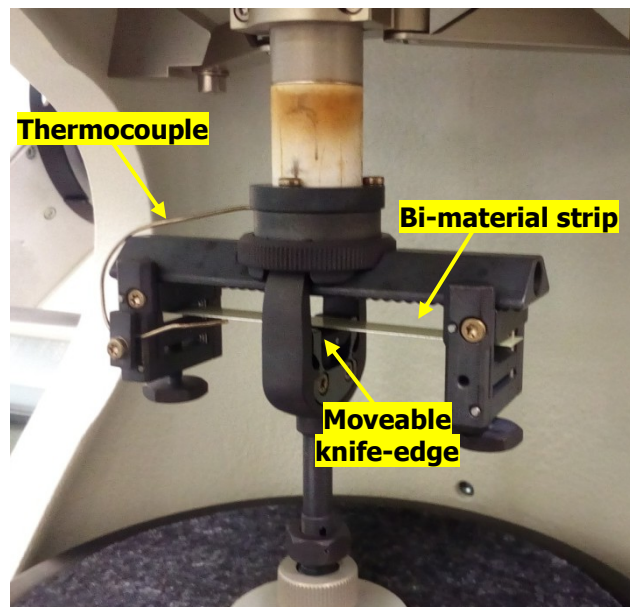
Fig. 3-8: Bi-material strip mounted in the 3-point bending clamp of the DMA/SDTA861^e.

Table 3-6: Test parameters for measurements in the 3-point bending mode of the DMA/SDTA861[e].

Specimen length	[mm]	30 … 80
Specimen width	[mm]	10
Specimen thickness	[mm]	0,26
Temperature range	[°C]	+30 … +220
Heating rate	[°C/min]	5
Maximum force	[mN]	8
Maximum displacement	[µm]	1500
Frequency	[Hz]	1
Mode of offset control	-	no offset control

3.5 Rheometry

The Modular Compact Rheometer MCR501 from Anton Paar GmbH of the PCCL was used to determine the cure-induced dimensional changes of the epoxy resin (Fig. 3-9). The measurements were carried out using the parallel plate configuration with the diameter of the upper plate being 25mm.

Fig. 3-9: Modular Compact Rheometer MCR501 from Anton Paar GmbH.

The rheometer was preheated to 100°C for the specimen preparation. A metal ring with 25mm in diameter was placed onto the preheated plate and filled with resin powder in order to produce evenly shaped specimens. The specimens were formed by closing the

gap between the two plates of the rheometer and applying a maximum force of 30N. Both temperature and pressure were maintained constant until the gap between the plates reached a stable value. Finally, the ring was removed and the specimens were cooled down to room temperature. Some of the specimens were prepared in the vacuum press P200PV from Dr. Colling GmbH. The press was heated to 100°C and the temperature was kept constant for 60min. During the whole press cycle a pressure of 8bar was applied. Figure 3-10 shows one of the resin disks placed on the bottom plate of the rheometer.

Each measurement was divided into 4 different test segments; the measurement parameters are listed in Table 3-7. At the beginning of the measurements, the temperature was kept constant at 30°C for 5min either without applying any pressure or applying a pressure of 0,01N to determine the initial specimen thickness. Then the disks were heated to 200°C with a constant heating rate of 5°C/min. During heating, the normal force was set to 0,05N. This rather low force value was chosen to ensure contact between the plates and the resin without having a significant impact on the specimen dimensions. In the following isothermal segment, the temperature was kept constant at 200°C for 60min and 90min respectively. The normal force was increased to 0,1N. In a last step the specimen was cooled down to room temperature. The cooling of the
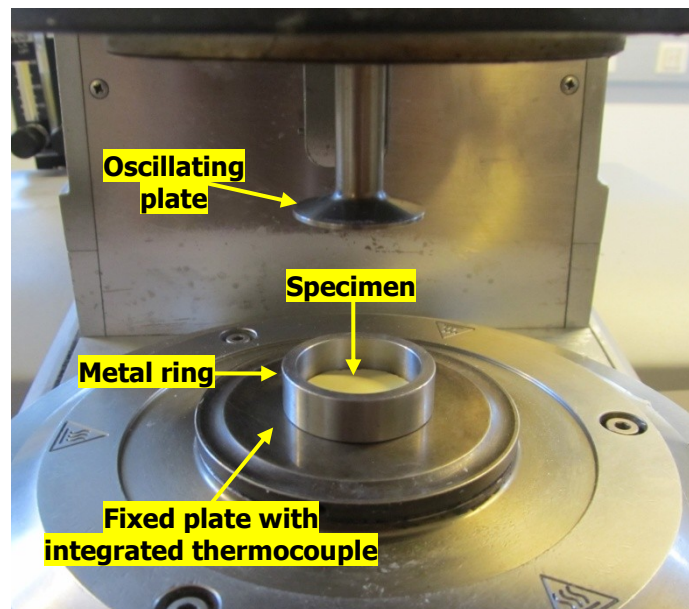

Fig. 3-10: Resin disk placed on the lower plate of the Modular Compact Rheometer MCR501 from Anton Paar GmbH.

Table 3-7: Test parameters for the rheometer measurements.

		Stabilizing	heating	Isothermal	Cooling

				curing	
Temperature range	**[°C]**	+30	+30 ... +200	+200	+200 ... +30
Heating rate	**[°C/min]**	-	5	-	Air controlled
Holding time	**[min]**	5	-	60 / 90	-
Normal force	**[N]**	0 / 0,01	0,05	0,1	0,1
Shear amplitude	**[%]**	2 / 0,5	2 / 0,5	2 / 0,5	2 / 0,5
Angular frequency	**[rad/s]**	4	4	4	4

rheometer is air-controlled and could therefore not be influenced. The angular frequency was set to 4rad/s. For the determination of the maximum shear amplitude a shear force scan is usually carried out. However, because only limited measurement time was available and having no suitable specimens for the force scans, the shear amplitude was estimated based on the results of the dynamic-mechanical force scan and on previous rheological measurements where similar materials were examined. A shear amplitude of 2% was chosen during the first measurement, but was then reduced to 0,5% considering the advice and the experience of the measurement supervisor.

3.6   Thermomechanical analysis

For the thermomechanical measurements 2 different test instruments from Mettler-Toledo Inc. at both AT&S and the Chair of Materials Science and Testing of Polymers at the Montanuniversität Leoben were used. Figure 3-11 displays the TMA/SDTA841[e] Thermomechanical Analyser at university. At AT&S the predecessor model TMA/SDTA840[e] was used for measuring. However, this had no influence on the measurement procedure or the setting parameters. Measurements were carried out in expansion mode in order to determine the cure shrinkage of the resin specimens and in 3-point bending mode to analyze the deformation behavior of the bi-material strips.

Fig. 3-11: TMA/SDTA841^e Thermomechanical Analyser from Mettler-Toledo Inc..

Figure 3-12 displays a resin specimen fixed between the sample holder and the measurement probe of the test instrument. Specimens with very smooth and plane-parallel surfaces are needed in order to determine the specimen thickness accurately. The specimen was placed additionally between two fused silica disks to ensure perfect contact between the surface of the specimen and the probe but also to avoid local intrusion of the probe. A flat probe with 3mm in diameter was used with the test instrument at AT&S; measurements at university were performed using a 3mm ball-point probe (Ehrenstein et al. 2004).

Table 3-8 lists the parameters used for the measurements in expansion mode. A force of 0,01N was applied in accordance with the ASTM E 831-2003 standard which recommends loads of 1g to 3g. A very high heating rate of 20°C/min was chosen to heat the specimens from ambient temperature to 200°C. The temperature was kept constant at 200°C for 60min to ensure total curing of the resin. Finally the specimens were cooled down to room temperature with a cooling rate of 5°C/min. Unlike the TMA/SDTA841^e, the cooling device of the TMA/SDTA840^e operates without the use of liquid nitrogen. As a result, the cooling performs worse the closer the temperature in the test chamber gets to the ambient temperature (Ehrenstein et al. 2004).

Regarding the resin specimens and the fused silica disks, strong adhesion was detected. Depending on the specimen preparation temperature, some of the specimens would stick
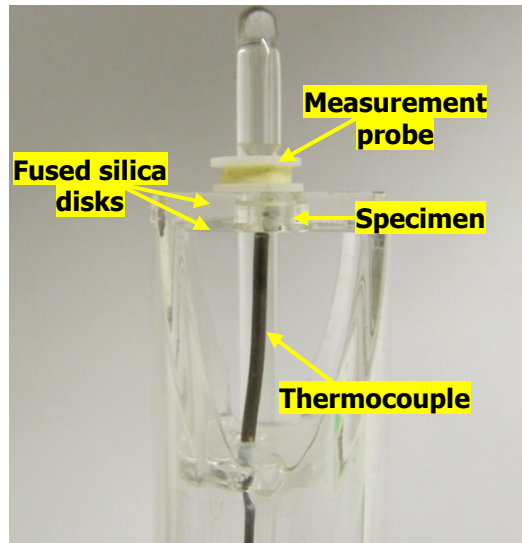
Fig. 3-12: Specimen fixed between the sample holder and the measurement probe of the TMA/SDTA841[e] used for the measurements in expansion mode.

to the disks permanently and distort the measured thicknesses. As a consequence, very thin polytetrafluorethylene (PTFE) films were used to separate the specimens and the disks. Thus any impact on the measured dimensional changes of the specimens caused by resin adhesion was prevented.

Table 3-8: Test parameters for measurements in the expansion mode of both the TMA/SDTA840[e] and the TMA/SDTA841[e].

		TMA/SDTA840[e]	TMA/SDTA841[e]
Specimen diameter	**[mm]**	3 … 4	3 … 4
Specimen thickness	**[mm]**	~ 1	~ 1
Measurement probe	**-**	Flat probe, 3mm	Ball-point probe, 3mm
Force	**[N]**	0,01	0,01
Temperature range	**[°C]**	+30 … +200	+30 … +200
Heating rate	**[°C/min]**	20	20
Holding time	**[min]**	60	60
Cooling rate	**[°C/min]**	max 5	5

Measurements in 3-point bending mode were performed using a special bending accessory. The bi-material strips were placed on two quartz cylinders and fixed by lowering the measurement probe until a contact force of 0,01N was reached (Fig. 3-13).

The measurement length can be varied by placing the cylinders in different notches of the supporting device; a measurement length of 12mm was chosen. Again a thin PTFE film was put between the specimen and the measurement probe to avoid adhesion. Since the aforementioned fused silica disks cannot be used in this measurement mode, this was also an important precaution in order to not damage or contaminate the probe with the resin.

The test parameters for 3-point bending measurements are listed in Table 3-9. By analogy with the measurements in expansion mode, the force applied to the strips was chosen as small as possible with 0,01N. A heating rate of 5°C/min was chosen to heat the specimens to 200°C. The temperature was kept constant for 45min; afterwards the specimens were cooled down to room temperature.

Again the flat probe and the ball-point probe were used, but in fact none of these probes has the ideal shape for measurements in 3-point bending mode. Using the flat probe, it is not even possible to measure the maximum deflection of the strip because no contact between the center of the curved strip and the probe exists during the measurements.
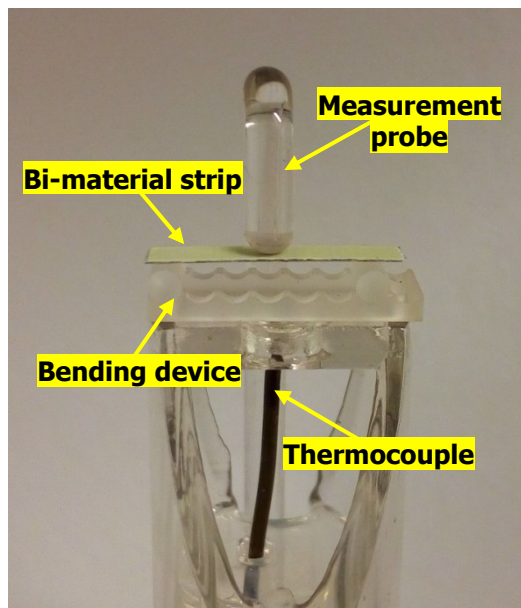

Fig. 3-13: Bi-material specimen fixed between the sample support for measurements in the 3-point bending mode and the measurement probe of the TMA/SDTA841^e.

Table 3-9: Test parameters for measurements in the 3-point bending mode of both the TMA/SDTA840^e and the TMA/SDTA841^e.

		TMA/SDTA840^e	TMA/SDTA841^e

Specimen width	[mm]	2,5 – 3	2,5 - 3
Specimen thickness	[mm]	0,26	0,26
Measuring length	[mm]	12	12
Measurement probe	-	Flat probe, 3mm	Ball-point probe, 3mm
Force	[N]	0,01	0,01
Temperature range	[°C]	+30 … +200	+30 … +200
Heating rate	[°C/min]	5	5
Holding time	[min]	45	45
Cooling rate	[°C/min]	max 5	5

Instead, the deformation of the strip is measured at the edge of the probe, with some offset from the center of the strip. Usually, test instruments from Mettler Toledo can be equipped with measurement probes with knife-edges. However, neither at AT&S nor at university was this type of probe available (Mettler Toledo 2017).

Table 3-10 shows the test parameters for the temperature modulated measurements. An underlying heating rate of 1°C/min was chosen to heat the specimens from ambient temperature to 220°C. For the sinusoidal modulation an amplitude of 5°C and a period of 300s were chosen. Little literature is available on how to choose the parameters for this kind of measurement technique and especially on how to measure resin materials. The test program was therefore inspired only by the work of Jakobsen et al. (2013) who investigated the shrinkage behavior of a glass-fiber reinforced epoxy resin with temperature modulated TMA in tensile mode.

Measurements were performed using the TMA/SDTA841[e] at university because of the possibility to cool the test chamber with liquid nitrogen. For temperature modulated measurements sufficient cooling during each modulation step is an important requirement. Both the test instrument and the specimen have to be able to follow the temperature variation easily.

Table 3-10: Test parameters for temperature modulated TMA measurements.

Specimen diameter	[mm]	3 … 4

Specimen thickness	[mm]	~ 1
Measurement probe	-	Ball-point probe, 3mm
Force	[N]	0,01
Temperature range	[°C]	+25 … +220
Underlying heating rate	[°C/min]	1
Oscillation amplitude	[°C]	5
Period	[s]	300

3.7 Finite element analysis of the test carrier

For the finite element analysis of the test carrier Abaqus FEA of the software company Dassault Systèmes was used. Strips were modeled according to the bi-material strips described in chapter 3.1.2. Since the shrinkage behavior of the pure resin was investigated, the prepreg layer was separated into its glass and resin contents. Based on the specification for finished fabric glass styles as well as on microsections of the strips, three models with differences in geometry were created. In a first approach, a glass layer and two resin layers with equal thicknesses were modeled (Fig. 3-14). The thicknesses of the individual layers of model 1 were calculated based on the volumetric fiber content of the prepreg. Regarding model 2, the fabric woven from glass fibers was modeled following the geometric data of the IPC-4412A specification (Fig. A-17a). Individual yarns with a diameter of 53µm were modeled and placed in the specified distance. Regarding model 3, the geometry of the fabric was adapted to its actual dimensions after the press process as determined by microsectioning (Fig. A-18a). For this purpose, the individual yarns were modeled in a rectangular shape, with the width of the yarns being up to ten times higher than their height (IPC - Association Connecting Electronics Industries 2008).

Boundary constraints were applied in order to simulate the testing conditions of the TMA measurements. As indicated in Fig. 3-14, the degrees of freedom U3 and UR1 of the bottom edges of both the short ends of the strips were locked. More precisely these edges of the modeled strip could not move in z-direction or rotate around the x-axis,
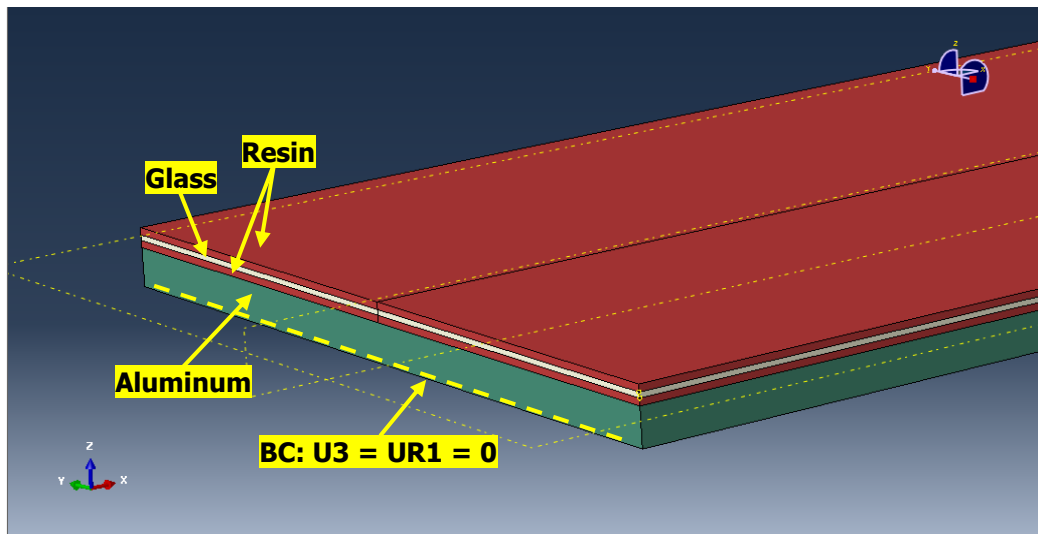
Fig. 3-14: Model 1 of the bi-material strip created in Abaqus FEA, modeled with a homogenous glass layer.

simulating the two supports of the 3-point bending accessory. No force was applied, since TMA measurements could demonstrate that the rather small force of 0,01N did not have any significant influence on the strip curvature. Regarding model 2 and model 3, only a quarter of the strip was modeled to reduce the necessary computing time.

A very simple approach was chosen to implement the determined cure shrinkage value into the simulation. Based on the assumption that the cure shrinkage could be treated in the same way as the CTE of the material, these two parameters were combined to one material characteristic which was then implemented into the software. Furthermore, it was assumed that the formation of cross-linking as well as the related cure shrinkage occurred only within a predefined temperature range. The thermal load was increased in a first step from 30°C to 200°C and in a second step from 200°C to 201°C. The CTE of the uncured resin was determined using the measurement data obtained by TMA and the thermal strains were calculated as described in chapter 2.3.5. As the thermal expansion of the material and the contraction due to the cross-linking overlap, the thermal strain at 201°C was reduced by subtracting the determined shrinkage value according to equation (3.1). Afterwards equation (2.9) was used to calculate the values of $\overline{\alpha}(\Delta T)$, which were then implemented in Abaqus FEA.

$$\varepsilon_{201°C}^{(th+s)} = \varepsilon_{201°C}^{(th)} - \varepsilon_s \tag{3.1}$$

Table 3-11: Material characteristics of aluminum, glass fibers, and resin used for the finite element analysis of the test carrier.

		Aluminum	**Glass fibers**	**Resin**
Young's modulus	**[MPa]**	73.000	73.300	500
Poisson's ratio	**[-]**	0,3	0,22	0,34
CTE (20°C – 200°C)	**[ppm/°C]**	24	5,5	100
CTE (200°C – 201°C)	**[ppm/°C]**	24	5,5	44,8

In this way, a material model with different characteristics depending on the temperature was created. It was assumed that during the first temperature step the modeled strips both expand and deform due to the mismatching CTEs of resin, glass fibers and aluminum. During the second step between 200°C and 201°C the further deformations of the strips were mainly due to the cure shrinkage of the resin.

The material characteristics used for the simulations are listed in Table 3-11. The values for aluminum and glass fibers are a combination of experimental results and values found in literature. The force scan described in chapter 3.4 was used to determine the Young's modulus of the uncured resin at room temperature. In reality, the Young's modulus is strongly depending on temperature. However, the determination of the temperature-dependent Young's modulus of the uncured or partially cured resin was not within the scope of this thesis and one value had to be sufficient for a first verification of the chosen implementation approach. For the Poisson's ratio, the value of the fully cured resin was accepted and was therefore an assumption as well. TMA measurements were used to determine the CTE of the uncured resin, which was assumed to be constant up to a temperature of 200°C.

4 RESULTS AND DISCUSSION

4.1 Evaluation of the cure shrinkage

4.1.1 Density measurements

As can be seen in Fig. 4-1, the volumetric shrinkage values obtained by pycnometry showed large scattering. The negative values indicate that some of the specimens did not show overall shrinkage as expected but instead an increase in volume. Calculating the mean values and the standard deviations for the two investigated specimen types confirmed that the scattering of the measured data was too large to derive any reliable information (Table 4-1). The individual measurement results are listed in Table A-1 in the appendix.

The scattering of the results could be explained by considering the fact that this measurement technique only works well if the specimens are free of adhering bubbles when immersed in the measurement liquid. However, even after a detergent was added to the distilled water, bubbles on the specimens could be detected. The shrinkage results of the resin specimens that were prepared at 110°C showed even larger scattering than those of the specimens that were prepared at the higher temperature. An explanation for this apparently different material behavior could be found when having a closer look at the surfaces of the resin specimens. The porosity of the material increased with decreasing specimen preparation temperature. Neither by cutting nor by grinding was it possible to prepare specimens with smooth surfaces because of the porosity of the resin; consequently the probability of bubble adhesion was extremely high.

Table 4-1: Mean values and standard deviations of volumetric shrinkage obtained from pycnometer measurements of specimens prepared at different temperatures.

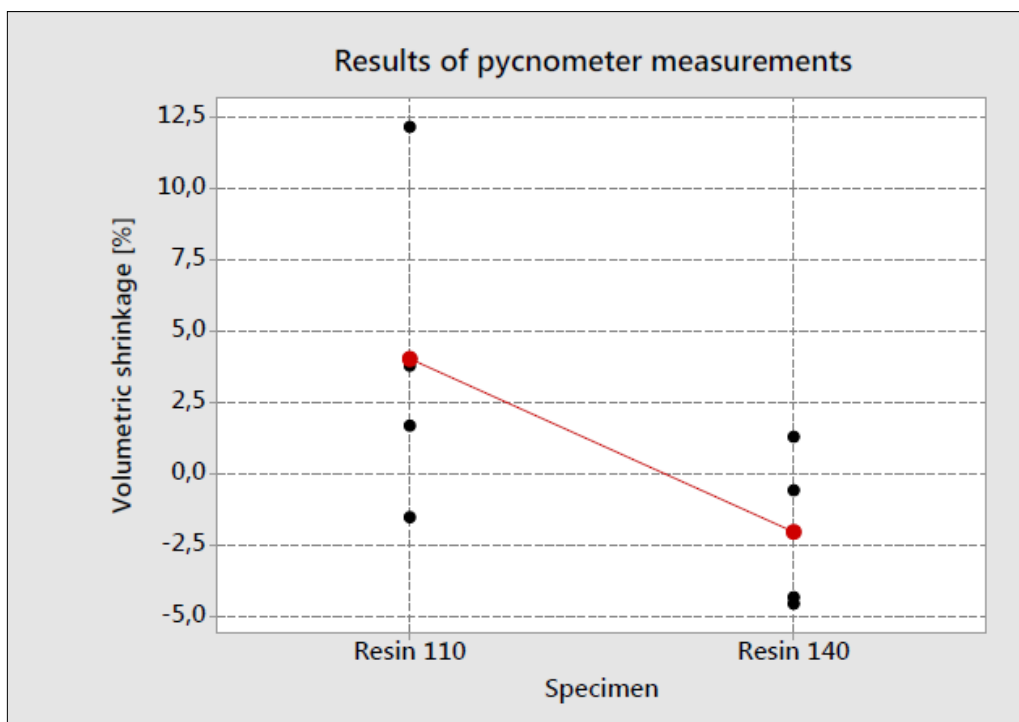| No.	Specimen	Curing Device	Curing parameters	Pressure during curing	Mean (SD) of vol. shrinkage
-	-	-	-	[N]	[%]
01-04	Resin 110	DSC	iso200°C / 60min	-	4,0240 (5,8434)
05-08	Resin 140	DSC	iso200°C / 60min	-	-2,0432 (2,8733)

Fig. 4-1: Individual results and mean values of volumetric shrinkage obtained from pycnometer measurements of specimens prepared at different temperatures.

Hydrostatic weighing of the specimens before and after curing was an attempt to achieve more accurate results than with pycnometry. Furthermore, the influence of pressure applied during the specimen preparation was analyzed. Figure 4-2 illustrates the distribution of the measurement results and the corresponding mean values obtained by hydrostatic weighing. Compared to the results of the pycnometer measurements, the first thing to notice is the small scattering of the data. However, having a closer look at the mean values and standard deviations listed in Table 4-2, the scattering is still rather large. The dimensional changes of the individual specimens are listed in Table A-3 in the appendix. Again some of the specimens showed an increase in volume after curing.

Careful interpretation of the data led to the assumption that the results of the density measurements were primarily influenced by the pressure applied during the specimen preparation. All the specimens that were prepared in DSC crucibles showed quite reasonable values for volumetric cure shrinkage. A decrease in volume was detected for most of the specimens that were prepared at 120°C in the press and cured in the TMA, but not for those that were cured in the heating chamber. The same trend could be detected for the specimens that were prepared at 140°C in the press.

The differences in the results might be explained by considering two facts. First, the pressure applied in the press during the specimen preparation had an influence on the molecular structure of the resin. When comparing the densities of the specimens before curing, those that were prepared in the crucibles showed significantly lower values than those that were prepared in the press (Table A-3). Apparently the applied pressure during the specimen preparation led to more densely packed molecular chains and therefore to higher densities of these specimens. At temperatures higher than the T_g, the mobility of the molecular chains increases. It can be assumed that reorientation and relaxation processes led to a reduction of residual stresses and thus to an increase in volume. Afterwards, at still higher temperatures, the formation of cross-links led again to a decrease in volume. More specifically, even though the volumetric changes due to the cure shrinkage were the same for both types of specimens, overlapping effects like relaxation processes made it impossible to determine the actual shrinkage values with the described measurement method (Ehrenstein et al. 2004).

Furthermore, as could be proven both by DSC and DMA measurements, curing was initiated at temperatures close to 120°C. Depending on the distribution and the size of the

Table 4-2: Mean values and standard deviations of volumetric shrinkage obtained by hydrostatic weighing of specimens that were prepared at different temperatures and cured in different heating devices.

| No.	Specimen	Curing device	Curing parameters	Pressure during curing	Mean (SD) of vol. shrinkage
-	-	-	-	[N]	[%]
01-05	Resin 120	Heating chamber	iso200°C, 60min	-	-1,263 (0,695)
06-10	Resin 120	TMA	HR20 / iso200°C / 60min	0,01	1,819 (2,671)
11-15	Resin 140	Heating chamber	iso200°C, 60min	-	-1,300 (1,008)
16-20	Resin 140	TMA	HR20 / iso200°C / 60min	0,01	0,403 (2,021)
21-25	Resin DSC	Heating chamber	iso200°C, 60min	-	3,147 (1,123)
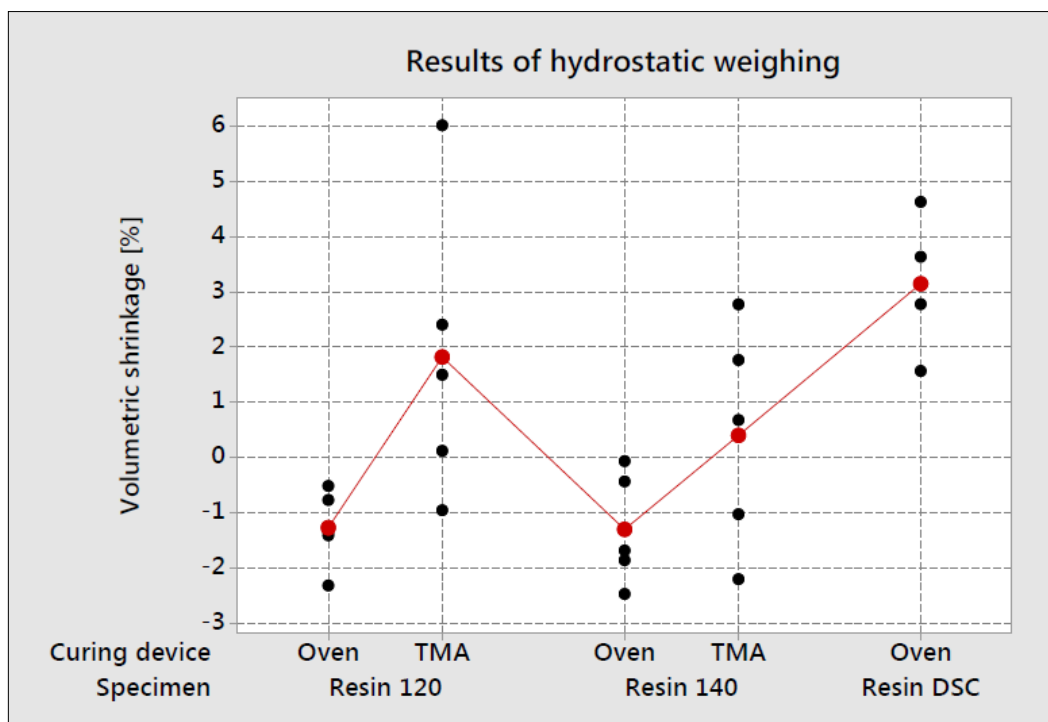
Fig. 4-2: Individual results and mean values of volumetric shrinkage obtained from hydrostatic weighing of specimens that were prepared at different temperatures and cured in different heating devices.

hardener particles, cross-links already existed in some of the specimens that were prepared at 120°C. At temperatures higher than the T_g of the resin, the mobility of the molecular chains was limited by these cross-links, though relaxation processes at elevated temperatures still led to an increase in volume before curing. However, the specimens that were heated between two fused silica disks in the test chamber of the TMA were apparently affected by the test environment. This might explain why some of the specimens cured in the TMA showed volumetric shrinkage. On the other hand, the force applied by the measurement probe was extremely small and should not have had any influence on the material behavior at least after the cross-linking process was initiated.

4.1.2 Differential scanning calorimetry

The heat flow curves of the resin powder recorded at different heating rates are displayed in Fig. 4-3. These curves provided information about the temperature range in which the curing of the resin takes place. With increasing heating rates the onset temperature of the cross-linking as well as the related curing peak are shifted to higher temperatures. Difficulties occurred when trying to determine the temperature at which the resin was

fully cured. All the curves showed an endothermic peak following the exothermic curing peak. Since the composition of the resin material was mostly unknown, only assumptions could be made about the nature of the reaction causing these peaks. Most likely the endothermic peak was caused by thermal decomposition of the resin. This could be confirmed by thermogravimetric analysis, with the investigated specimen showing a weight loss of already 1,8% at 300°C (Fig. A-2). The exothermic reaction subsequent to the thermal decomposition might be related to thermo-oxidative degradation. Air that was trapped inside the specimens during the specimen preparation probably contaminated the atmosphere in the crucibles. As a consequence, oxidation of the organic material took place. Volatile oxidation products led to a further decrease in specimen weight (Seyler and Moody 1997, Mettler Toledo 2000).

Curved baselines were used to determine the curing enthalpy of the resin powder. This is a common technique used when a reaction is accompanied by a change in heat capacity resulting in a baseline shift. This shift often occurring during cross-linking reactions in thermosets makes it impossible to evaluate the reaction enthalpy by applying a straight
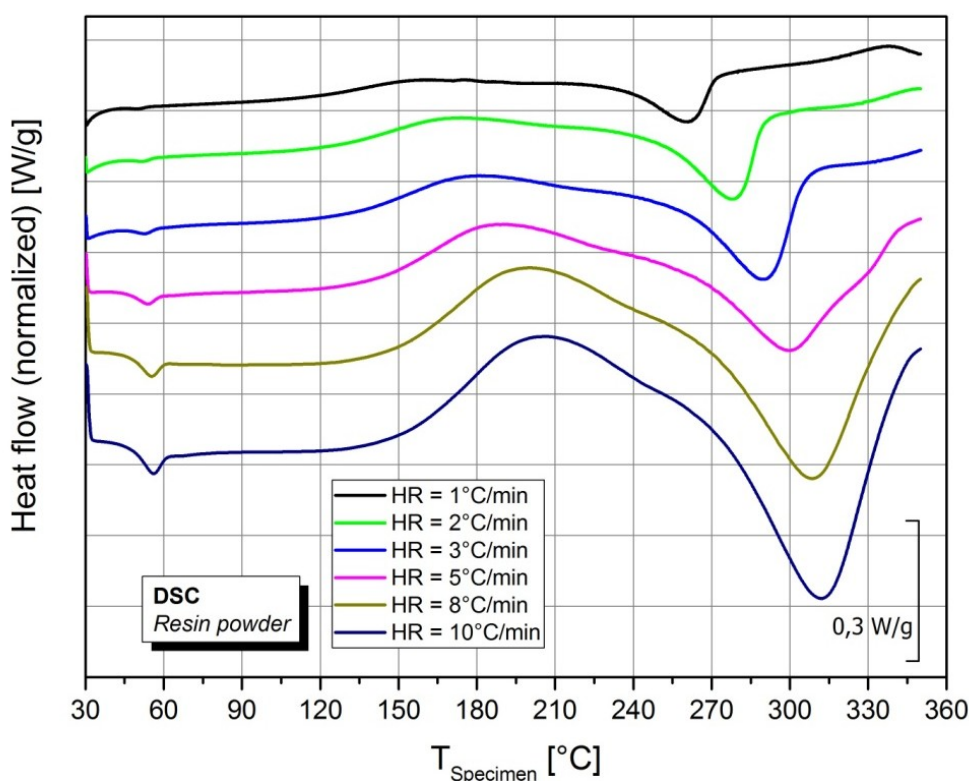

Fig. 4-3:   Dynamic heat flow curves of the resin powder recorded using heating rates between 1°C/min and 10°C/min.

line to the curve. As mentioned before, the subsequent endothermic peak made it even more difficult to find an appropriate endpoint for the evaluation of the enthalpy. The METTLER TOLEDO STAR[e] system offers several different types of baselines that allow an accurate integration of the curves. The baseline type "spline" was chosen, which can be described as a second-order polynomial determined by two tangents aligned to the limits of the evaluation range (Ehrenstein et al. 2004, Riesen 2007).

The model-free kinetic algorithm after Vyazovkin described in chapter 2.3.2 was applied using the determined curing enthalpies. In a first step the conversions depending on temperature were determined for all the heating rates (Fig. A-3a); these curves where then used to calculate the activation energy (Fig. A-3b). Finally, the isothermal curves of conversion over time could be determined. For 5 different temperatures the conversion depending on curing time was predicted (Fig. 4-4); Table 4-3 lists the according values. As can be seen, considerable differences exist between the predicted values. The lower the curing temperature, the longer it takes to fully cure the resin. According to the predictions, the conversion increases rapidly at the beginning of the cross-linking at all
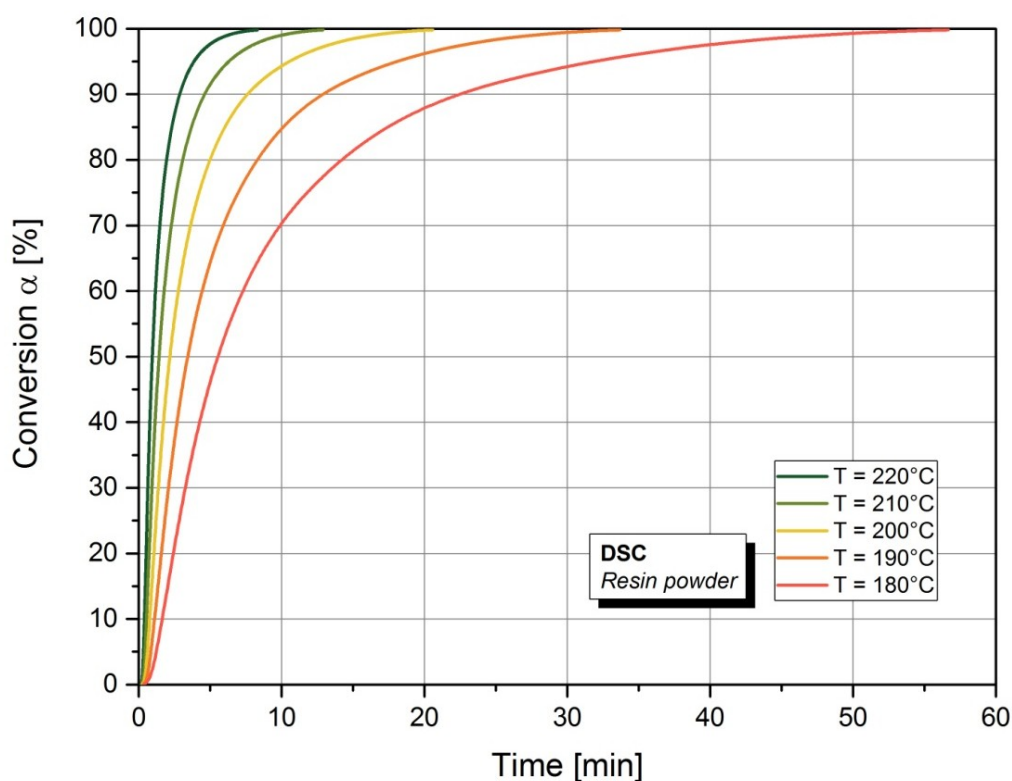

Fig. 4-4: Conversion depending on curing time predicted for curing temperatures between 180°C and 220°C.

Table 4-3: Specific conversion values depending on curing time predicted for curing temperatures between 180°C and 220°C.

Conversion	Curing time				
	@180°C	@190°C	@200°C	@210°C	@220°C
[%]	[min]	[min]	[min]	[min]	[min]
10	1,64	1,10	0,76	0,54	0,39
25	2,82	1,82	1,21	0,82	0,57
50	5,54	3,42	2,17	1,42	0,94
75	11,79	6,96	4,22	2,63	1,68
90	22,47	12,91	7,62	4,61	2,86
95	31,89	18,09	10,55	6,31	3,87
99	47,76	27,63	16,41	9,99	6,23

temperatures. At higher degrees of cure the differences in curing time are expected to become larger depending on the curing temperature.

The T_g of the uncured resin could also be derived from Fig. 4-3. Analyzing the curves regarding the midpoint temperature of the transition found the T_g to be approximately 52°C. At higher heating rates, the transition area is more pronounced and can be evaluated easily. The overshoot of the heat flow visible as an endothermic maximum is due to the time-delayed mobilization of the polymer chains (Ehrenstein et al. 2004).

Isothermal measurements were performed in order to determine the melting point of the hardener and therefore the start of the curing process. Resin powder was heated to 100°C, 110°C and 120°C respectively and the heat flow curves were recorded over a period of 100min. The mean values and standard deviations of 3 measurements at each temperature are depicted in Fig. 4-5. A horizontal baseline was used to determine the individual curing enthalpies. This is done by defining an evaluation limit and applying a straight line through this point; the integral of the enclosed area is then calculated. The mean values and standard deviations of the normalized enthalpies were summarized in Table 4-4. The enthalpy values of the individual measurements are listed in Table A-2 in the appendix (Riesen 2007).

When analyzing the measurements performed at 100°C, no signs of curing were detected. The enthalpy values of the measurements performed at 110°C and 120°C revealed curing of the resin to a certain extent. Uniform properties of the resin are difficult to predict though, since epoxy resin, dicy and accelerator form an inhomogeneous mixture. Dicy particles can segregate due to resin flow during heating and lead to unevenly distributed cross-links. Larger dicy particles, in turn, can remain intact in the fully cured material and not react with the resin at all. Therefore it is not unusual to obtain different temperatures for dicy melting when analyzing different specimens, even when they were prepared in exactly the same way. As can be derived from Table 4-4, the evaluation of the measurements performed at 110°C resulted in a rather high standard deviation compared to the mean value and also to the measurements at other temperatures. The individual measurements did not show any signs of curing except for one measurement. By comparison, quite similar enthalpy values were obtained by evaluating the curves recorded at 120°C. Based on these measurements it was concluded that the dicy definitely starts melting at approximately 120°C but that it cannot be excluded that individual particles already start melting earlier (Gilbert 1988).
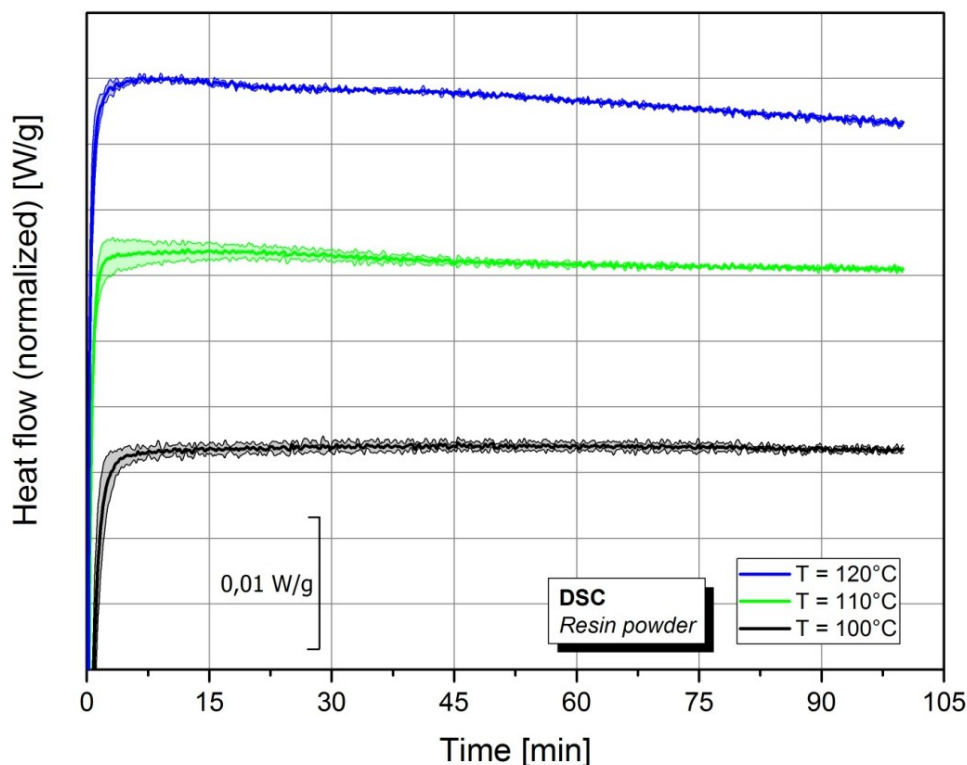

Fig. 4-5: Isothermal heat flow curves of the resin powder recorded at 100°C, 110°C, and 120°C.

Table 4-4: Mean values and standard deviations of the normalized enthalpies obtained from isothermal heat flow curves of resin powder at different temperatures.

Specimen	Temperature	Mean (SD) of normalized enthalpy
-	[°C]	[J/g]
Resin powder	100	-2,7 (0,7)
	110	1,8 (2,2)
	120	9,4 (0,1)

In a next step, all the resin specimens that were prepared at different temperatures were compared to each other using both isothermal measurements and dynamic measurements with constant heating rates. The averaged curves are depicted in Fig. 4-6 and Fig. 4-7. Again the curing enthalpies of the individual curves were determined using spline baselines for the dynamic measurements and horizontal baselines for the isothermal measurements. The mean values and standard deviations were calculated and
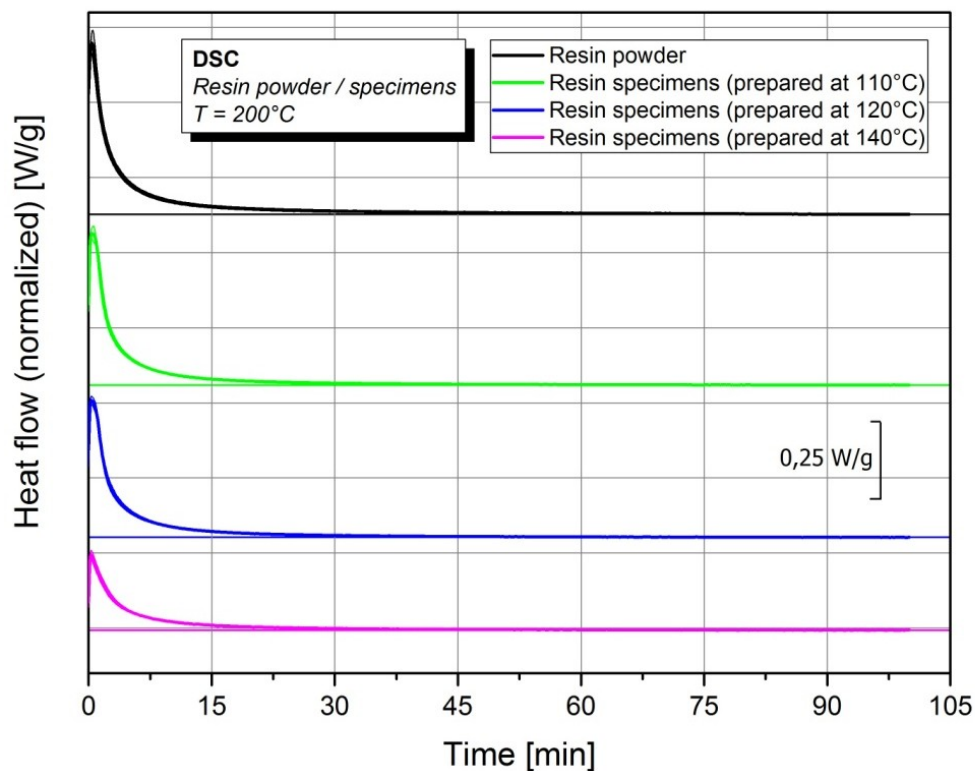

Fig. 4-6: Isothermal heat flow curves of the resin powder and resin specimens that were prepared at 110°C, 120°C, and 140°C.

summarized in Table 4-5. The enthalpy values of the individual measurements can be looked up in Table A-4 in the appendix.

When having a look at the isothermal measurements, a high standard deviation of the mean enthalpy of the resin powder can be observed. The reason for this was one outlier with a significant higher enthalpy. Since it was figured out that mostly no curing occurred at 110°C, all specimens with enthalpy values higher than 120J/g were considered as being uncured at the beginning of the measurements. The particular high enthalpy value of approximately 150J/g might be explained by a different composition of the resin powder in this specific crucible than in the others. The concentration of the hardener might have been higher and therefore enabled the cross-linking density to become higher than the average. Striking is also the high standard deviation of the specimens prepared at 120°C. This could be related to the differently advanced curing reactions of the individual specimens. The reaction enthalpies showed either almost no difference to the ones measured with resin powder or were noticeably lower. These variations could confirm the previously made assumption that the melting of the dicy started at temperatures slightly above or below 120°C. By comparison, the specimens prepared
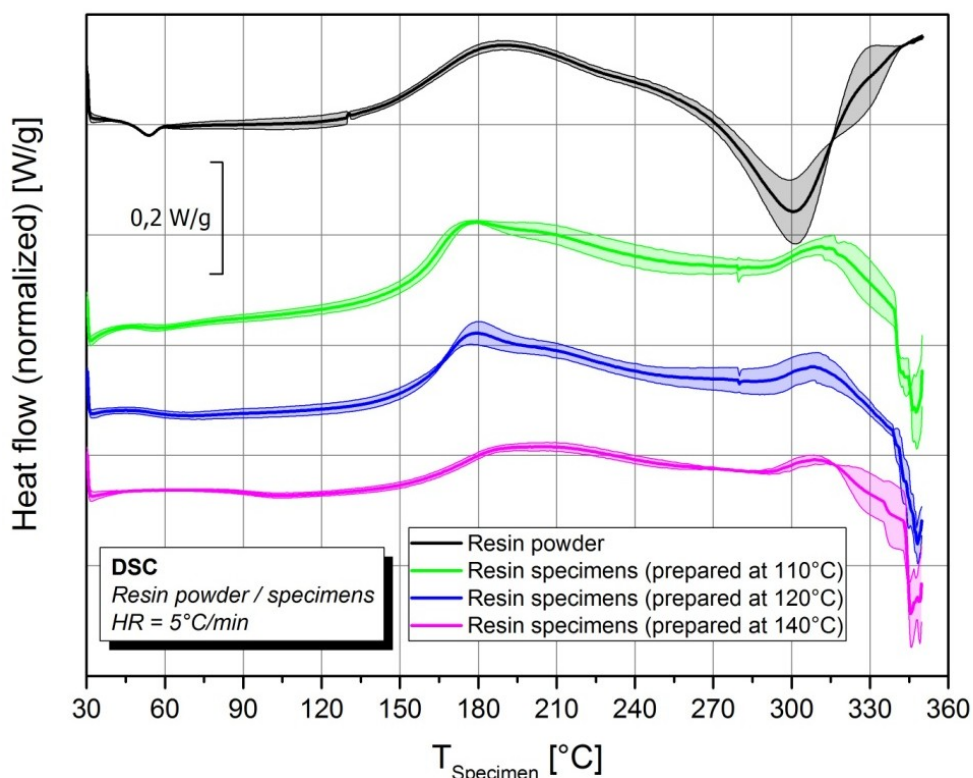

Fig. 4-7: Dynamic heat flow curves of the resin powder and resin specimens that were prepared at 110°C, 120°C, and 140°.

Table 4-5: Mean values and standard deviations of the normalized enthalpies obtained from isothermal and dynamic heat flow curves of the resin powder and specimens that were prepared at different temperatures.

No.	Specimen	Heating rate	Curing temperature (isothermal)	Curing time (isothermal)	Mean (SD) of normalized enthalpy
-	-	[°C/min]	[°C]	[min]	[J/g]
01-03	Resin powder	-	200	100	129,3 (11,1)
04-06	Resin 110	-	200	100	121,7 (2,7)
07-09	Resin 120	-	200	100	109,6 (7,0)
10-12	Resin 140	-	200	100	74,7 (2,2)
13-15	Resin 120	20	200	100	97,2 (8,8)
16-18	Resin powder	5	-	-	52,3 (0,7)
19-21	Resin 110	5	-	-	53,1 (2,1)
22-24	Resin 120	5	-	-	50,5 (0,5)
25-27	Resin 140	5	-	-	25,1 (0,6)

at 140°C showed significant lower reaction enthalpies. With a mean value of approximately 75J/g, these specimens were already 40% cured compared to the ones assumed to be still uncured. However, this percentage only refers to the condition of the untreated resin powder scratched out of the prepregs. Since these prepregs are already B-staged as described in chapter 2.1, the resin powder and all specimens prepared from it are already partially cured. For this reason, a distinction has to be made between total and relative degree of cure. In this study only the degree of cure relative to the B-staged condition could be determined.

Analysis of the dynamic measurements provided similar results than the isothermal measurements. As can be derived from Table 4-5, the reaction enthalpies of the resin powder and of the specimens prepared at 110°C differed only slightly. Only one of the specimens showed a higher enthalpy value which could again be attributed to fluctuations of the resin composition. Assuming that enthalpy values of 52J/g and higher referred to

specimens that were not cured during their preparation, the differences between the resin powder and the specimens prepared at 120°C were quite small. The relative degree of cure of those specimens was only approximately 3%. This value would be even lower than the 8% determined in isothermal measurements. Vast discrepancies were noticed though between the resin powder and the specimens prepared at 140°C. Apparently those specimens were already more than half cured compared to the initial curing condition of the powder.

When performing isothermal measurements, the crucibles with the specimens are introduced only after the measuring cell was preheated at the required temperature. This allows the specimens to reach the measurement temperature within half a minute. By comparison, measurements with defined heating of the specimens prior to the isothermal segment were performed. In accordance with the test parameters used during the TMA measurements, a heating rate of 20°C/min was used to increase the specimen temperature from ambient to 200°C. Thus it was possible to examine the influence of the dynamic heating on the curing enthalpy. The recorded heat flows depicted in Fig. 4-8 were evaluated using horizontal baselines. The beginning of the isothermal segment was
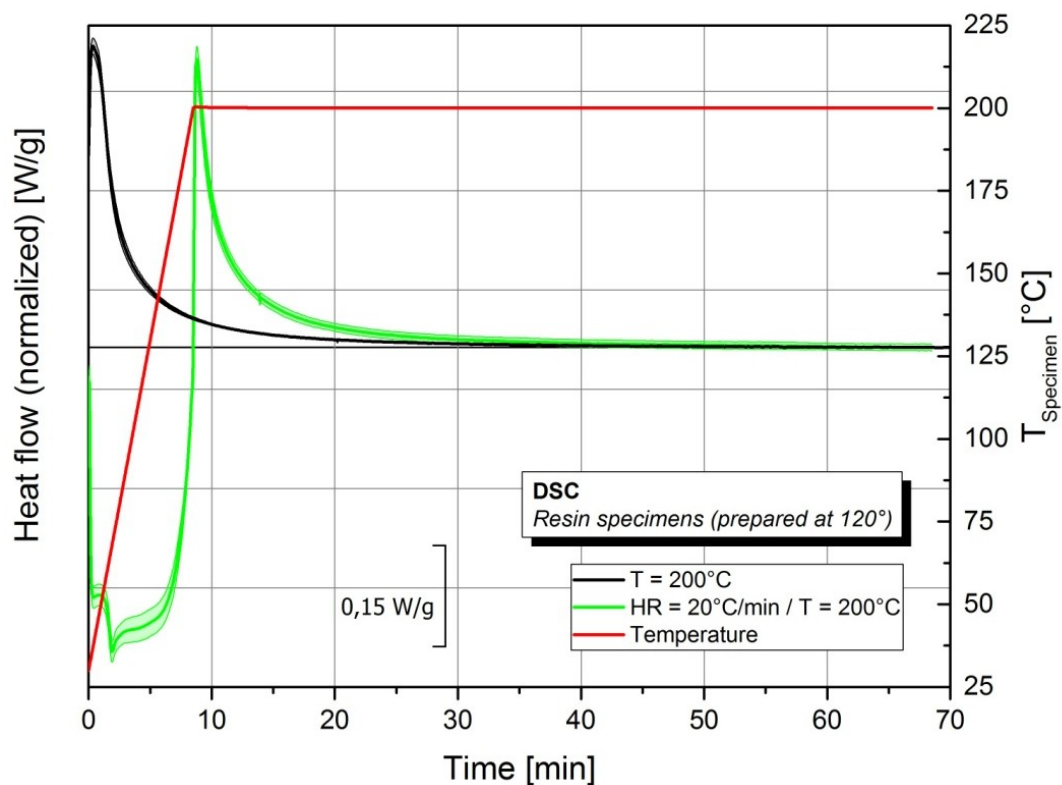

Fig. 4-8:   Comparison of isothermal heat flow curves with and without a preceding heating segment of resin specimens that were prepared at 120°C.

used as the lower evaluation limit. The curves as well as the mean enthalpy values were compared to the results of the isothermal measurements. As can be derived from Table 4-5 differences could be detected, indicating that the curing reaction already started during heating (Widmann 2000).

4.1.3   Dynamic mechanical analysis

The dynamic mechanical measurements in shear mode were carried out in order to determine the gelation temperature T_{gel} of the epoxy resin. At T_{gel}, the material behavior changes from liquid-like to solid-like due to the evolving cross-linking of the polymer chains. As a consequence, the mechanical properties of the resin change likewise, as can be seen in Fig. 4-9. The T_{gel} can be derived as the second intersection point of the curves of the storage modulus G' and the loss modulus G''. Two additional measurements were performed and the points of gelation were evaluated (Fig. A-4 and Fig. A-5); Table 4-6 lists the results as well as the calculated mean value and the standard deviation. Gelation of the investigated resin was found to occur at approximately 122°C (Billotte et al. 2013).
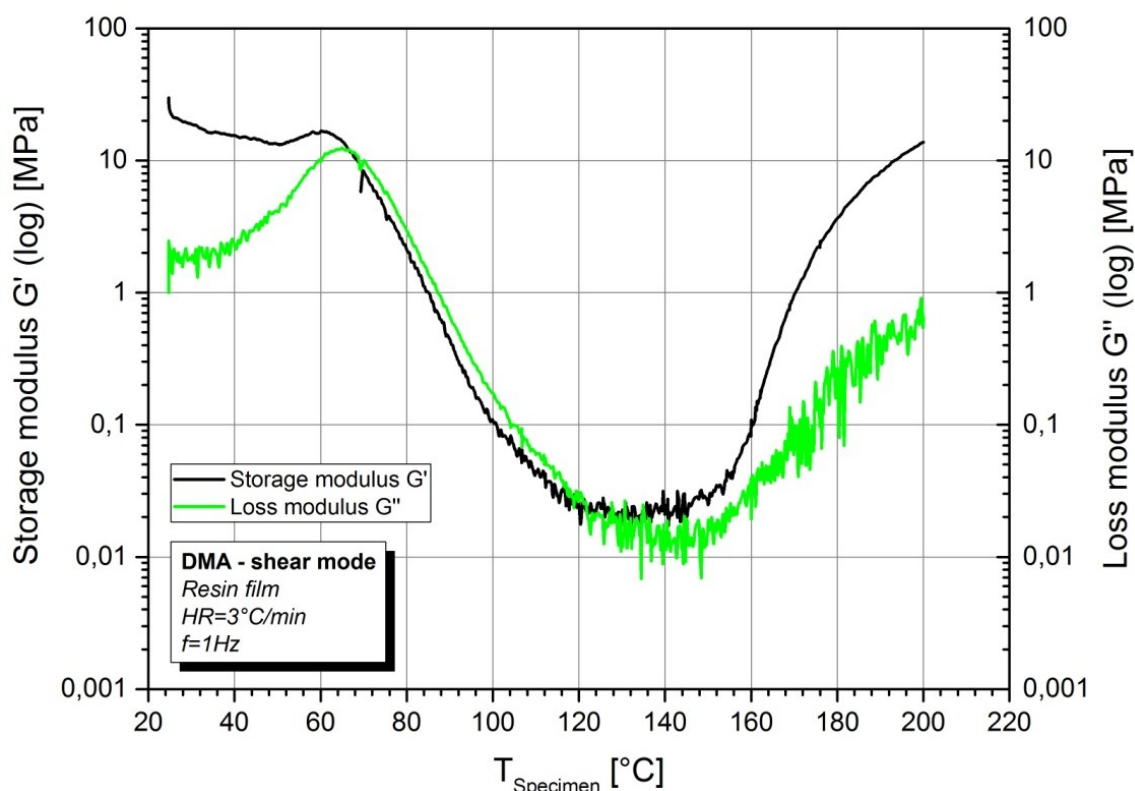

Fig. 4-9:   Storage modulus G' and loss modulus G'' over temperature measured in the shear mode of the DMA/SDTA861[e] (specimen 1).

Table 4-6: T_{gel} of the resin determined as the second intersection point of G′ and G″.

Specimen no.	$T_{Crossover} = T_{gel}$	Mean (SD) of T_{gel}
-	[°C]	[°C]
01	119	
02	122	121,7 (2,5)
03	124	

It can be assumed that the increased mobility of the molecular chains above the T_g is affected when the temperature exceeds the T_{gel} of the resin. In other words, the resin can adjust to shrinkage without the formation of stresses in the material at temperatures below the T_{gel}. This would also mean that the cure shrinkage of the resin would not have an impact on the warpage behavior of an electronic module until a molecular network with a certain amount of cross-links was formed throughout the resin material. So a distinction can be made between total occurring cure shrinkage and cure shrinkage relevant regarding warpage issues (Schoch et al. 2004).

Figure 4-10 shows the displacement curves of two bi-material strips with different lengths, measured in the 3-point bending configuration of the DMA/SDTA861[e]. As can be seen from the curve progression, at higher temperatures the curvatures of the strips became too large for the test instrument to follow because the displacement sensor core reached its displacement limit. As can be seen in Fig. 4-10, the maximum displacement of the test instrument is even larger than the maximum value specified in the user manual.

The measureable deformation of a strip increases with smaller specimen length. As a consequence smaller strips were used, but even when using the smallest possible specimens with a length of only 30mm the resulting deformation was larger than 1500μm. The point where the test instrument lost contact with the strip only moved to higher temperatures when using smaller specimen lengths. Additionally, as can be derived from Fig. 4-10 when having a look at the curve behavior of the shorter specimen, the measurements showed a tendency to become more unstable with decreasing strip length. This can be explained by considering the very small force which is necessary to compensate the weight of a strip. On the other hand, if the applied force is significantly higher than the weight of a strip, the specimen does not stay in place during measuring
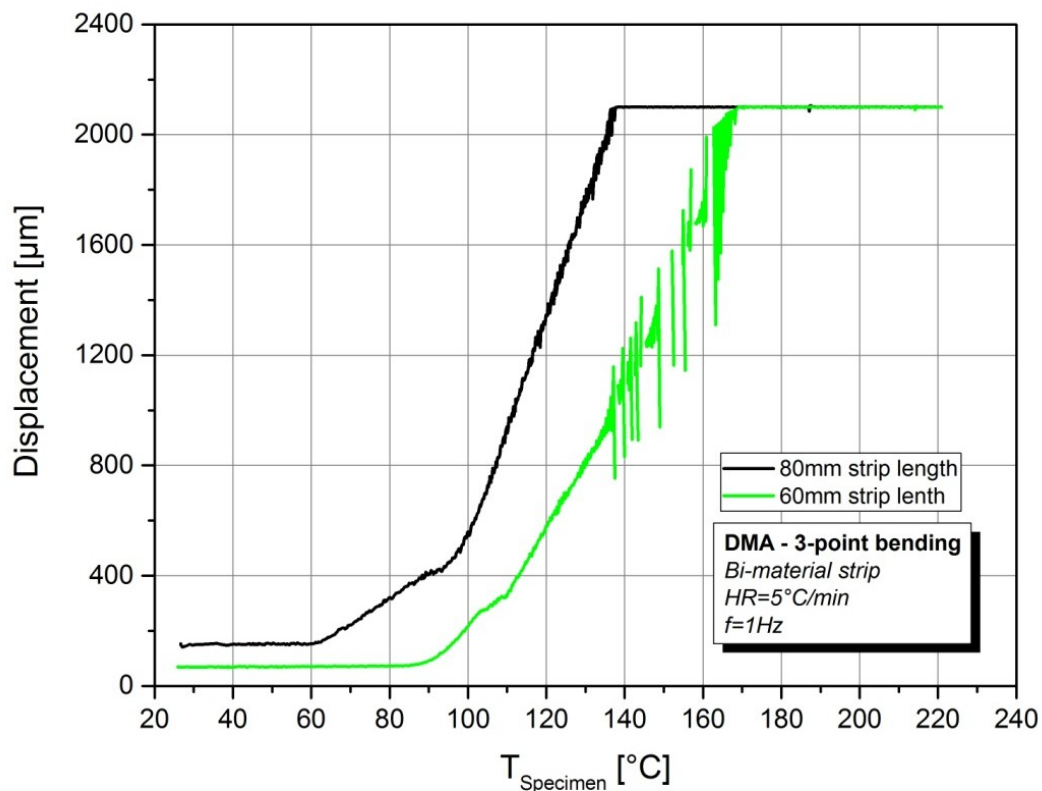
Fig. 4-10: Displacement of the bi-material strip during heating recorded with the DMA/SDTA861[e].

but lifts off the supporting knife-edges. When using a strip size of 30mm the required force would be smaller than 3mN; the test instrument cannot reliably apply forces smaller than 5mN though.

4.1.4   Rheometry

The measurements carried out with the rotational rheometer provided information about the thickness changes of the specimens caused by thermal expansion as well as by cure shrinkage. Figure 4-11 shows the gap distance between the two parallel plates of the rheometer depending on time or rather temperature recorded for one of the investigated specimens.

At first, the temperature was kept constant at 30°C for 5min. The gap between the plates did not change during this measurement segment, which proved that the specimen had had enough time to adjust to room temperature; its dimensions remained stable. During heating, the specimen thickness increased due to thermal expansion until suddenly at approximately 100°C the curve progression changed and the gap became smaller.

Eventually, when reaching a temperature of 150°C, the gap distance increased again with a similar slope as before. This material behavior can be explained using the same considerations about the cross-linking condition of the resin as in chapter 4.1.1. Even though some cross-links might already have existed after the specimen preparation, the material was still able to relax at elevated temperatures. Only after the formation of a closer meshed network, the thermal expansion became again the predominant force and once more resulted in an increase in specimen thickness.

The major part of the cross-links was expected to form during the isothermal segment at 200°C. Indeed the gap decreased until a small plateau emerged at the end of the segment. However, as the recorded graph shows, the gap did not decrease immediately but at first became still larger. Two different explanations might exist for this curve behavior. For one thing, the shrinkage might have still been overlapped by thermal expansion, which would indicate that it took some time for the specimen to gain an even temperature distribution. Secondly, this might be an effect caused by the force control of the rheometer, since the applied forces were in the range of its lower working limit. It is possible that it took some time until the force was properly adjusted to the new value of
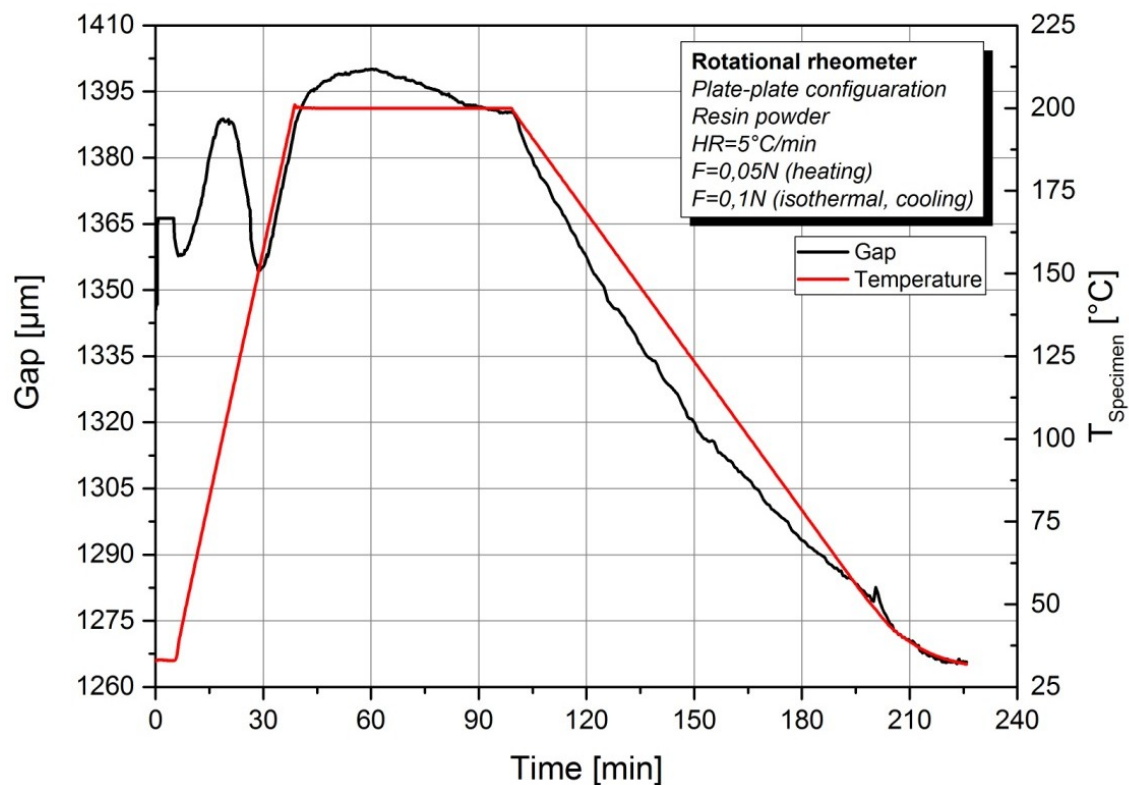

Fig. 4-11: Gap between the two plates of the MCR501 rheometer over time and in relation to the specimen temperature (specimen 1).

0,1N in the heating segment. During cooling, the distance between the plates was constantly decreasing. The slope of the curve changed due to the changing material behavior of the cured resin at temperatures in the regime of the glass transition.

The decrease in gap distance at the beginning of the heating segment cannot be explained by the material characteristics of the resin. As already mentioned in chapter 4.1.2, the T_g of the uncured resin was found to be approximately 52°C. If the applied pressure would have been too high and led to a significant deformation of the specimens, this should have happened continuously at least until cross-linking started. Besides, the pressure applied in TMA measurements was 5 times higher and did not lead to any visible decrease in specimen thickness in the above considered temperature range. However, as this curve behavior could be observed in 3 out of 4 measurements it should not be ignored. One possible explanation might be that the force control of the rheometer was not able to increase the force according to the specified parameters. According to the manufacturer Anton Paar GmbH, the rheometer has a resolution of 0,002N and a guaranteed accuracy of 0,03N. Figure 4-12 depicts the curve progression of the normal force over time related to the gap height shown in Fig. 4-11. Apparently the rheometer is
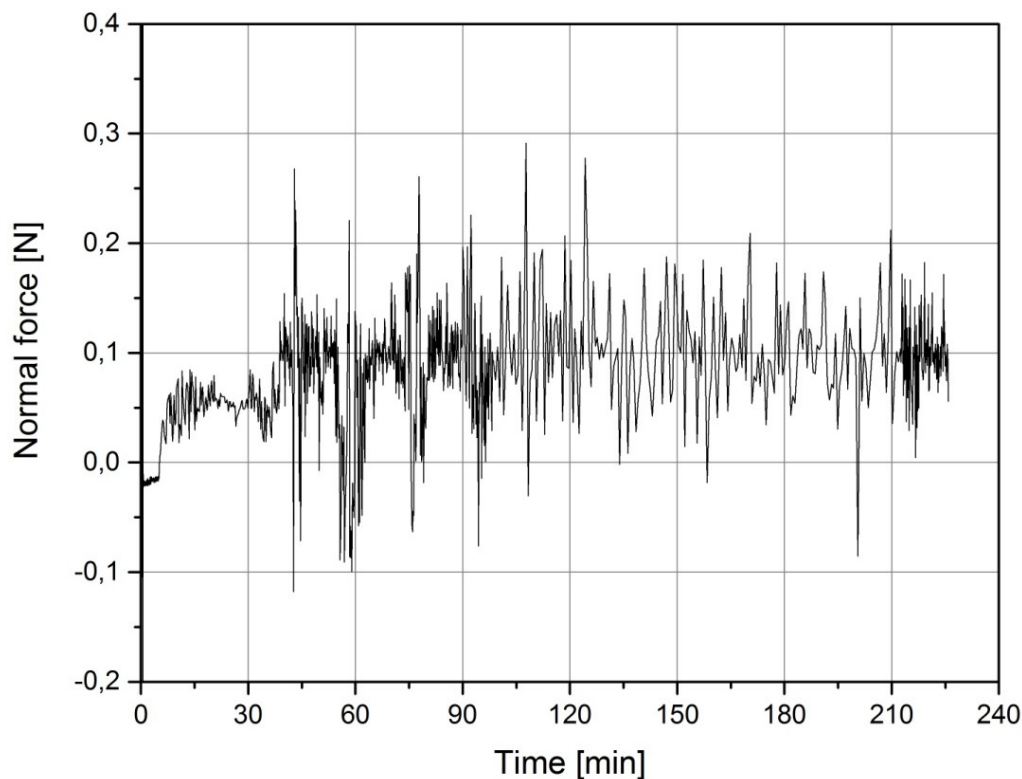

Fig. 4-12: Normal force over time measured in the plate-plate configuration of the MCR501 rheometer.

Table 4-7: Linear cure shrinkage values obtained from rheometer measurements and the calculated mean value and standard deviation.

Specimen no.	Linear cure shrinkage	Mean (SD) of linear cure shrinkage
-	[%]	[%]
01	0,72	0,75 (0,04)
02	(0,43)	
03	not evaluable	
04	0,78	

able to apply small loads, but not with the indicated accuracy. The drop was only observed when increasing the force from 0,01N to higher values. Even though the recorded data did not show unusually high deviations, the assumption that the rheometer could not handle these small forces properly was the only reasonable explanation for the detected gap change (Anton Paar GmbH 2006).

By evaluating the gap distance at the beginning and at the end of the isothermal measurement segment, the cure shrinkage could be calculated. The recorded graphs of the further measurements are depicted in Fig. A-6 to Fig. A-8 in the appendix. All the analyzed specimens showed a similar material behavior during the isothermal curing and the cooling to room temperature and therefore resulted in similar curve progressions. Significant differences could only be noted regarding the heating segment. Depending on the amount of cross-links that were already formed during the specimen preparation, the resin was more or less able to relax. Accordingly, the graphs showed a large decrease in gap distance or no drop at all. Noteworthy are the jumps visible in some graphs, especially regarding the curve progression depicted in Fig. A-6. These jumps could again be attributed to the difficulties of the force control handling the rather low force values. The cure shrinkage of specimen 03 was not determined because of the jump in the gap distance at the end of the isothermal segment (Fig. A-7).

The determined shrinkage values are listed in Table 4-7. Good correlation could be found between two of the specimens, with 0,72% and 0,78% shrinkage respectively. However, one has to keep in mind that some of the shrinkage already occurred during heating. The

decreasing slope of the curve at the end of the heating segment noticeable in some of the graphs can be interpreted as the simultaneous occurrence of thermal expansion and cure shrinkage. The measured dimensional changes are therefore smaller than the actual occurring shrinkage.

The comparably low shrinkage value of 0,43% derived from Fig. A-6 can be explained when regarding the isothermal segment of the measurement. The holding time of 20min was apparently not sufficient for the resin to be fully cured. This assumption is supported by the fact that no plateau was reached at the end of the segment and therefore the dimensions of the specimen still changed due to curing at the beginning of the cooling segment.

4.1.5   **Thermomechanical analysis**

Thermomechanical measurements were performed using specimens that were prepared at different temperatures. The specimens were heated to 200°C at a high heating rate; then the dimensional changes of the specimens at constant temperature were recorded. In order to represent the specific dimensional changes of each specimen type, typical displacement curves are depicted in Fig. 4-13; all the measured displacement curves are depicted in Fig. A-9 to Fig. A-12 in the appendix. Striking is the influence of the specimen preparation temperature on the material behavior during heating. By contrast, at the isothermal conditions as well as during cooling, the dimensional changes of all the specimens were quite similar. The non-linear decrease in temperature at the end of the measurements was due to the fact that the used measurement instrument could not be cooled with liquid nitrogen and the required cooling rate could therefore not be realized.

Table 4-8: Mean values and standard deviations of the linear cure shrinkage of specimens prepared at different temperatures determined by means of TMA.

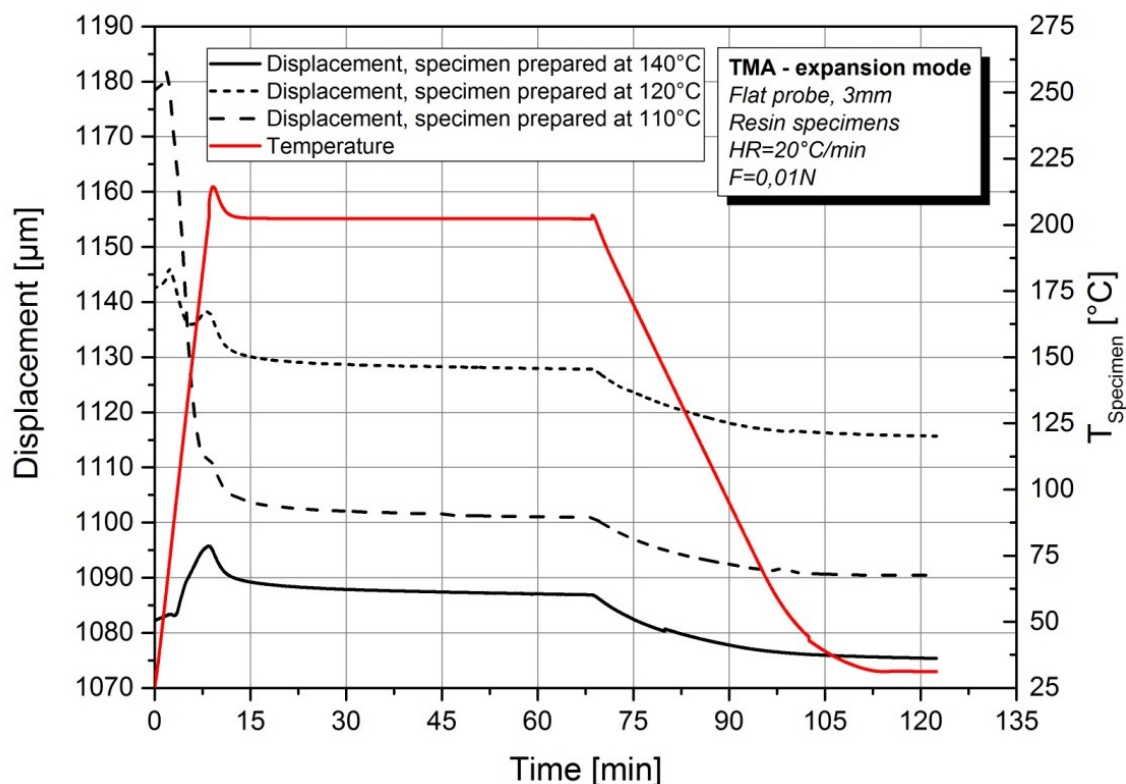| Specimen no.	Specimen	Mean (SD) of linear cure shrinkage
-	-	[%]
01 – 03	Resin 110	0,997 (0,065)
04 – 12	Resin 120	0,982 (0,176)
13 – 14	Resin DSC	0,906 (0,092)
15 – 18	Resin 140	0,774 (0,035)

Fig. 4-13: Displacement curves of specimens that were prepared at different temperatures, measured in the expansion mode of the TMA.

The mean shrinkage value of the specimens that were prepared at 110°C was with approximately 1% slightly higher than the shrinkage determined for the specimens that were prepared at 120°C (Table 4-8). The mean shrinkage value of the specimens that were prepared at 140°C was one forth lower. The different shrinkage values as well as the differences in the curve behavior at the beginning of the measurements were a direct consequence of the different specimen preparation temperatures. Higher specimen preparation temperatures led to an increased cross-linking density in the material, whereas at 110°C no cross-links were built at all. During measuring the mobility of the molecular chains increases at temperatures higher than the T_g; therefore a decrease in specimen thickness might be due to material relaxation. However, the chain mobility and consequently the dimensional changes are affected by the amount of formed cross-links. Furthermore the formation of cross-links during the specimen preparation resulted in lower determined shrinkage values (Ehrenstein et al. 2004).

Specimens that were prepared in DSC crucibles were used for measurements as well. However, due to their porous and uneven surfaces, the results of the specimens that were prepared in the press are assumed to be more reliable.

Figure 4-14 shows the dimensional change over temperature of one of the specimens recorded by applying the temperature modulated technique. As can be seen, the thickness of the specimen changed in accordance with the sinusoidal temperature profile. Several intermediate steps were necessary to separate the measurement data into the reversing dimensional changes and the non-reversing dimensional changes.

First, the derivation of the dimensional changes of the specimen with respect to time was calculated (Fig. A-13). In a next step, Fourier method was used for the deconvolution of the derived dimensional changes. This mathematical procedure is implemented in the METTLER TOLEDO STAR^e system and allowed easy handling of the huge amount of data. Applying the software option called "ADSC" provided the total rate of dimensional change as well as the rates of the reversing and the non-reversing dimensional changes (Fig. A-14). Integration of the data with respect to time finally enabled the determination of the total dimensional changes L_{total} and the changes due to thermal expansion and cure
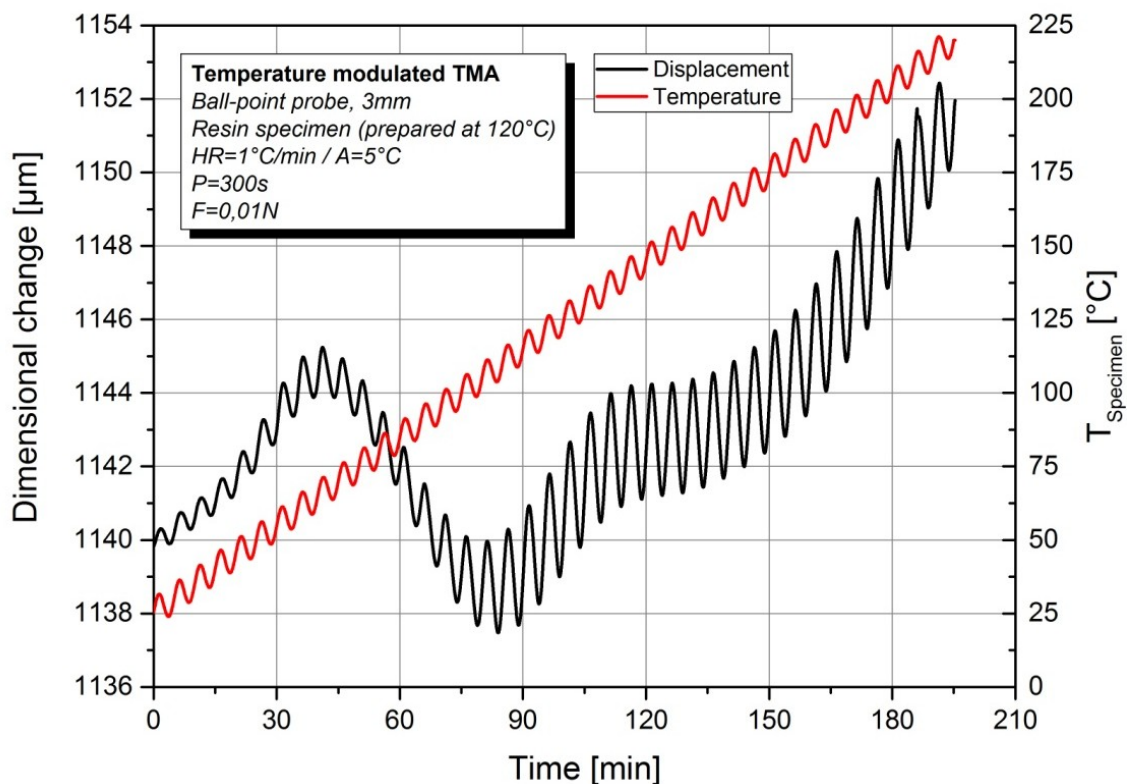

Fig. 4-14: Dimensional change of the specimen depending on time and temperature recorded by applying the temperature modulated technique (specimen 1).

shrinkage, $L_{reversing}$ and $L_{non-reversing}$, respectively. L_{total}, $L_{reversing}$, and $L_{non-reversing}$ are depicted graphically in Fig. 4-15 (Riesen 2000).

Several important characteristics of the investigated resin could be derived from Fig. 4-15. At the beginning of the measurement, $L_{non-reversing}$ remained rather constant while $L_{reversing}$ was increasing continuously due to the thermal expansion of the specimen. The slope of $L_{non-reversing}$ dropped only after reaching a temperature of 63°C, indicating an irreversible decrease in specimen thickness. Again this can be explained by relaxation processes due to the increased mobility of the molecular chains, since the specimen temperature already exceeded the T_g of the material. Another significant decrease in thickness could be detected beginning at approximately 130°C, which could be related to the formation of cross-links and therefore might mark the onset of the chemical shrinkage. However, since a continuous decrease in specimen thickness up to 220°C was recorded, it was assumed that the resin was not fully cured at the end of the measurement. This could be proven by cooling the specimen to room temperature and subsequently repeating the measurement. The dimensional changes of the specimen recorded during this second experiment are depicted in Fig. 4-16. $L_{non-reversing}$ remained quite constant until a temperature of
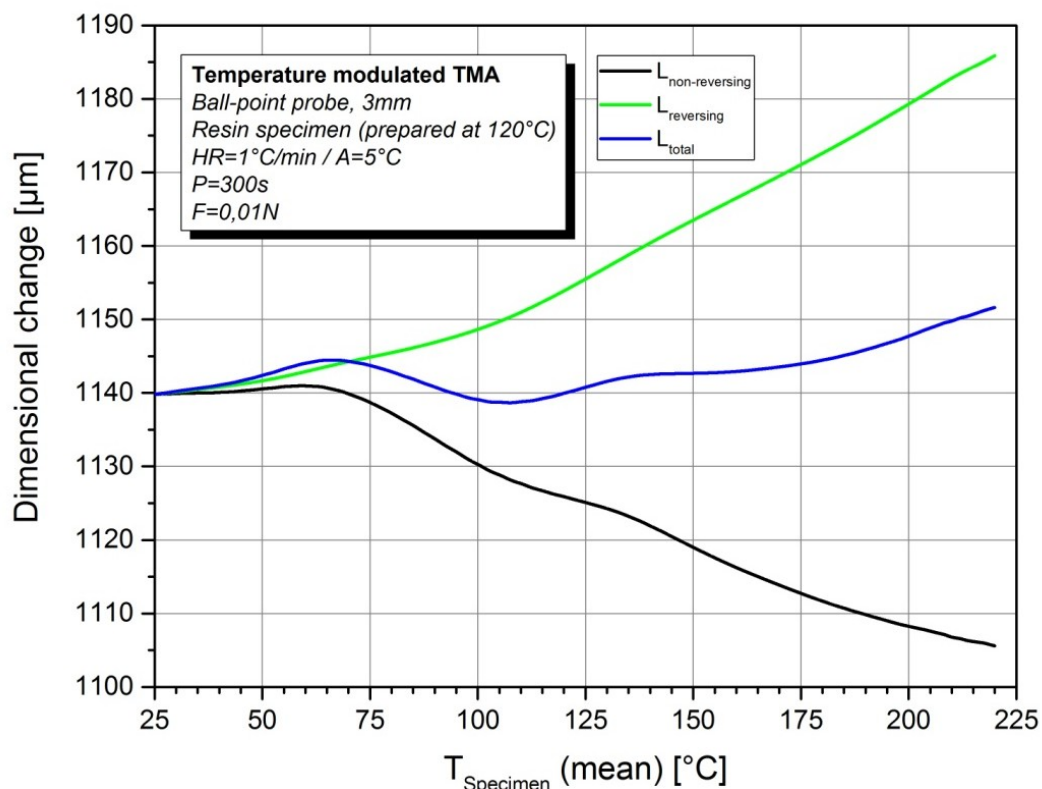

Fig. 4-15: Deconvolution of the measured data in non-reversing and reversing dimensional change, 1st run (specimen 1).

approximately 150°C was reached. Then again the specimen thickness started decreasing irreversibly due to the chemical shrinkage of the resin (Jakobsen et al. 2013).

Nevertheless, the thickness change of the specimen was evaluated in the temperature range between 130°C and 220°C in order to have a comparable value for the conventional TMA measurements. Two additional measurements were performed and evaluated as well (Fig. A-15 and Fig. A-16). The determined shrinkage values are listed in Table 4-9.

The noticeable change in slope of $L_{reversing}$ at the beginning of the measurement indicates the glass transition range of the material. Basically it is possible to determine the T_g of the material by fitting tangents to the curve and evaluating their intersection point. For this method to work properly, however, the starting temperature of the measurement has to be at least 30°C lower than the beginning of the glass transition. Consequently this evaluation method could not be applied (Ehrenstein et al. 2004).

The reversing dimensional changes of the specimen can be used to determine the CTE as described in chapter 2.3.5. The mean coefficient $\overline{\alpha}(\Delta T)$ was calculated using the values of $L_{reversing}$ depicted in Fig. 4-16. The data of the second experiment was chosen in order to
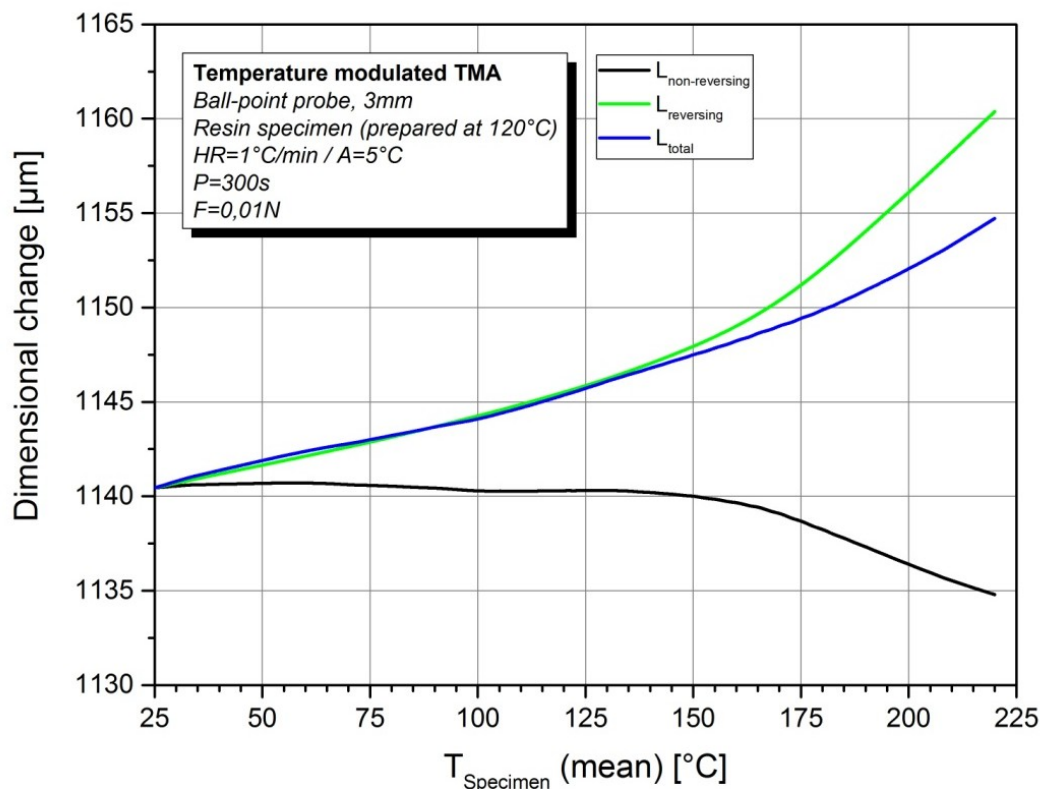

Fig. 4-16: Deconvolution of the measured data in non-reversing and reversing dimensional change, 2nd run (specimen 1).

Table 4-9: Linear cure shrinkage obtained from TMA measurements by applying the temperature modulated technique.

Specimen no.	Specimen	Run	Linear cure shrinkage	Mean (SD) of linear cure shrinkage
-	-	-	[%]	[%]
01	Resin 120	1st	1,742	1,884 (0,200)
02	Resin 120	1st	2,025	
03	Resin 140	1st	1,064	-
01	Resin 120	2nd	0,482	-

be able to compare the determined CTE with the values currently used at AT&S for the fully cured resin. These values were determined by Frewein (2016) using conventional TMA measurements; consequently several differences compared to the described measurements exist. The specimens were prepared in the same way as described in chapter 3.1.1, but the maximum curing temperature in the press was 200°C. To ensure the highest possible degree of cure, the specimens were additionally annealed at 200°C for another 2 hours after preparation. During the measurements, the flat probe with 3mm in diameter was used and a constant pressure of 0,1N was applied. Figure 4-17 depicts the values for $\overline{\alpha}(\Delta T)$ he evaluated in comparison to the values determined in temperature modulated TMA.

The first thing to notice is that the values which were determined using the temperature modulated technique were higher throughout the whole measurement range. The discrepancies became even larger after the measurement temperature exceeded the T_g of the resin. Then again, the overall curve progressions were quite similar. The most likely explanation might be that the specimen used for the temperature modulated measurement was not fully cured; this would also correlate with the interpretation of the curves depicted in Fig. 4-16. The CTE of the resin decreases with increasing degree of cure because the formation of cross-links reduces the ability of the resin to thermally expand. As the mobility of the polymer chains increases at temperatures higher than the T_g, the degree of cure might have an even bigger influence on the CTE at elevated temperatures. What is more, measurement parameters as the heating rate and the shape of the measurement probe also have an influence on the recorded data. Since the
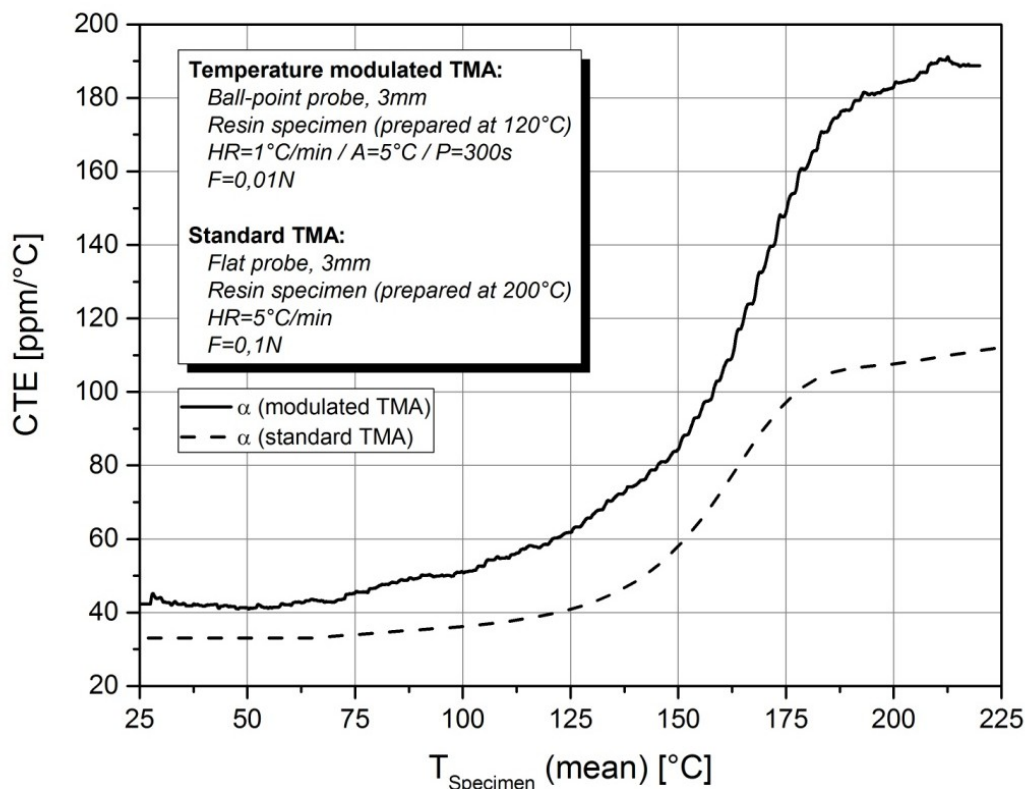
Fig. 4-17: CTE curves measured by applying the temperature modulated technique and measured by Frewein (2016) using conventional TMA measurements.

measuring methods were quite different, this might also explain the differences in CTE to a certain extent. Finally, the temperature modulated TMA is a rather complex technique. Most of the measurement parameters have to be chosen depending mainly on the material behavior of the specimen. In addition, several preconditions have to be met for the Fourier deconvolution to work properly. The phase lag between the excitation signal and the response signal, for example, determines how long the period of one temperature cycle has to be. On the other hand, in order to successfully depict a transition in the material behavior a minimum of 5 cycles is required across the area of transition. The interaction of all these parameters influences the measurement results (Ehrenstein et al. 2004, Blaine 2005).

4.1.6   Comparison of the shrinkage results of the different test methods

The results of all the investigated measurement methods were compared considering the differences in both temperature and pressure conditions during the respective specimen preparation process. The results for the volumetric cure shrinkage and the linear cure shrinkage are listed in Table 4-10.

The volumetric cure shrinkage can be obtained by density measurements. However, no reasonable results could be obtained by pycnometry, since the porous surfaces of the specimens led to severe difficulties due to bubble adhesion. What is more, the pressure applied during the specimen preparation had an influence on the density of the specimens. Regarding hydrostatic weighing, similar measurement difficulties were encountered, but with the use of larger specimens the scattering of the measured values could be reduced. It was even possible to measure the density of specimens that were prepared without applying any pressure; evaluation of the density of these specimens before and after curing resulted in an average volumetric shrinkage value of 3,147%. Compared to the other measurement methods, the scattering of the results was still rather large though.

The rotational rheometer as well as the TMA measurements were suitable for the determination of the thickness changes of the specimens due to curing and therefore provided results for the linear cure shrinkage. Compared with the results of the conventional TMA measurements, the shrinkage values determined by rheometry were up to one forth lower. The lower values could be explained by the moderate heating rates which had to be used and the amount of cross-links already formed during heating. The shrinkage values determined by TMA varied in accordance with the different specimen preparation temperatures. As was to be expected, with 0,997%, the highest shrinkage values were obtained using specimens that were prepared at temperatures below the melting temperature of the hardener. The specimens that were prepared at 120°C in the press showed with 0,982% a deviation of only approximately 2% but were much easier to handle regarding the specific specimen preparation for TMA measurements. By contrast, the average shrinkage of the specimens that were prepared in the DSC crucibles at the same temperature but without applying pressure was several percent lower. These specimens were definitely not the most suitable specimens for the investigated measurements since they were very thin and porous; the specimen condition might well be an explanation for the deviations of the measured shrinkage values. Since the volumetric shrinkage is 3 times the linear shrinkage, the results of conventional TMA and of hydrostatic weighing matched sufficiently well. Noticeable are the low shrinkage values obtained using specimens that were prepared at 140°C. Comparison with the other specimens clearly showed that for reasonable shrinkage measurements the specimen preparation temperature has to be in the range of the melting temperature of the hardener or below.

Table 4-10: Comparison of the investigated measurement methods for determining the cure shrinkage.

Measurement method	Specimen preparation pressure	Specimen preparation temperature	Mean (SD) of volumetric cure shrinkage	Mean (SD) of linear cure shrinkage
-	[bar]	[°C]	[%]	[%]
Pycnometry	10	110 / 140	not evaluable	-
Hydrostatic weighing	-	120	3,147 (1,123)	-
Rotational rheometer	0,6 / (8)	100	-	0,750 (0,040)
TMA	-	120	-	0,906 (0,092)
	10	110	-	0,997 (0,065)
	10	120	-	0,982 (0,176)
	10	140	-	0,774 (0,035)
Temperature modulated TMA	10	120	-	1,884 (0,200)
	10	140	-	1,064 (-)

Compared with the results of conventional TMA, the results of the temperature modulated TMA measurements were extraordinarily high for both investigated types of specimens. The shrinkage values of the specimens that were prepared at 120°C were nearly twice as high, with approximately 1,88% compared to 0,98%. Since the temperature modulated TMA is a technique which requires knowledge about both the material behavior of the specimen and the suitable choice of measurement parameters, the results of conventional TMA were thought to be more reliable. As a consequence, a linear shrinkage value of 1% was implemented in the material model of the investigated resin in the used finite element software.

4.2   Analysis of the prepreg lamination process

Microsections of the unprocessed prepregs as well as of the bi-material panels were prepared. This was done in order to analyze the influence of the lamination process on

the resulting thickness of the prepreg layer. As can be seen in Fig. 4-18a, the prepregs had a rather uneven surface and thickness distribution, with the thickness varying between 80μm and 130μm. The geometry of the fabric already differed from the round shaped bundles specified in IPC-4412A (IPC - Association Connecting Electronics Industries 2008).

The microsections of the panels which were prepared at 140°C and 200°C respectively are depicted in Fig. 4-18b and Fig. 4-18c. The lamination process led to constantly thick prepreg layers with a thickness of approximately 90μm. Apparently the different press temperatures did not have any influence on the layer thickness, since no differences between the panels could be detected. During the panel manufacturing, resin is pressed out of the fabric. It was assumed that at temperatures higher than the T_{gel} of the resin the formation of cross-links stops the resin flow. The thickness of the prepreg layers measured after the lamination process was used for the creation of the simulation model of the test carrier.

Regarding PCB manufacturing, some processes require only partially cured prepregs. Between the first lamination step and the final curing several manufacturing steps take place. As a consequence, warpage of both partially and fully cured builds is a severe issue
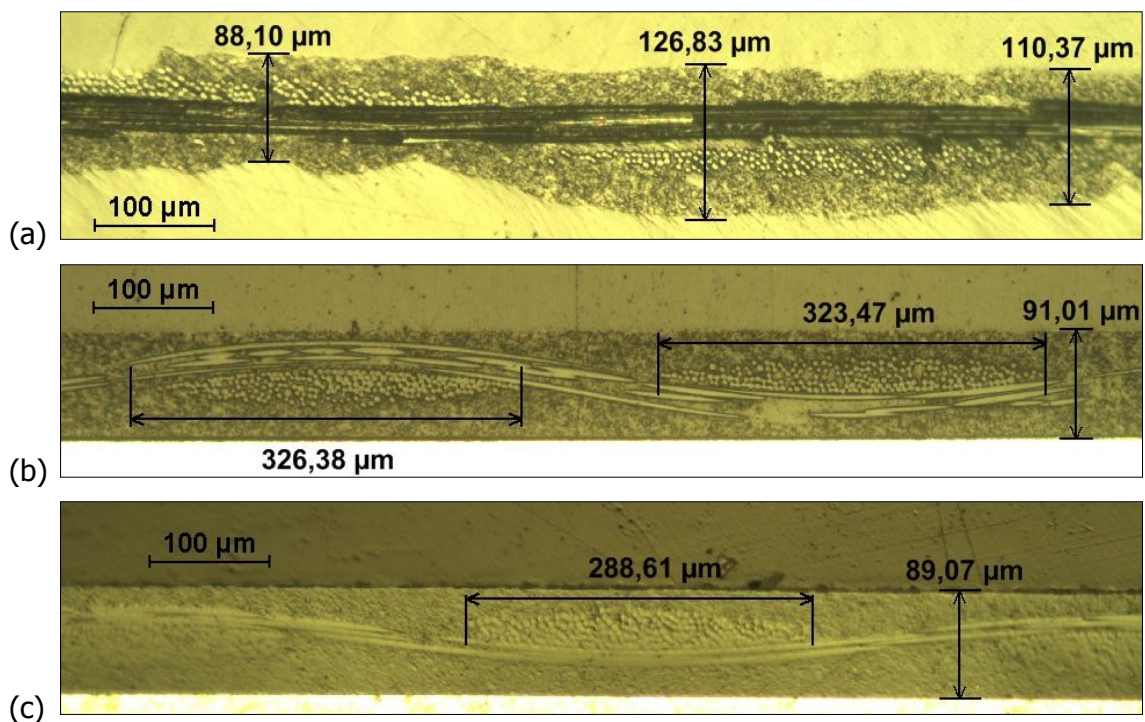

Fig. 4-18: Microsections parallel to the weft direction of (a) the unprocessed prepreg, (b) a panel that was prepared at 140°C, and (c) of a panel that was prepared at 200°C.

regarding the producibility of the boards. Depending on the degree of cure of the resin, different lamination temperatures were expected to result in differently warped panels. The warpage behavior of the bi-material panels that were either partially cured at 110°C, 120°C, and 140°C respectively or fully cured at 200°C was analyzed. The extent of warpage was compared directly after the partial curing step (Fig. 4-19a) and again after the final lamination step (Fig. 4-19b).

As can be derived from Fig. 4-19a, the panels that were prepared at 110°C and 120°C showed only marginal deflections. Again this could be explained considering the starting temperature of the curing reaction. At 110°C no cross-links should have formed at all, whereas the formation of a rather limited amount of cross-links was to be expected in the resin layer of the panel prepared at 120°C. However, the bonding between the prepreg layer and the aluminum sheet of the panel that was prepared at 110°C was not sufficient for further processing. By comparison, significant deformation of the panel that was prepared at 140°C could be observed. The panel with the fully cured prepreg layer showed the most extensive warpage behavior.
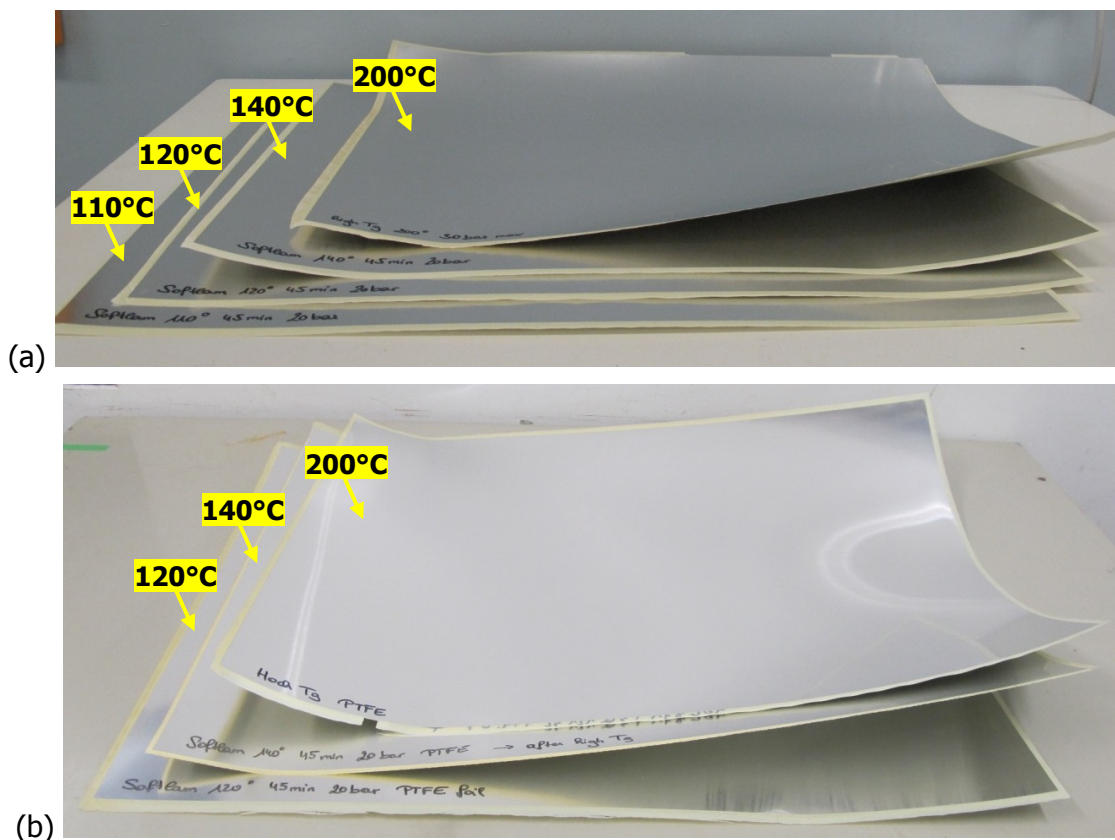

(a)

(b)

Fig. 4-19: (a) Panels that were prepared at 110°C, 120°C, 140°C, and 200°C.

(b) Panels that were prepared at 120°C and 140°C after final lamination, as well as the panel that was prepared at 200°C.

After the final lamination at 200°C, the panel that was prepared at 120°C still showed only marginal warpage compared to the others (Fig. 4-19b). It was concluded that the overall deformation of the panels can be reduced by applying temperatures slightly below or above T_{gel} during the first lamination step. This is likely due to the fact that at these temperatures the molecular chains of the resin are still rather moveable and can adjust to the applied pressure but still already attach to the aluminum layer. This presumption fits into the overall picture regarding the material behavior of the investigated resin that could be achieved during this work (Ehrenstein et al. 2004).

4.3 Deformation behavior of the test carrier

4.3.1 Results of the experimental deformation analysis

The deformation curves of the bi-material strips measured in the 3-point-bending mode of the TMA under different test conditions are displayed in Fig. 4-20. Obviously the irreversible deformations of the strips were quite independent of the chosen heating rate but were mainly influenced by the measuring time. It can be seen that the recorded displacements of the probe did not reach plateaus at isothermal temperatures.
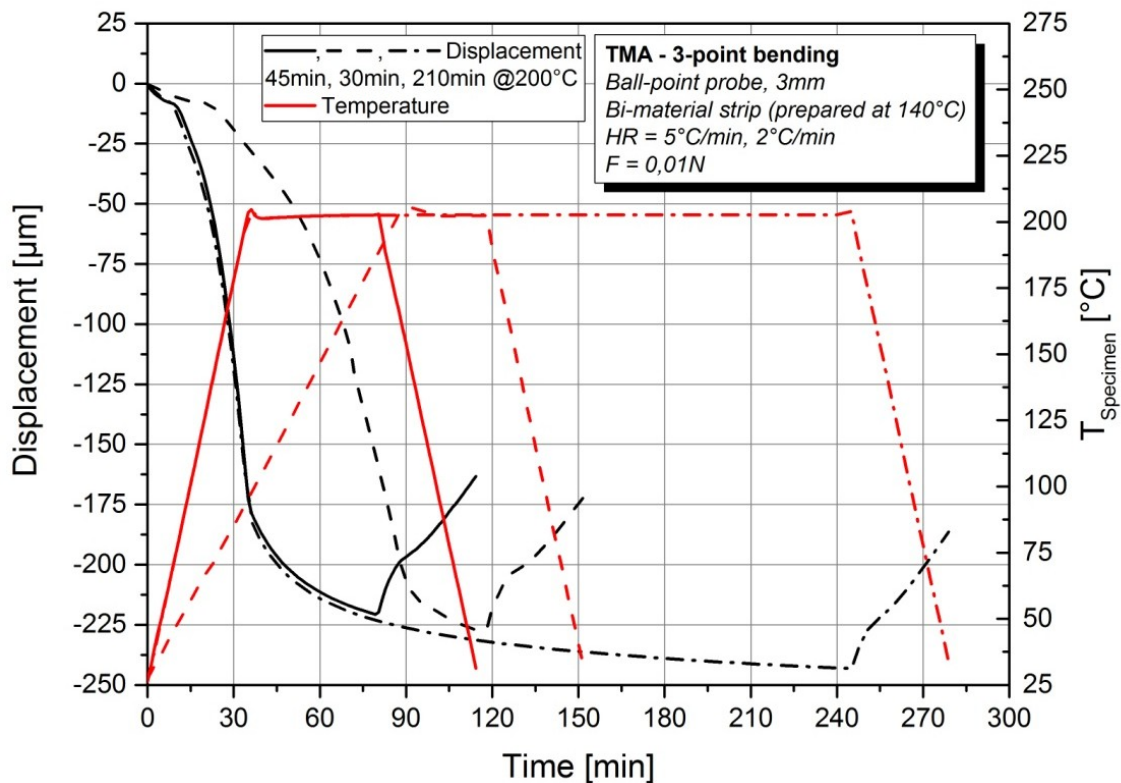

Fig. 4-20: Displacement over time and temperature of bi-material strips prepared at 140°C, depending on the chosen heating rates and holding times.

Considering the results of the DSC measurements, at least the strip that was cured for 3 hours at 200°C should have been fully cured, but nevertheless it deformed until the end of the measurement.

This material behavior can likely be explained considering the different characteristics of the strip materials. First, the differences in CTE of aluminum, glass and resin cause internal stresses in the strip during heating. At isothermal conditions additionally the cross-linking processes within the resin have to be considered. As mentioned in chapter 2.3.1, volumetric shrinkage is a direct result of the different bond types between the resin molecules before and after curing. By contrast, the glass fibers show virtually no dimensional changes at all. Over time and at elevated temperatures, the internal stresses decline to a certain extent because of the viscoelastic material behavior of the resin. This relaxation processes highly depend on time and temperature and are a possible reason for the further increase in strip curvature after curing (Khoun and Hubert 2010, Ehrenstein 2011).

The displacement curve depicted in Fig. 4-21 demonstrates that the force applied by the probe did not affect the deformation behavior of the specimens, at least not of the cured
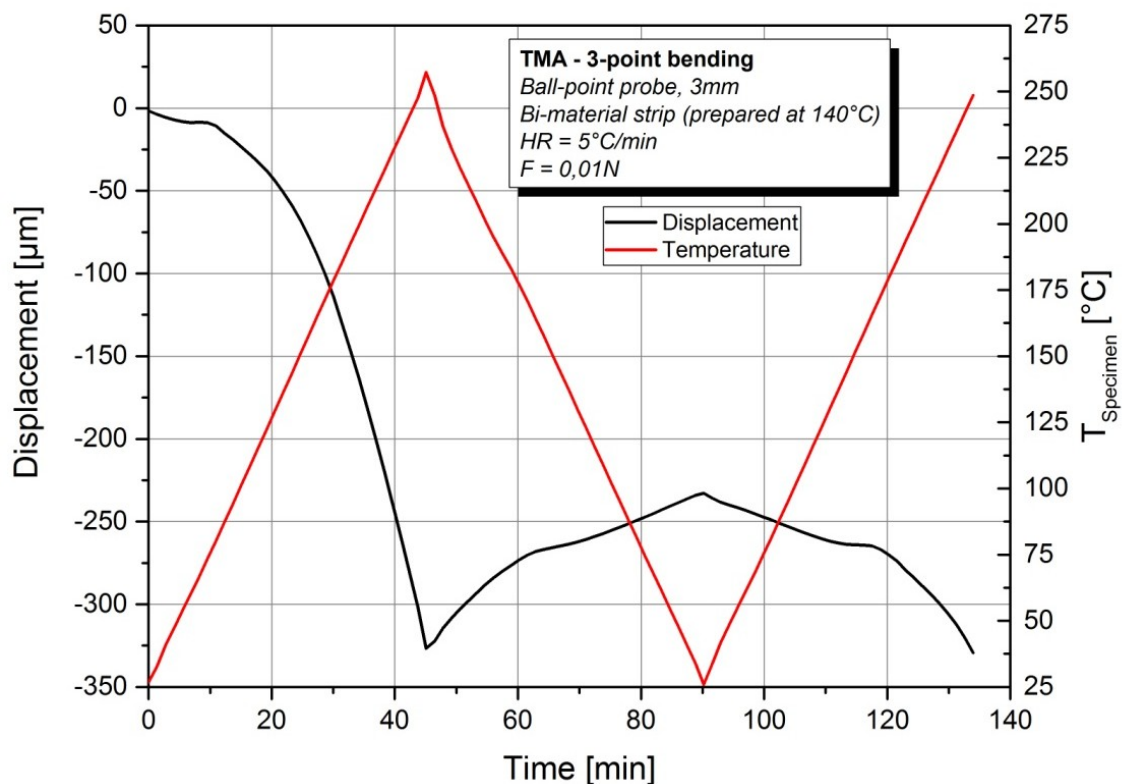

Fig. 4-21: Displacement over time and temperature of a bi-material strip that was prepared at 140°C.

strips. The specimen was heated to 250°C and then cooled to ambient temperature. The results of the subsequent heating showed that the probe displacement recorded during the second heating segment mirrored the curve progression in the cooling segment. This also indicates that after curing the curvature of the strip was caused only by the differences in CTE of the layer materials. As expected, this thermally-induced deformation is entirely reversible.

Measurements were performed using bi-material strips that were prepared at both 120°C and 140°C. The recorded displacement curves are depicted in Fig. 4-22. The curvatures of the strips that were prepared at 140°C were evaluated at the end of the heating segment and at the end of the isothermal segment respectively (Table 4-11). Noticeable is the deformation behavior of the strips that were prepared at 120°C. It seems that at first the thermal expansion of the aluminum layer dominated, until at temperatures slightly higher than the T_g of the resin the expansion of the prepreg layer increased; the bending of the strip was even reversed. Only at higher temperatures did the curvature change again, aluminum being again the outer and thus the more expanded layer of the strip. This unexpected deformation behavior might possibly be explained considering the pressure
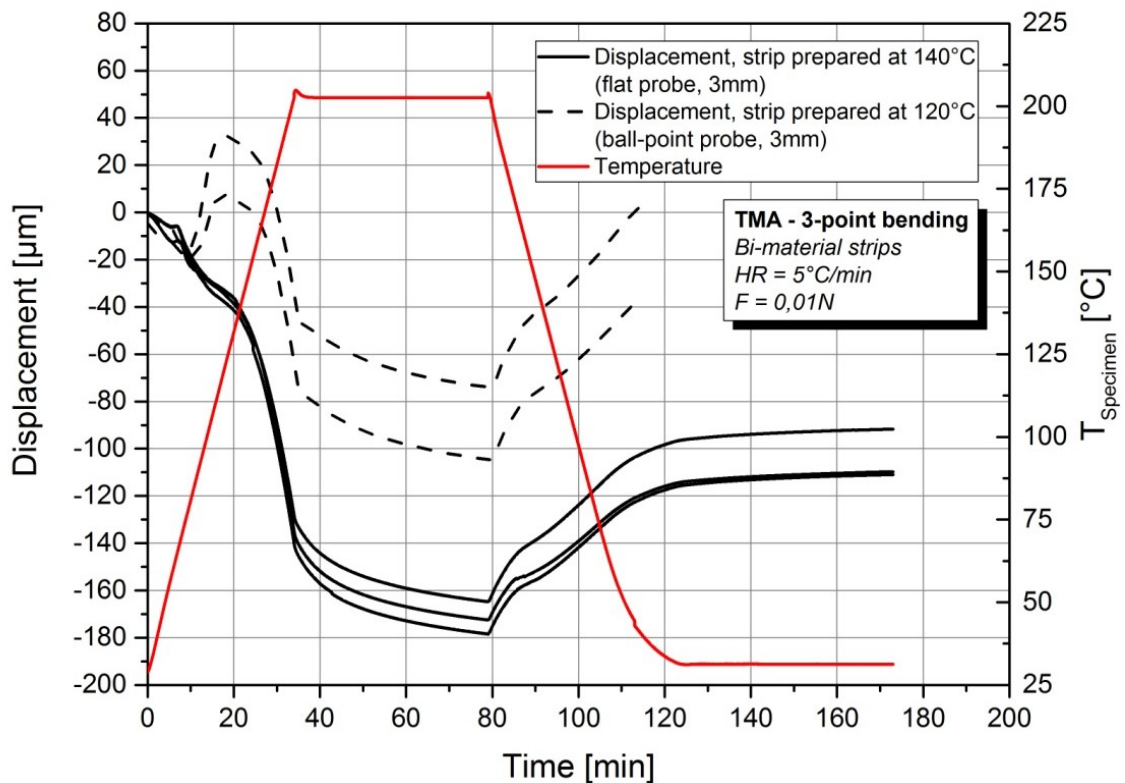

Fig. 4-22: Displacement depending on time and temperature of bi-material strips that were prepared at 120°C and 140°C.

Table 4-11: Displacements of the bi-material strips prepared at 140°C at the end of the heating segment and at the end of the isothermal segment respectively.

No.	Specimen	Displacement after heating segment	Displacement after isothermal segment
-	-	[µm]	[µm]
01	Strip (prod @140°C)	132	164
02	Strip (prod @140°C)	140	171
03	Strip (prod @140°C)	145	178
Mean (SD)		139,2 (5,1)	171,2 (5,5)

during the strip lamination. As could be demonstrated by hydrostatic weighing of the pure resin specimens, the applied pressure led to densely packed molecular chains. At temperatures higher than the T_g of the resin, the mobility of the molecular chains increased and they sought to return to a state of equilibrium. However, the mobility of the chains was hindered at the bonding surface of the strip and in-plane by the glass fibers as well. These hindrances combined with the high chain mobility might be the reason for an unexpected deformation behavior of the prepreg layer and therefore of the whole strip (Ehrenstein 2011).

4.3.2 Results of the finite element analysis

The results of the finite element analysis of model 1 are depicted in Fig. 4-23. The different colors represent the displacement of the strip in z-direction of the defined coordinate system. The legend assigns the colors to the corresponding value ranges. The model was evaluated according to the test carrier. A node in the center of the outer resin layer was chosen to represent the contact point between the measurement probe of the TMA and the strip. The displacement of this node was evaluated after both simulation steps, resulting in a displacement due to thermal expansion and a displacement due to resin shrinkage. The deformations of model 2 and model 3 are depicted in Fig. A-17b and Fig. A-18b in the appendix and were evaluated in the same way.

The nodal displacements of all models are listed in Table 4-12. The first thing to notice are the rather low values achieved with model 2 compared to the results of the other models. The similar results of model 1 and model 3 can be explained by considering the
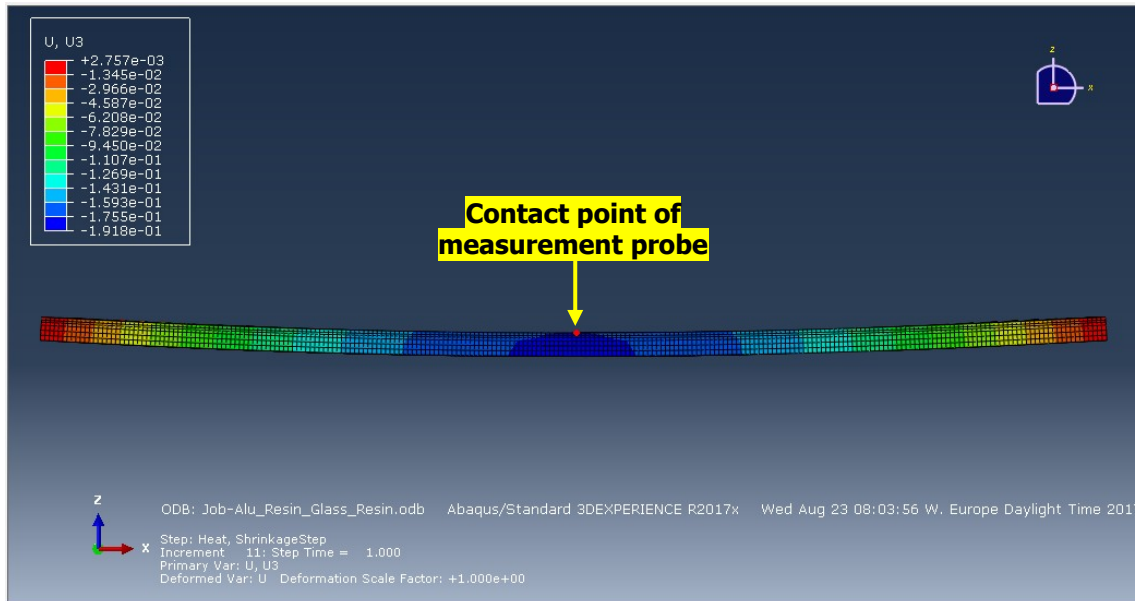
Fig. 4-23: Deformation of the modeled strip at the end of the shrinkage step (model 1).

geometry and the distribution of the glass fibers. Whereas an even glass layer was created in model 1, several individual flat yarns were created in model 3. These geometric approaches are similar and represent the actual geometry of the fiber fabric by far better than the ideal yarn shape realized in model 2. Considering the geometry, the mismatch in the CTEs of resin and glass fibers apparently had a higher impact on the strip curvature either with increasing surface area of the fibers or with increasing fiber content. This could be an explanation for the striking low deformation values of model 2. With 27µm, however, model 2 achieved the highest deformation due to the cure shrinkage of the resin. It was assumed that a higher resin content within the fiber layer resulted in an increasing deformation of the strip due to resin shrinkage.

Table 4-12: Nodal displacements of the different models representing the deformation of a strip after thermal expansion and after cure shrinkage respectively.

Model	Displacement after step 1 (CTE only)	Displacement after step 2 (CTE + shrinkage)	Displacement due to cure shrinkage
-	[µm]	[µm]	[µm]
Model 1	175	190	15
Model 2	30	57	27
Model 3	141	159	18

4.3.3 Comparison of the experimental results and the finite element analysis

The simulation results of the different finite element models as well as the displacement values recorded by TMA are listed in Table 4-13. Comparison of the deformation values showed good agreement between the experimental results and the results of the deformation analysis of model 1 and model 3. The analysis results of model 2 did not correlate with the measured values after the first simulation step. However, the second simulation step provided deformation results in a similar size range than the measurements. As already discussed in chapter 4.3.2, these results were not entirely unexpected. The prepreg manufacturing process leads to severe geometric changes of the fiber fabric; this could be confirmed by microsectioning as described in chapter 4.2. For this reason, the evenly distributed glass layer represented the actual fiber fabric better than individual yarns arranged according to the fabric specification. Model 1 slightly overestimated the deformation due to thermal expansion compared to the results of the TMA measurements, whereas the results of model 3 corresponded exceptionally well.

By contrast, both model 1 and model 3 underestimated the deformation of the strip due to the cure shrinkage of the resin. Several considerations might explain these discrepancies. First of all, as could be proven by Frewein (2016), the influence of the glass fabric on the thermal behavior of the resin is not negligible. Due to the lower CTE of the fibers, the resin cannot expand freely. Thus it is likely that the fiber-matrix interface affects the shrinkage behavior of the resin as well. This would also correlate with the assumption that the glass fiber content affects the shrinkage behavior of the resin and subsequently that the lower fiber content in model 2 led to a decreased impact of the

Table 4-13: Comparison of the simulation results and the experimental results in terms of displacement after thermal expansion and after cure shrinkage.

Test carrier / model	Displacement after thermal expansion	Displacement after shrinkage	Displacement due to shrinkage
-	[µm]	[µm]	[µm]
Test carrier	139	171	32
Model 1	175	190	15
Model 2	30	57	27
Model 3	141	159	18

fibers on the resin behavior. Furthermore, several assumptions were made regarding the material characteristics of the uncured and the partially cured resin. As mentioned in chapter 3.7, assumptions were made for the temperature-dependent Young's modulus as well as for the Poisson's ratio. What is more, both the CTE and the chemical shrinkage of the resin depend on the degree of cure; the degree of cure, in turn, depends on curing time and temperature. As for the evaluation of the TMA measurements, thermal expansion and cure shrinkage occurred simultaneously during the heating segment at temperatures higher than the T_{gel} of the resin. Considering all these assumptions and approximations to reality, it was more important to reach the same magnitude of deformation by simulation as by TMA measurements than to achieve the exact same results. Regarding the results listed in Table 4-13 this worked sufficiently well for model 1 and model 3.

5 SUMMARY AND OUTLOOK

Reasonable results for the cure-induced shrinkage of the investigated epoxy resin were obtained from measurements in the expansion mode of the TMA. Specimens that were prepared at 110°C and 120°C respectively were used for the measurements, since at those temperatures only marginal curing or even no curing at all could be expected during the specimen preparation. A dynamic segment with a high heating rate was followed by an isothermal segment at the specified curing temperature of the material. The dimensional changes of the specimens under isothermal conditions were due only to cure shrinkage. Analyzing the thicknesses of the specimens before and after curing resulted in a shrinkage value of approximately 1% for the investigated resin. This value could be successfully implemented into the material model of the resin in the finite element software Abaqus FEA. Strips consisting of aluminum layers and prepregs were prepared and measured in the 3-point bending mode of the TMA; in addition simulation models of the strips were created and thermally stressed. Comparison with the experimental results showed that the deformation behavior of the strips due to both thermal expansion during heating and cure shrinkage under isothermal conditions could be sufficiently well approximated by 2 of the models. In conclusion, the described test procedure was found to be the most suitable method among the investigated measurement techniques for determining the cure-induced shrinkage of the epoxy resin.

However, most of the investigated methods were only suitable to a limited extend or not suitable at all for the determination of the cure shrinkage. Several ideas for improving the measurements and also the implementation of the shrinkage value into the finite element software came up during this work. Most promising were the results of the temperature modulated TMA measurements, thus this method should definitely be explored in more detail. Compared to the conventional TMA measurements, the determined shrinkage values were significantly higher. For this reason, future work should focus on the selection of the measurement parameters and their influence on the deconvolution of the dimensional changes of the specimens in particular, as well as on the comparability of the results with those of other measurement methods.

The rotational rheometer described in this work cannot be recommended for the shrinkage determination for two reasons. First, compared to the TMA measurements, a rather low heating rate had to be chosen because of the thermal inertia of the test instrument. As a result, the cross-linking process was already quite advanced at the

beginning of the isothermal measurement segment. Consequently, the evaluation of the dimensional changes that occurred under isothermal conditions provided but a fraction of the total cure shrinkage. What is more, the rheometer obviously was not able to handle the small forces applied to the specimens during measuring. Jumps in the displacement curves due to insufficient force control can lead to possibly distorted shrinkage results. On the other hand, the simple specimen preparation with adjustable pressure control was a major advantage of the rheometer compared to the other investigated test instruments.

Regarding the density measurements, pycnometry and hydrostatic weighing provided insufficient shrinkage values because of the porous surface condition of the specimens and the resulting problem of bubble adhesion. Furthermore, the pressure applied during the specimen preparation had an influence on the density of the specimens. As a result, weighing of the specimens after their preparation and after curing provided misleading results. In addition, the impact of stress relaxation at temperatures higher than the T_g could not be taken into account; this was only possible when using measurement instruments that continuously recorded the dimensional changes of the specimens.

The influence of the pressure applied during the specimen preparation on the characteristics of the resin should definitely be analyzed in future. As could be demonstrated, the applied pressure led to an increased specimen density, which did not influence the total occurring cure shrinkage of the resin but rather the reasonable applicability of the different test procedures. However, further investigation of the specimen preparation process and the resulting specimen characteristics is recommended in order to acquire a deeper knowledge of the influence of pressure.

As regards the finite element analysis, a simple approach was chosen in order to implement the cure shrinkage of the resin into the simulation model. Even though this approach worked well for the presented simulation of the test carrier, there exist other ways of implementation which should be evaluated and might prove themselves more suitable for future applications. Further work is also needed in order to examine the influence of the glass fabric on the shrinkage behavior of the resin with a special focus on the development of a material model for the prepregs, combining the material characteristics of both constituents. Besides for a more accurate simulation of the curing process, additional material characteristics of the resin like Young's modulus and Poisson's ratio depending on both temperature and degree of cure remain to be determined.

6 LITERATURE

Anton Paar GmbH (2006). Betriebsanleitung Physica MCR xx1 Reihe

Billotte C., Bernard F. M. and *Ruiz E.* (2013). Chemical shrinkage and thermomechanical characterization of an epoxy resin during cure by a novel in situ measurement method. European Polymer Journal 49, 3548–3560

Blaine R. L. (2005). Modulated thermomechanical analysis - measuring expansion and contraction simultaneously. http://www.tainstruments.com/, as on 02.08.2017

Boyle M. A., Martin C. J. and *Neuner J. D.* (2001). In "Epoxy resins", (Miracle, D. B; Donaldson, S.L; ed.), 78–89

Coombs C. F. J. (Hrsg.) (2001). Printed Circuits Handbook, 5th edition, The McGraw-Hill Companies, Inc., US

Dassault Systèmes (2017). Homepage of Dassault Systèmes. http://abaqusdoc.ucalgary.ca, as on 12.12.2017

Ehrenstein G. (2011). Polymer-Werkstoffe, Struktur - Eigenschaften - Anwendung, 3th edition, Carl Hanser Fachbuchverlag, München

Ehrenstein G. W., Trawiel P. and *Riedel G.* (2004). Thermal Analysis of Plastics, Theory and Practice, Carl Hanser Fachbuchverlag, München

Frewein M. (2016). Development and evaluation of an appropriate characterization method for the anisotropic measurement of the thermal expansion of individual printed circuit board layers, Bachelor thesis, Institute of Material Science and Testing of Polymers, Montanuniversität Leoben, A.

Frick A. and *Stern C.* (2006). DSC-Prüfung in der Anwendung, Carl Hanser Fachbuchverlag, München

Frick A. and *Stern C.* (2011). Praktische Kunststoffprüfung, Carl Hanser Fachbuchverlag, München

Gilbert M. D. (1988). "Mechanism and kinetics of the dicyandiamide cure of epoxy resins", Dissertation, Department of Polymer Science and Engineering, University of Massachusetts Amherst, U.S.

Haider M., Hubert P. and *Lessard L.* (2007). Cure shrinkage characterization and modeling of a polyester resin containing low profile additives. Composites Part A: Applied Science and Manufacturing 38, 994–1009

IPC - Association Connecting Electronics Industries (1999). IPC-TM-650 Test Methods Manual, 2.4.22 - Bow and Twist (Percentage)

IPC - Association Connecting Electronics Industries (2008). IPC-4412A, Specification for Finished Fabric Woven from "E" Glass for Printed Boards. Amendment 1

Jakobsen J., Jensen M. and *Andreasen J. H.* (2013). Thermo-mechanical characterisation of in-plane properties for CSM E-glass epoxy polymer composite materials - Part 1: Thermal and chemical strain. Polymer Testing 32, 1350–1357

Khoun L. and *Hubert P.* (2010). Cure shrinkage characterization of an epoxy resin system by two in situ measurement methods. Polymer Composites 31, 1603–1610

Kravchenko O. G., Li C., Strachan A., Kravchenko S. G. and *Pipes R. B.* (2014). Prediction of the chemical and thermal shrinkage in a thermoset polymer. Composites Part A: Applied Science and Manufacturing 66, 35–43

Menard K. P. (2008). Dynamic Mechanical Analysis, A Practical Introduction, 2th edition, Taylor & Francis, Hoboken

Mettler Toledo (1997). STARe System TMA/SDTA840 Operating Instructions

Mettler Toledo (2000). METTLER TOLEDO Thermal Analysis UserCom 11, Interpreting DSC curves part 1: dynamic measurements

Mettler Toledo (2003). Model Free Kinetics. http://www.mt.com/ta/, as on 15.08.2017

Mettler Toledo (2005). STARe System DMA/SDTA861e Operating Instructions

Mettler Toledo (2017). Homepage of Mettler Toledo. http://www.mt.com/, as on 12.12.2017

Ortega-Rivas E. (2012). Non-thermal Food Engineering Operations, 1th edition, Springer-Verlag, s.l.

Riesen R. (2000). METTLER TOLEDO Thermal Analysis UserCom 12, Force and temperature modulated TMA measurements of fibers

Riesen R. (2007). METTLER TOLEDO Thermal Analysis UserCom 25, Choosing the right baseline

Rovitto M. (2016). "Electromigration Reliability Issue in Interconnects for Three-Dimensional Integration Technologies", Dissertation, Fakultät für Elektrotechnik und Informationstechnik, Technische Universität Wien, A.

Schoch K. F., Panackal P. A. and *Frank P. P.* (2004). Real-time measurement of resin shrinkage during cure. Thermochimica Acta 417, 115–118

Schuerink G. A., Slomp M., Wits W. W., Legtenberg R. and *Kappel E. A.* (2013). Modeling printed circuit board curvature in relation to manufacturing process steps. Procedia CIRP 9, 55–60

Seyler R. J. and *Moody R.* (1997). Oxidation as a contamination in measurements involving self-generated atmospheres. Oxidative behavior of materials by thermal analytical techniques - ASTM STP 1326

Stommel M., Stojek M. and *Korte W.* (2011). FEM zur Berechnung von Kunststoff- und Elastomerbauteilen, Carl Hanser Fachbuchverlag, München

Wang J., Laborie M.-P. G. and *Wolcott M. P.* (2005). Comparison of model-free kinetic methods for modeling the cure kinetics of commercial phenol–formaldehyde resins. Thermochimica Acta 439, 68–73

Widmann J. (2000). METTLER TOLEDO Thermal Analysis UserCom 12, Interpreting DSC curves; Part 2: Isothermal measurements

Yu H., Mhaisalkar S. G. and *Wong E. H.* (2005). Cure shrinkage measurement of nonconductive adhesives by means of a thermomechanical analyzer. Journal of ELECTRONIC MATERIALS 34, 1177–1182

APPENDIX

Table A-1: Volumetric shrinkage values obtained from pycnometer measurements of specimens that were prepared at different temperatures.

No.	Specimen	Mass	Density before curing	Curing device	Curing parameters	Pressure during curing	Density after curing	Volumetric shrinkage	Mean (SD) of vol. shrinkage
-	-	[g]	[g/cm³]			[N]	[g/cm³]	[%]	[%]
01	Resin 110	0,0278	1,5223	DSC	iso200°C / 60min	-	1,5483	1,6831	4,0240 (5,8434)
02		0,0279	1,3449				1,3978	3,7821	
03		0,0405	1,4960				1,4735	-1,5243	
04		0,0412	1,2840				1,4618	12,1551	
05	Resin 140	0,0225	1,6360	DSC	iso200°C / 60min	-	1,5681	-4,3287	-2,0432 (2,8733)
06		0,0230	1,4919				1,5113	1,2892	
07		0,0261	1,5496				1,5407	-0,5805	
08		0,0318	1,6055				1,5356	-4,5530	

Table A-2: Normalized enthalpy values obtained from isothermal heat flow curves of the resin powder at different temperatures.

No.	Specimen	Curing temperature	Curing time	Normalized enthalpy	Mean (SD) of normalized enthalpy
-	-	[°C]	[min]	[J/g]	[J/g]
01	Resin powder	100	100	-2,6	-2,7 (0,7)
02				-2,0	
03				-3,4	
04	Resin powder	110	100	4,4	1,8 (2,2)
05				0,5	
06				0,6	
07	Resin powder	120	100	9,5	9,4 (0,1)
08				9,3	
09				9,4	

Table A-3: Volumetric shrinkage values obtained from hydrostatic weighing of specimens that were prepared at different temperatures.

No.	Specimen	Mass	Density before curing	Curing device	Curing parameters	Pressure during curing	Density after curing	Volumetric shrinkage	Mean (SD) of vol. shrinkage
-	-	[g]	[g/cm³]	-	-	[N]	[g/cm³]	[%]	[%]
01	Resin 120	0,06572	1,595	Heating chamber	iso200°C / 60min	-	1,574	-1,334	-1,263 (0,695)
02		0,036	1,591			-	1,569	-1,402	
03		0,03876	1,583			-	1,571	-0,764	
04		0,03446	1,579			-	1,571	-0,509	
05		0,02052	1,597			-	1,561	-2,306	
06	Resin 120	0,0228	1,575	TMA	HR20 / iso200°C / 60min	0,01	1,599	1,501	1,819 (2,671)
07		0,02304	1,582			0,01	1,584	0,126	
08		0,02522	1,597			0,01	1,582	-0,948	
09		0,02465	1,581			0,01	1,600	2,407	
10		0,01817	1,548			0,01	1,647	6,011	
11	Resin 140	0,0542	1,583	Heating chamber	iso200°C / 60min	-	1,576	-0,426	-1,300 (1,008)
12		0,045238	1,594			-	1,565	-1,853	
13		0,0333	1,58			-	1,582	-0,063	
14		0,03695	1,581			-	1,543	-2,463	
15		0,04460	1,575			-	1,549	-1,679	
16	Resin 140	0,02169	1,583	TMA	HR20 / iso200°C / 60min	0,01	1,567	-1,021	0,403 (2,021)
17		0,02149	1,585			0,01	1,551	-2,192	
18		0,01815	1,597			0,01	1,608	0,684	
19		0,01685	1,612			0,01	1,640	1,767	
20		0,02087	1,576			0,01	1,621	2,776	
21	Resin DSC	0,01225	1,353	Heating chamber	iso200°C / 60min	-	1,404	3,632	3,147 (1,123)
22		0,01156	1,400			-	1,440	2,778	
23		0,01298	1,395			-	1,440	3,125	
24		0,01014	1,378			-	1,400	1,571	
25		0,00473	1,340			-	1,405	4,626	

Table A-4: Normalized enthalpy values obtained from isothermal and dynamic heat flow curves of resin powder and specimens prepared at different temperatures.

No.	Specimen	Heating rate	Curing temperature	Curing time	Normalized enthalpy	Mean (SD) of normalized enthalpy
-	-	[°C/min]	[°C]		[J/g]	[J/g]
01	Resin powder	-	200	100	120,4	129,3 (11,1)
02					141,8	
03					125,7	
04	Resin 110	-	200	100	123,5	121,7 (2,7)
05					118,6	
06					123,0	
07	Resin 120	-	200	100	114,4	109,6 (7,0)
08					101,6	
09					112,8	
10	Resin 140	-	200	100	77,2	74,7 (2,2)
11					73,2	
12					73,7	
13	Resin 120	20	200	100	94,3	97,2 (8,8)
14					107,2	
15					90,2	
16	Resin powder	5	-	-	52,6	52,3 (0,7)
17					51,5	
18					52,9	
19	Resin 110	5	-	-	51,9	53,1 (2,1)
20					51,9	
21					55,6	
22	Resin 120	5	-	-	50,4	50,5 (0,5)
23					50,1	
24					51,1	
25	Resin 140	5	-	-	25,0	25,1 (0,6)
26					24,6	
27					25,8	

Table A-5: Cure shrinkage obtained from TMA measurements in expansion mode, as well as the displacement of the probe at the end of the heating segment and at the end of the isothermal segment.

No.	Specimen	Displacement after heating segment	Displacement after isothermal segment	Linear cure shrinkage	Mean (SD) of cure shrinkage
-	-	[µm]	[µm]	[%]	[%]
01	Resin 110	1111,90	1100,94	0,986	0,997 (0,065)
02		1121,34	1109,37	1,067	
03		1133,13	1122,49	0,939	
04	Resin 120	1183,90	1172,35	0,976	0,982 (0,176)
05		1198,30	1184,90	1,118	
06		1102,70	1092,2	0,952	
07		1137,60	1128,40	0,809	
08		1119,60	1109,4	0,911	
09		1137,60	1127,80	0,861	
10		1144,00	1135,45	0,747	
11		1164,60	1150,60	1,202	
12		1168,30	1153,60	1,258	
13	Resin DSC	538,56	534,03	0,841	0,906 (0,092)
14		563,30	557,83	0,971	
15	Resin 140	1080,70	1072,00	0,805	0,774 (0,035)
16		1101,80	1093,80	0,726	
17		1132,79	1124,05	0,772	
18		1095,70	1087,00	0,794	
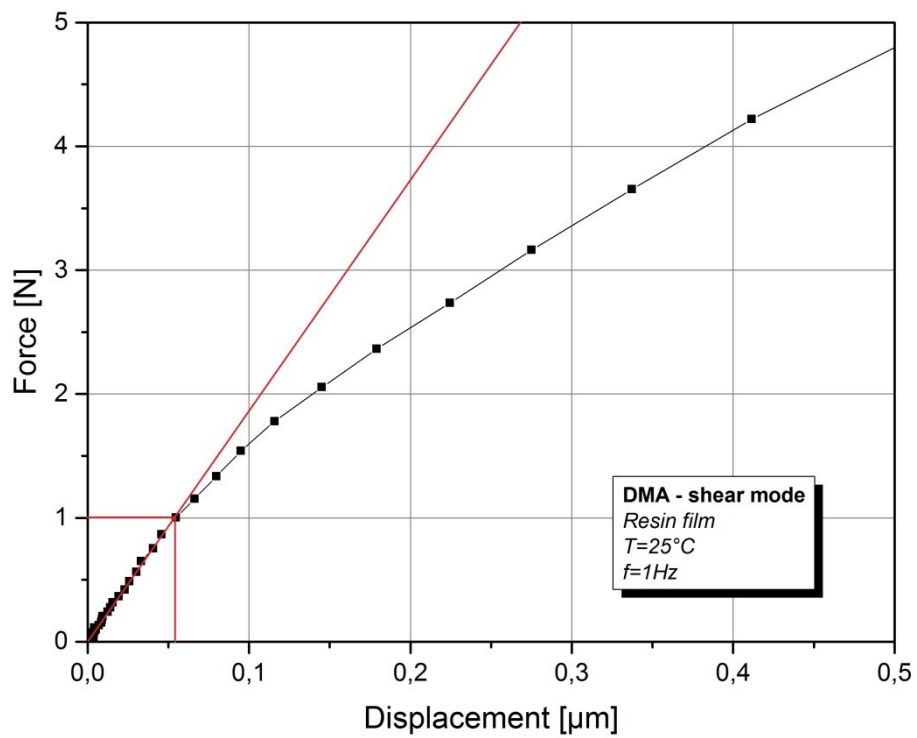
Fig. A-1: Force scan of an epoxy resin film performed in the shear mode of the DMA/SDTA861[e].
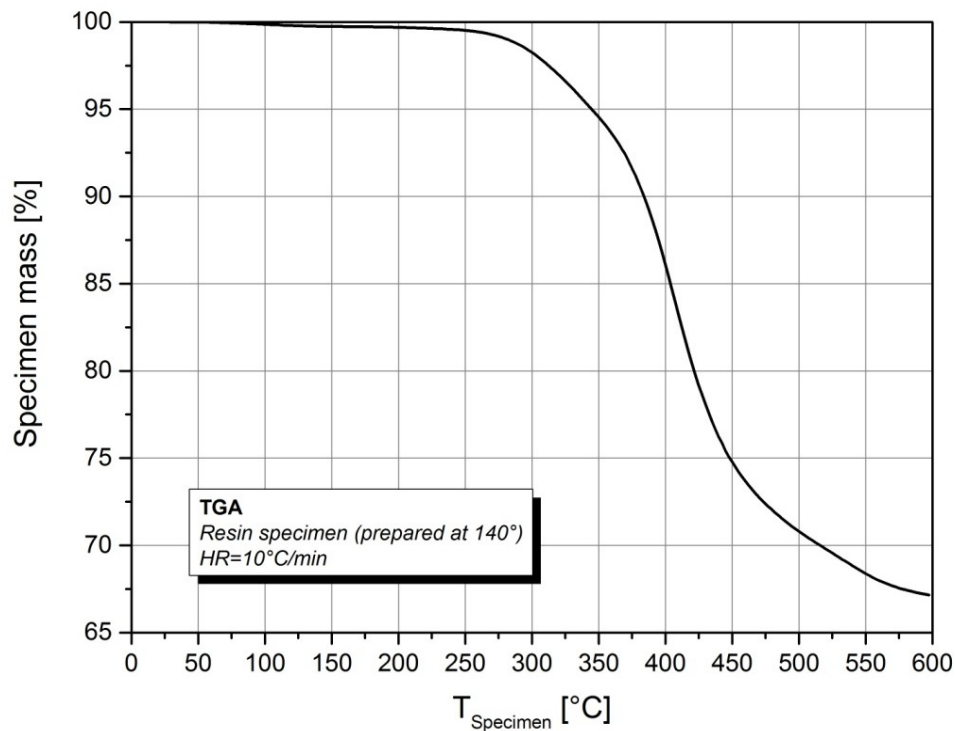
Fig. A-2: Results of a thermogravimetric analysis of a specimen prepared at 140°C carried out with a TG 209 F1 Libra® from Netzsch-Gerätebau GmbH.
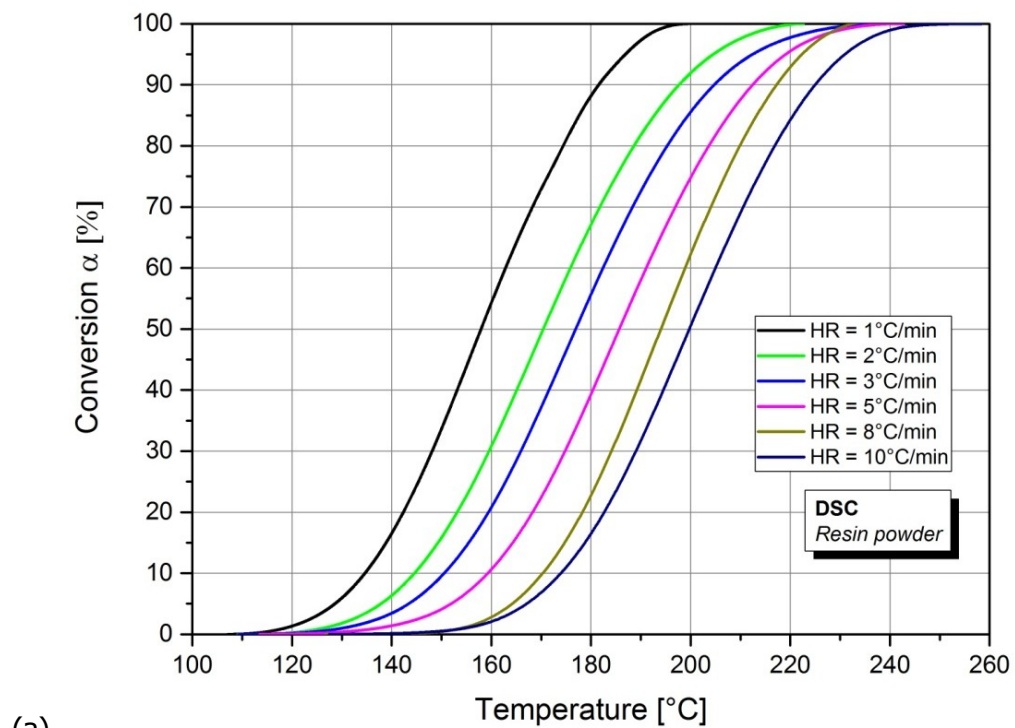
(a)
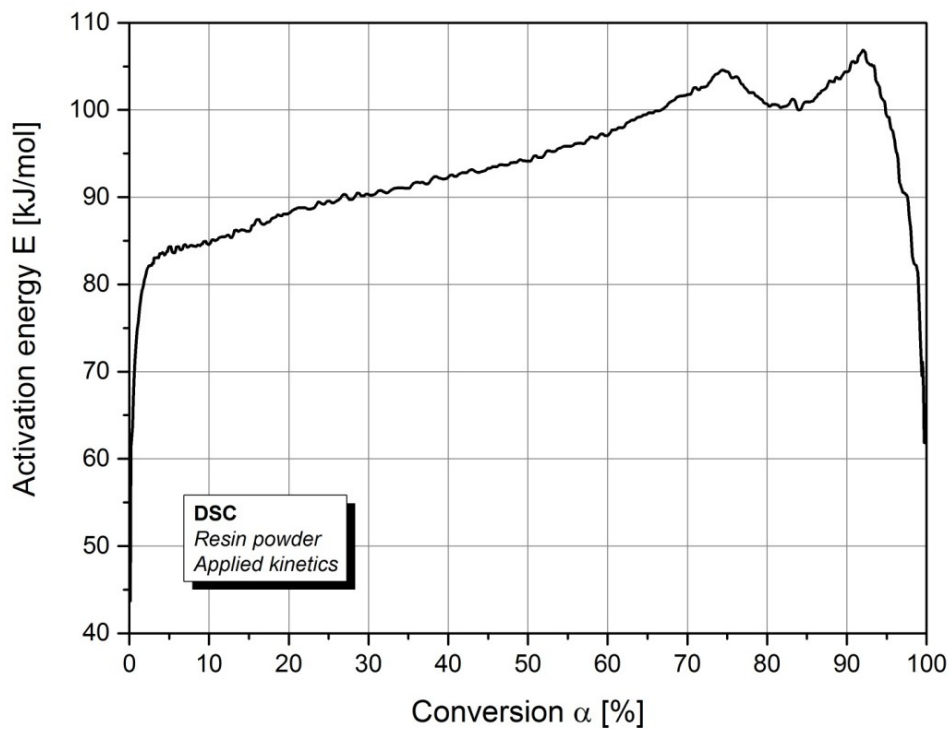
(b)

Fig. A-3: (a) Conversion depending on temperature for different heating rates.

(b) Activation energy determined by applying the Vyazovkin model-free kinetic algorithm.
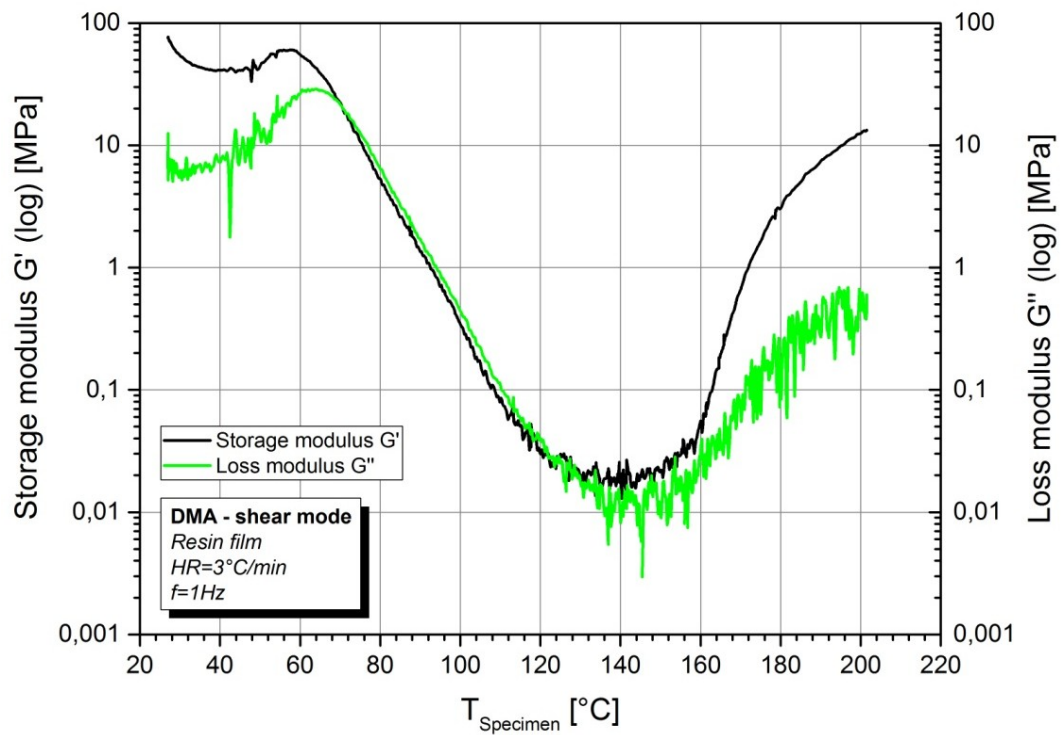
Fig. A-4: Storage modulus G′ and loss modulus G″ over temperature measured in the shear mode of the DMA/SDTA861[e] (specimen 2).
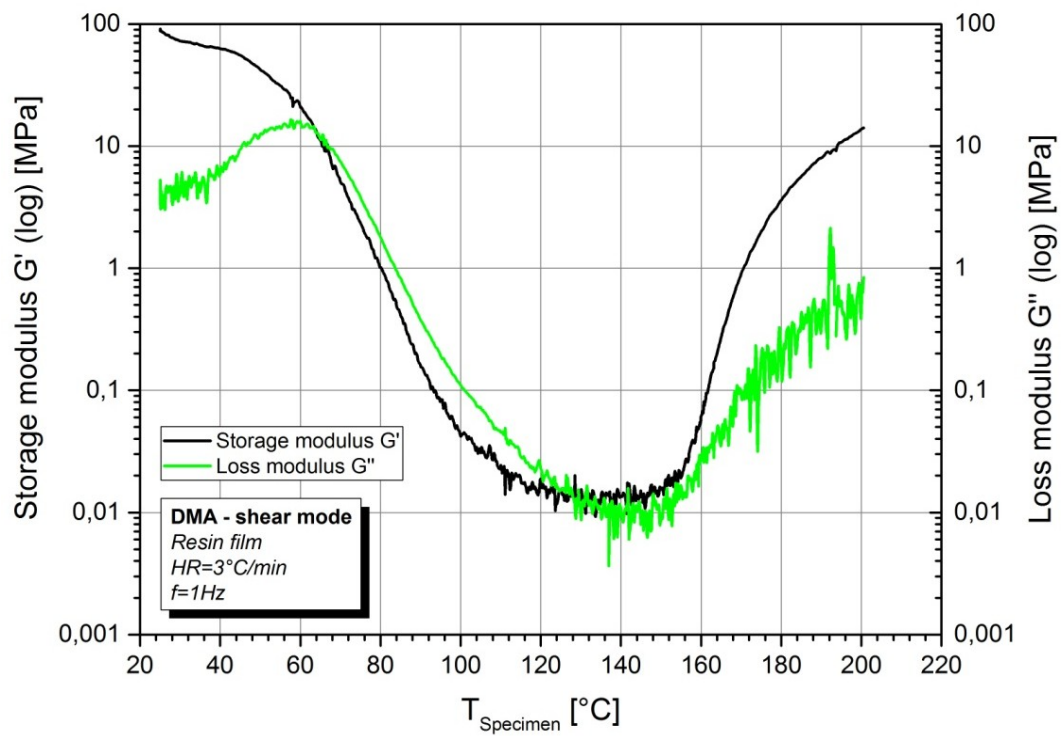
Fig. A-5: Storage modulus G′ and loss modulus G″ over temperature measured in the shear mode of the DMA/SDTA861[e] (specimen 3).
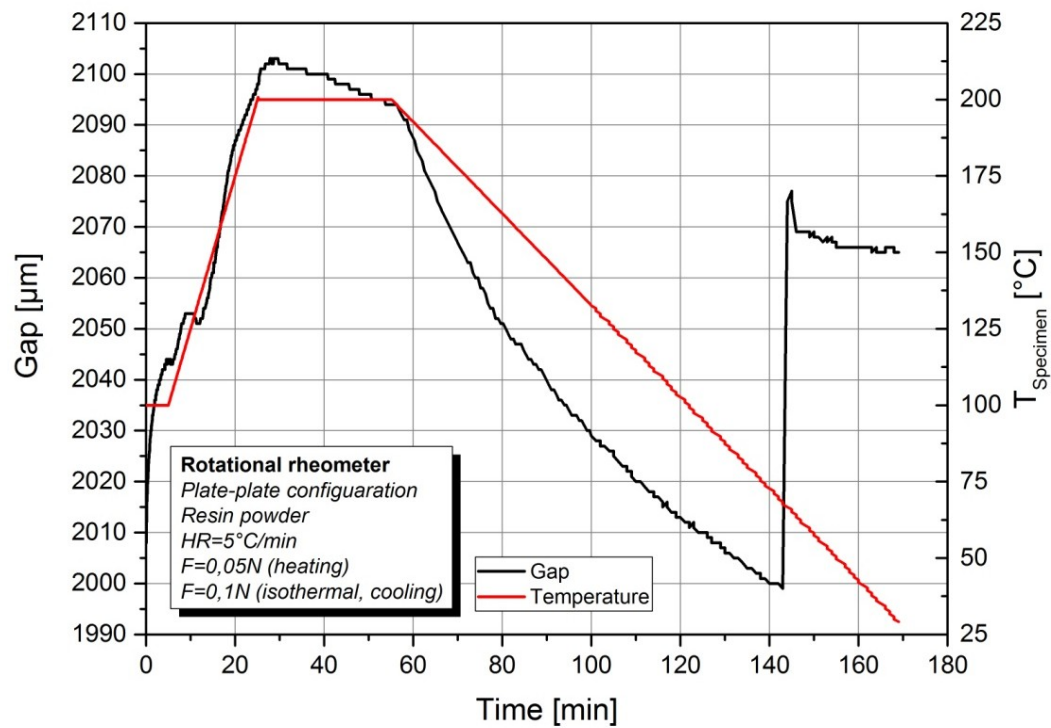
Fig. A-6:   Gap between the two plates of the MCR501 rheometer over time and in relation to the specimen temperature (specimen 2).
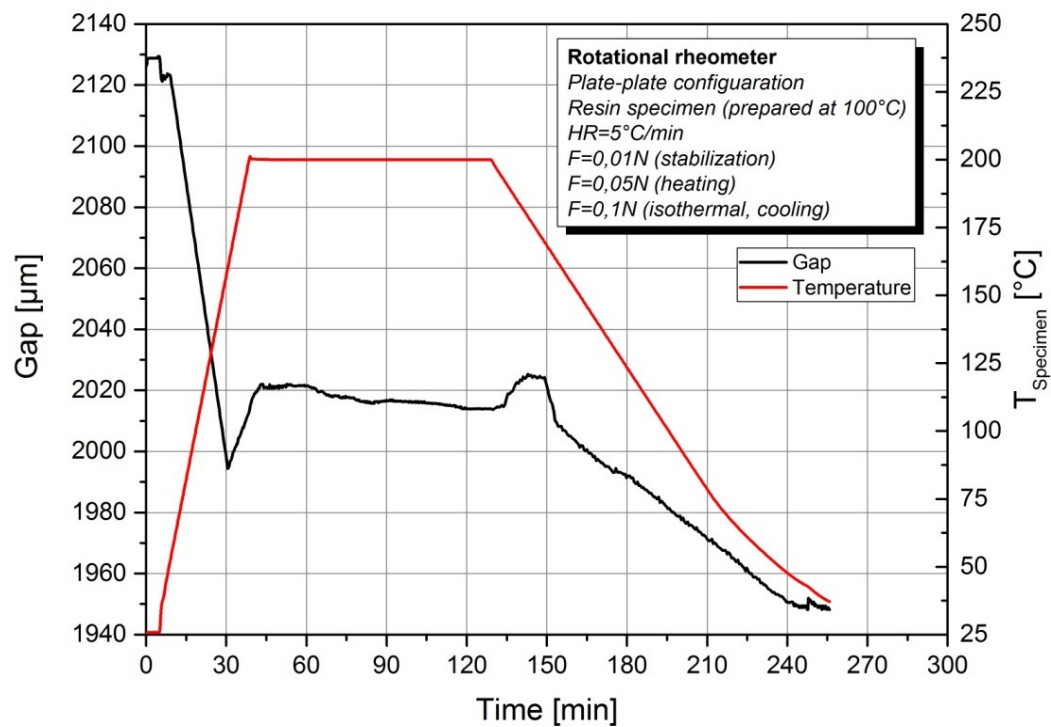
Fig. A-7:   Gap between the two plates of the MCR501 rheometer over time and in relation to the specimen temperature (specimen 3).
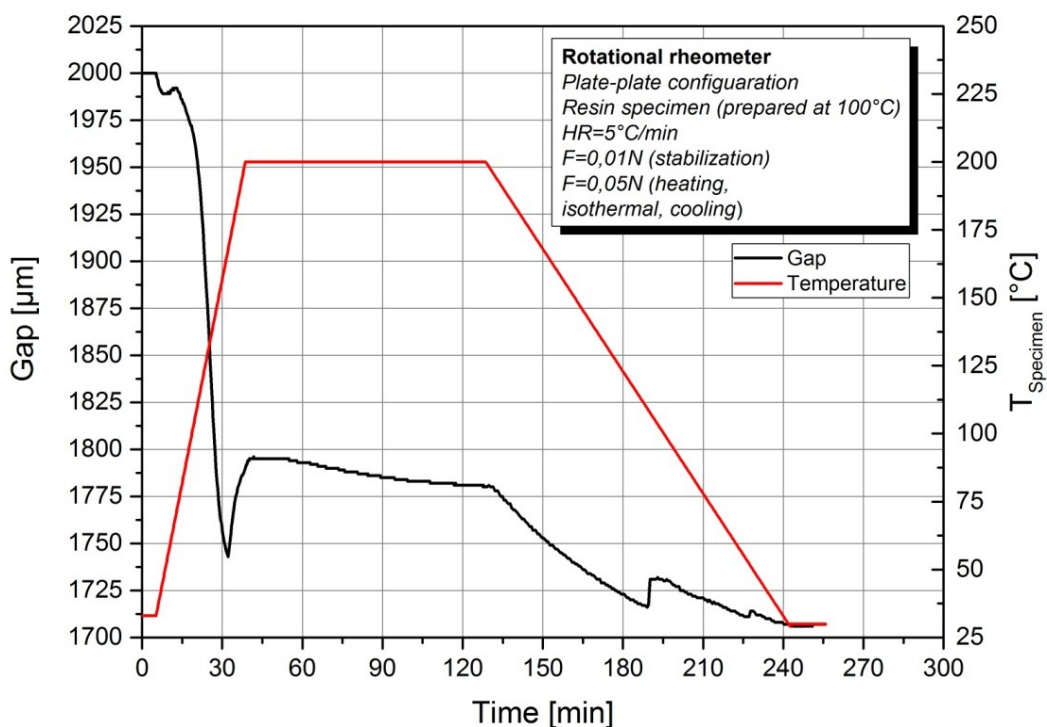
Fig. A-8: Gap between the two plates of the MCR501 rheometer over time and in relation to the specimen temperature (specimen 4).
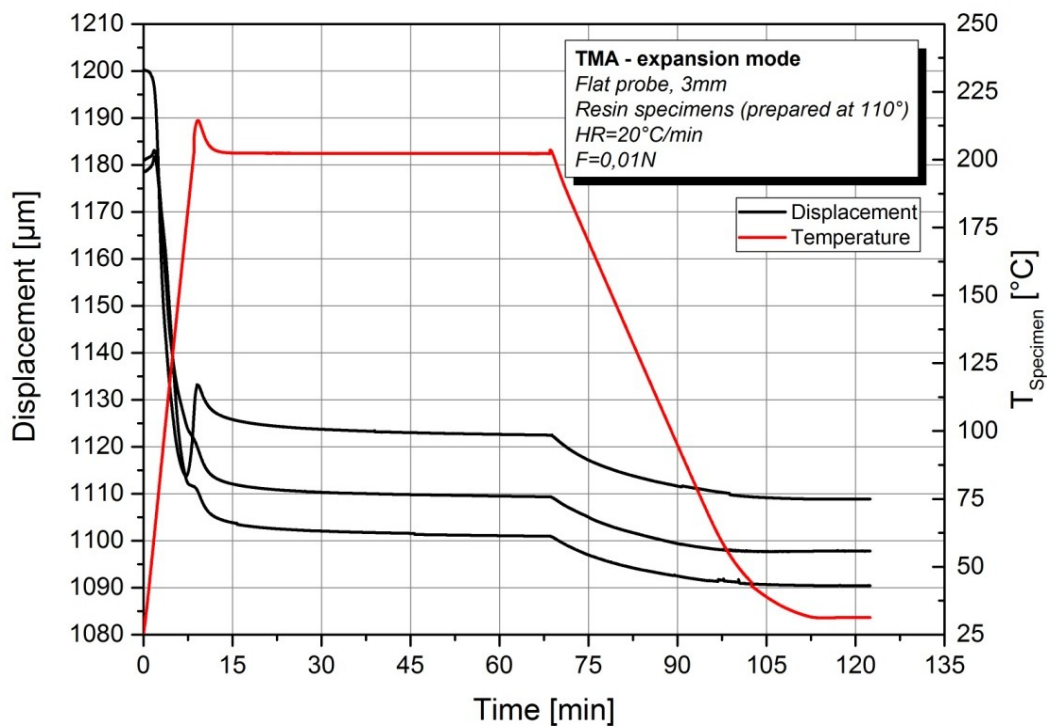
Fig. A-9: Dimensional changes over time of the specimens prepared at 110°C, measured in the expansion mode of the TMA (specimens 1-3).
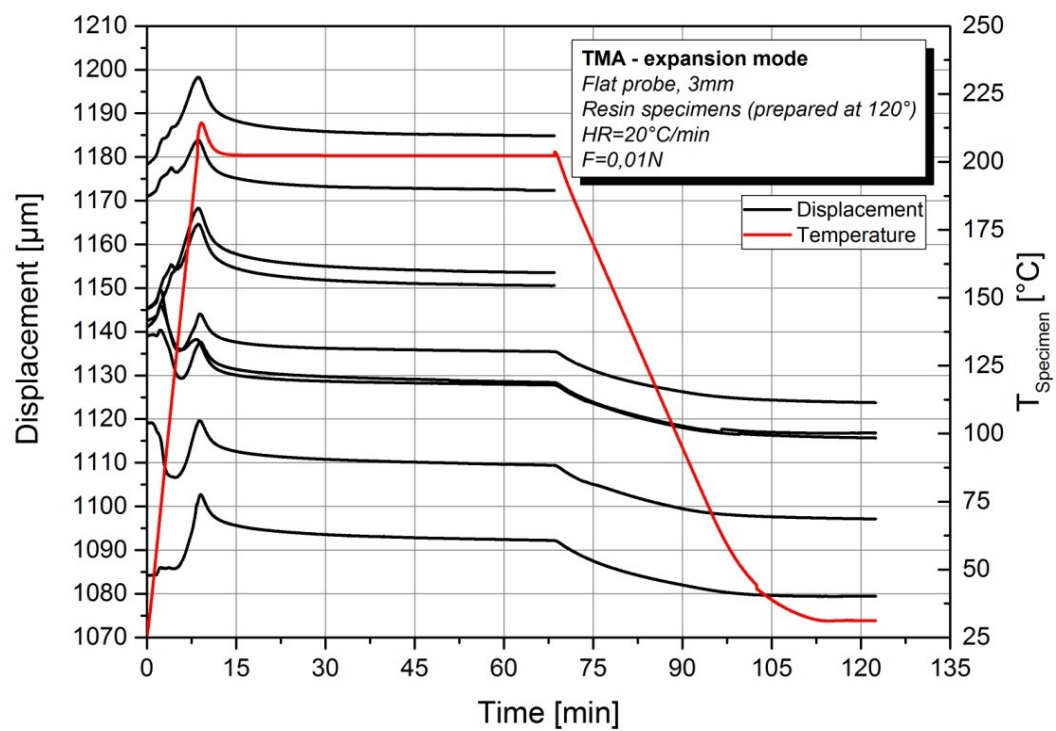
Fig. A-10: Dimensional changes over time of the specimens prepared at 120°C, measured in the expansion mode of the TMA (specimens 4-12).
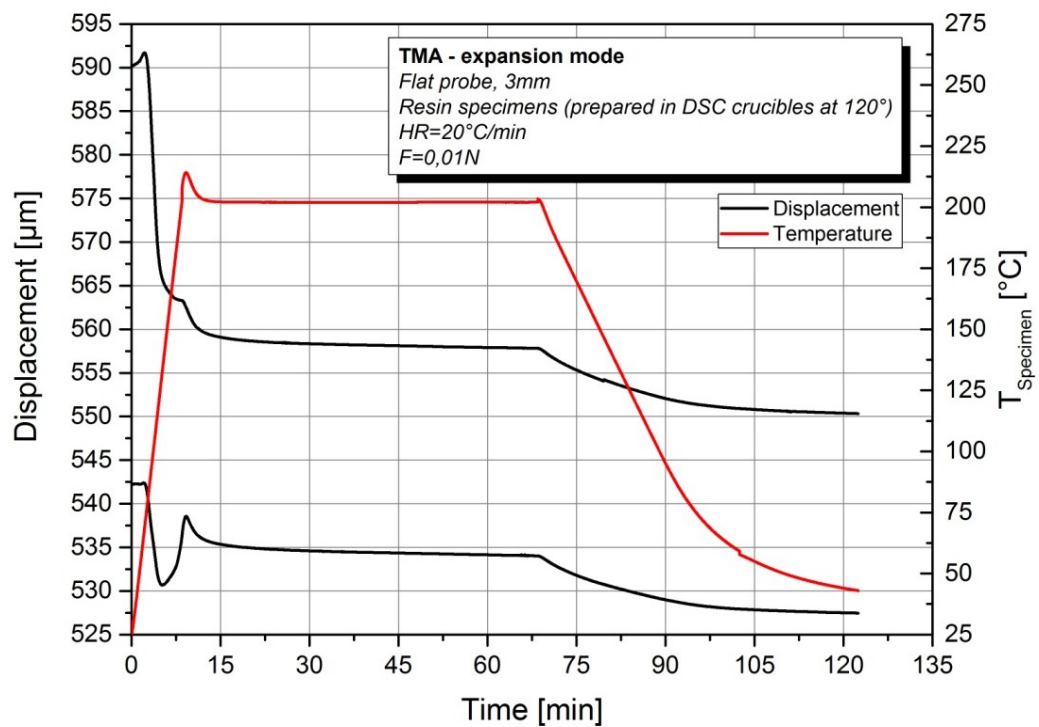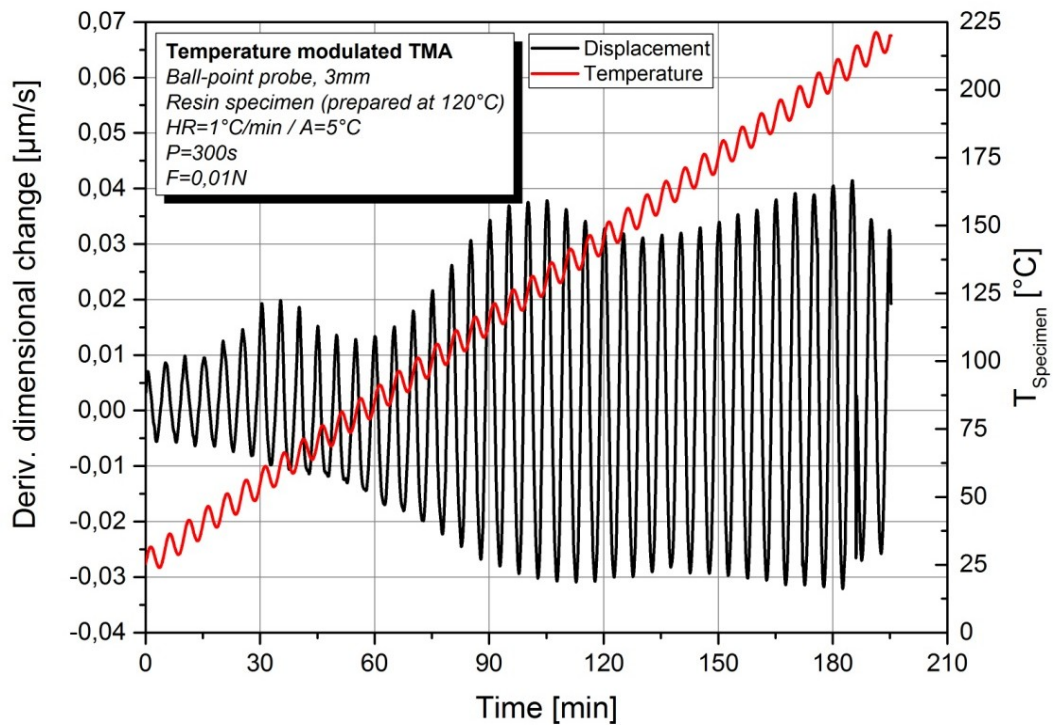

Fig. A-11: Dimensional changes over time of the specimens prepared at 120°C in DSC crucibles, measured in the expansion mode of the TMA (specimens 13-14).
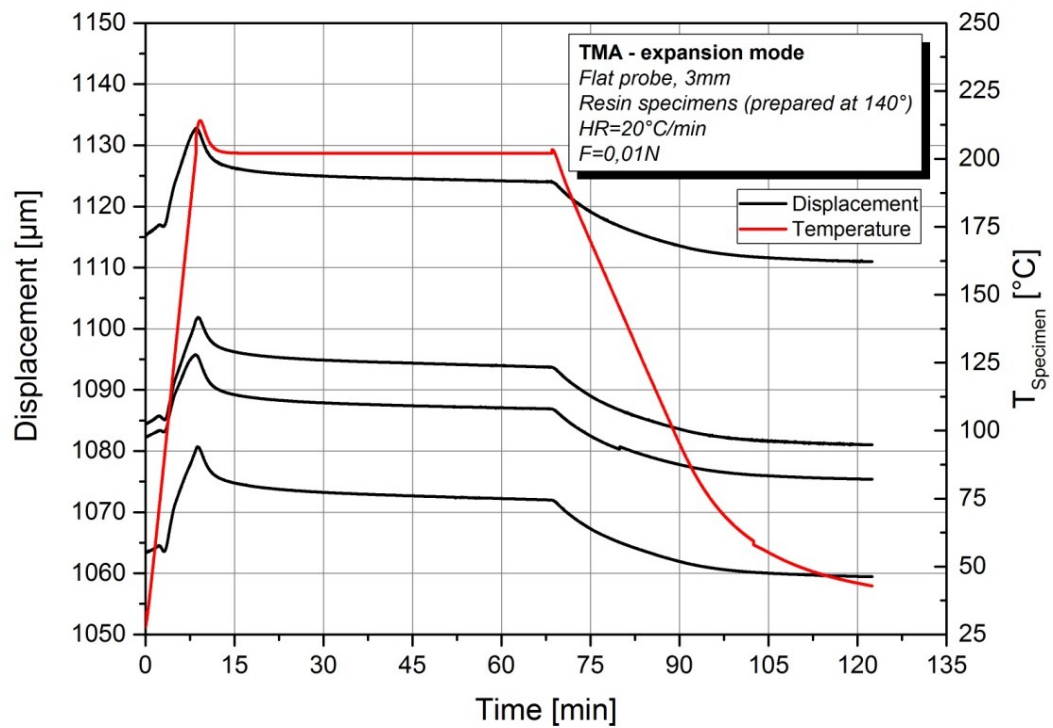
Fig. A-12: Dimensional changes over time of the specimens prepared at 140°C, measured in the expansion mode of the TMA (specimens 15-18).

Fig. A-13: First derivation of the dimensional change with respect to time (specimen 1).
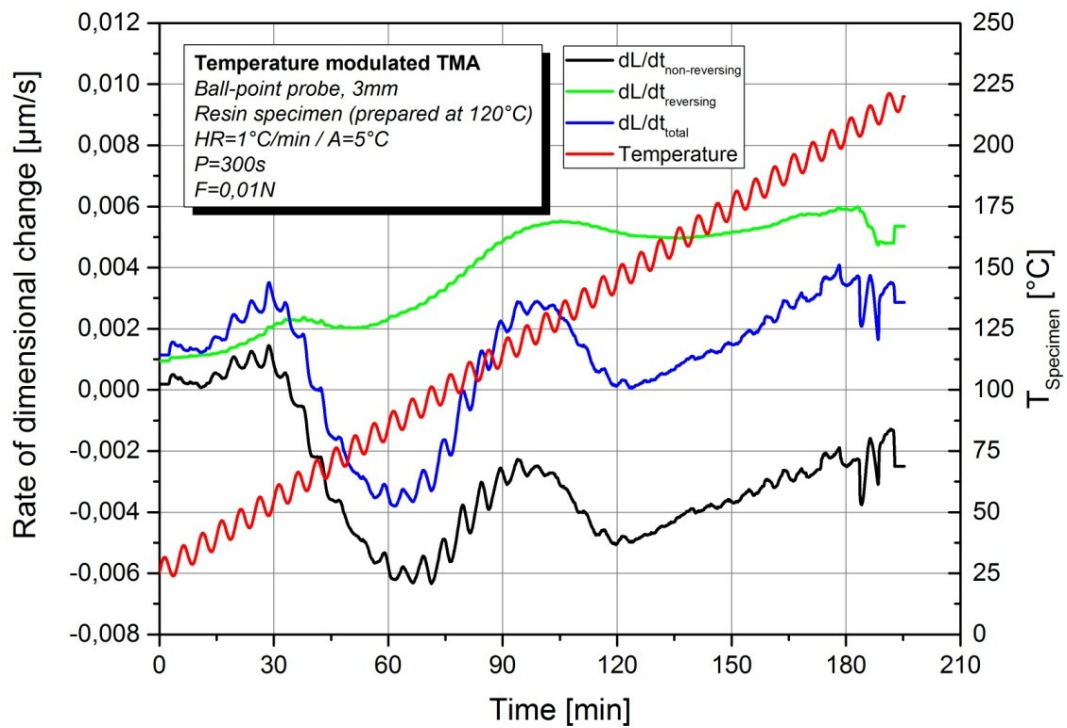
Fig. A-14: Total, reversing, and non-reversing rate of dimensional change obtained by applying the ADSC software option (specimen 1).
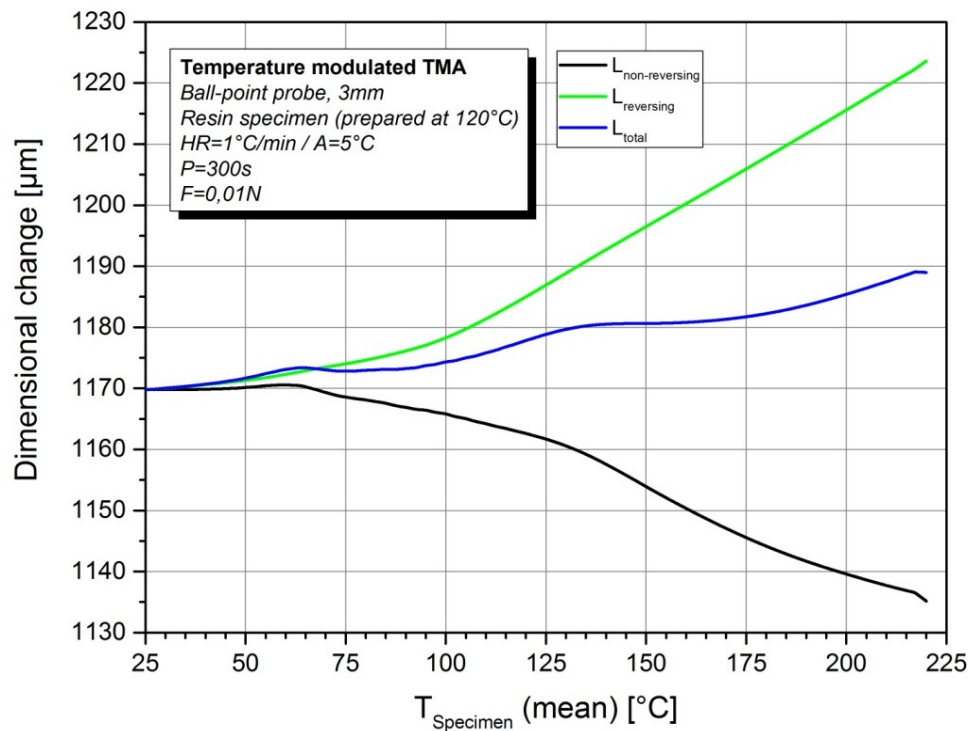

Fig. A-15: Deconvolution of the data recorded by applying temperature modulated TMA (specimen 2).
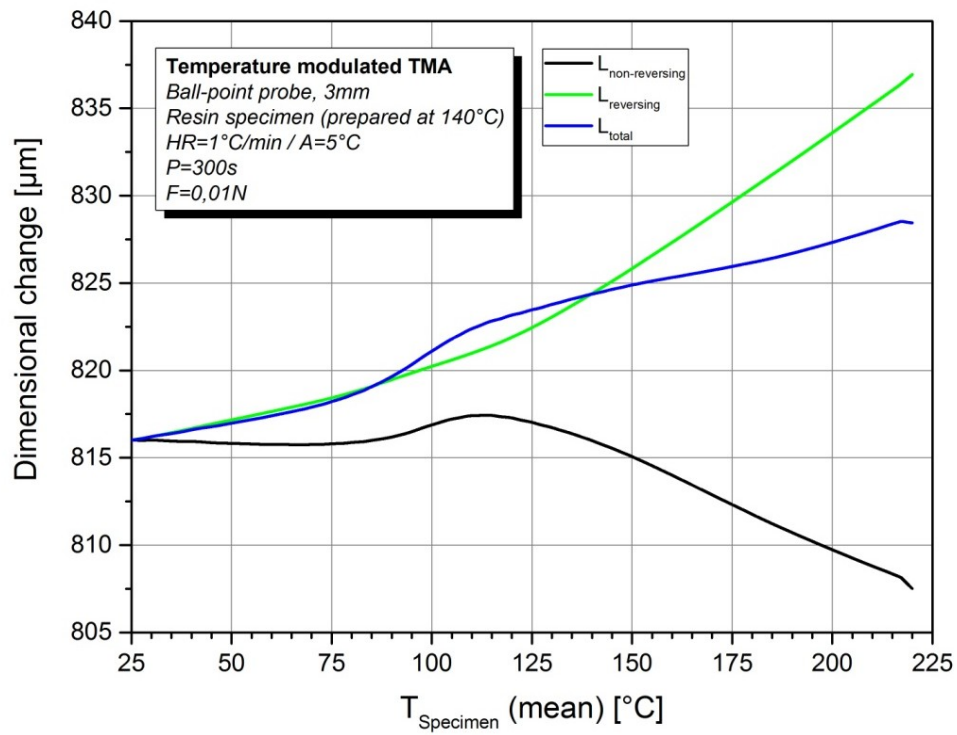
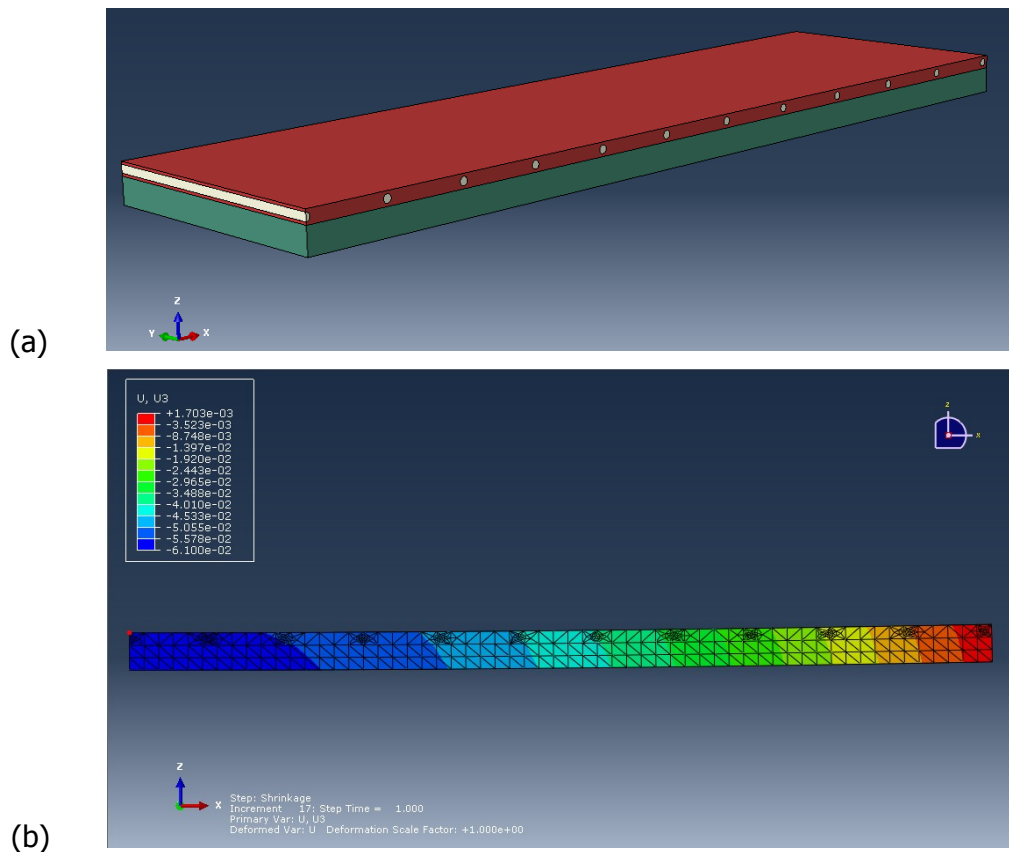**Fig. A-16:** Deconvolution of the data recorded by applying temperature modulated TMA (specimen 3).

(a)

(b)

Fig. A-17: (a) Geometry of model 2 and (b) final deformation of the modeled strip.
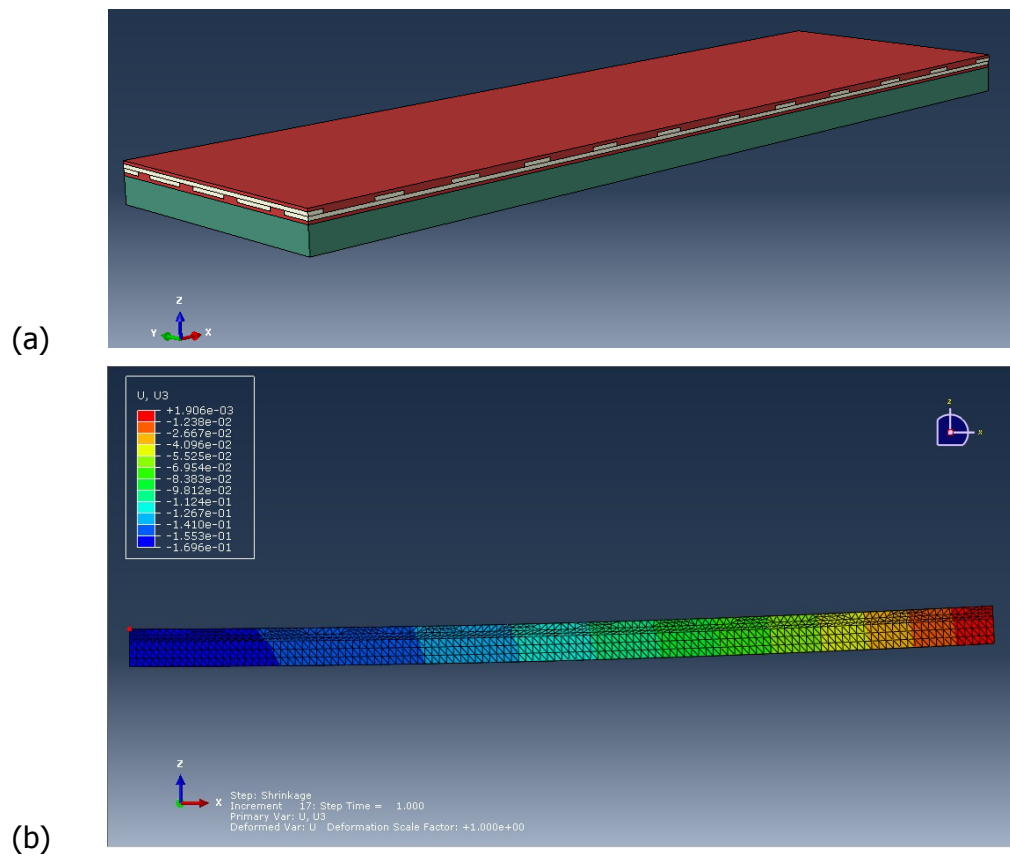
(a)

(b)

Fig. A-18: (a) Geometry of model 3 and (b) final deformation of the modeled strip.